Titre: Title:	Study of a tuneable microwave resonator based on liquid crystal
Auteur: Author:	Azin Mirfatah
Date:	2009
Type:	Mémoire ou thèse / Dissertation or Thesis
Référence: Citation:	Mirfatah, A. (2009). Study of a tuneable microwave resonator based on liquid crystal [Mémoire de maîtrise, École Polytechnique de Montréal]. PolyPublie. https://publications.polymtl.ca/8494/

URL de PolyPublie: PolyPublie URL:	https://publications.polymtl.ca/8494/
Directeurs de recherche: Advisors:	Jean-Jacques Laurin
Programme: Program:	Non spécifié

NOTE TO USERS

This reproduction is the best copy available.

UMI°

UNIVERSITÉ DE MONTRÉAL

STUDY OF A TUNEABLE MICROWAVE RESONATOR BASED ON LIQUID
CRYSTAL

AZIN MIRFATAH

DÉPARTEMENT DE GÉNIE ÉLECTRIQUE

ÉCOLE POLYTECHNIQUE DE MONTRÉAL

MÉMOIRE PRÉSENTÉ EN VUE DE L'OBTENTION

DU DIPLÔME DE MAÎTRISE ÈS SCIENCES APPLIQUÉES
(GÉNIE ÉLECTRIQUE)
AOÛT 2009

Library and Archives
Canada

Bibliothèque et
Archives Canada

Published Heritage
Branch

Direction du
Patrimoine de l'édition

395 Wellington Street
Ottawa ON K1A 0N4
Canada

395, rue Wellington
Ottawa ON K1A 0N4
Canada

Canada

UNIVERSITÉ DE MONTRÉAL

ÉCOLE POLYTECHNIQUE DE MONTRÉAL

Ce mémoire intitulé:

STUDY OF A TUNEABLE MICROWAVE RESONATOR BASED ON LIQUID
CRYSTAL

présenté par: MIRFATAH, Azin

en vue de l'obtention du diplôme de: Maîtrise ès sciences appliquées

a été dûment accepté par le jury d'examen constitué de:

M. BOSISIO Renato G., M.Sc.A., président

M. LAURIN Jean-Jacques, Ph.D., membre et directeur de recherche

M. AKYEL Cevdet, D.Sc.A., membre

To my parents, my brother, my husband

And to my daughter, Anita, who makes everything possible

ACKNOWLEDGEMENT

I am also very grateful to my parents and my brother Arash who provided me through my entire life. My deepest appreciation I must reserve for my husband Soroush, whose endless love, friendship and support I am very thankful for.

RÉSUMÉ

Un nouveau résonateur accordable utilisant des cristaux liquides comme diélectrique est présenté dans ce projet de maîtrise. Le cristal liquide est un matériau diélectrique non linéaire et polaire dont la polarisation peut être modifiée. En effet, ces matériaux peuvent être commandés par un champ électrique par le biais de leur permittivité diélectrique. Ainsi, pour un cristal liquide nématique anisotrope incorporé dans du substrat multicouche du résonateur, un changement de phase différentielle de 180° du coefficient de réflexion est prévue en bande X. Les variations de phase et les pertes par réflexion sont comparées pour des structures de cristaux liquides nématiques de la société Merck avec des propriétés différentes et référencés BL006, K15 et la MDA-05-893. Les recherches dans ce mémoire montrent qu'une faible tension (i.e. 5V) peut être utilisée pour faire varier la permittivité du substrat accordable et ainsi, le contrôle de la phase du signal réfléchi.

L'objectif principal de cette recherche est de parvenir à un résonateur accordable en bande X en utilisant des cristaux liquides comme diélectrique et de caractériser leur comportement en tant qu'antenne réseau-réflecteur microruban.

Au début, dans la partie théorique, quatre modèles différents: patch, microruban, résonateur demi-onde et résonateur en épingle à cheveux ont été décrit en soulignant leurs forces et faiblesses relatives. Les simulations sont effectuées à l'aide d'Ansoft -

HFSS ® et / ou Ansoft - Designer ® en bande X. Afin d'avoir une structure compacte avec de faibles pertes de rayonnement, la forme en épingle à cheveux est employée comme la conception la mieux adaptée. En fait, la symétrie impaire de la répartition de courant des deux côtés de l'épingle à cheveux conduit à l'annulation des champs rayonnés. Ainsi,les pertes sont seulement attribuées à la dissipation dans les conducteurs et les diélectriques.

Ensuite, dans la partie expérimentale, un résonateur en épingle à cheveux est fabriqué en utilisant la technologie multicouche et le cristal liquide est injecté dans la cavité fermée. Les coefficients de réflexion (S11) dans les cas parallèle et perpendiculaire des cristaux liquides sont mesurés en bande X à l'aide d'un analyseur de réseau. Les résultats numériques sont comparés avec la phase mesurée, les fréquences de résonance et l'atténuation du signal pour les deux orientations des molécules du cristal liquide. Les résonateurs sont fabriqués et les caractéristiques mesurées se trouvent en très bon accord avec les données simulées.

Dans la dernière partie du mémoire, le comportement de la structure de résonateur en épingle à cheveux utilisée comme élément d'antenne réseau-réflecteur est prédit, basé sur des données expérimentales. Enfin, les diagrammes de rayonnement d'une antenne réseau-réflecteur avec 301 éléments de cristaux liquides sont présentés.

ABSTRACT

A novel tuneable resonator using liquid crystal as a dielectric is proposed. Due to the bias-dependent permittivity of an anisotropic nematic liquid crystal embedded in the resonator's multilayer substrate, a differential phase shift of 180° in the reflection coefficient is predicted in X band. Phase ranges and reflection losses are compared for structures constructed using K15, BL006 and MDA-05-893 type liquid crystals which have been engineered by MERCK. The research conducted in this thesis shows that a small voltage (i.e.5 V) can be used to vary the permittivity of the tuneable substrate and thereby control the phase of the reflected signal.

The primary objective of this research is to achieve a tuneable resonator in X band using liquid crystal as a dielectric and characterizing its behaviour as a reflectarray.

First in the theory part, the four different types of designs: patch, microstrip, half wave resonator and hairpin resonator were sketched along with their relative strengths and weaknesses. Simulations are done using of Ansoft – HFSS ® and/or Ansoft – Designer ® in X-band. In order to provide compactness and low radiation losses, the hairpin shape is employed as the best suited resonator design. In fact, the odd symmetry of the current distribution on both sides of the hairpin leads to the cancellation of the currents responsible for the radiated fields. Therefore the most significant loss contribution left is from the dissipation in conductors and dielectrics.

Next, in the experimental part, the hairpin resonator is fabricated using multilayer technology and the liquid crystal is injected in the closed-cavity. The reflection coefficients (S11) in parallel and perpendicular liquid crystal states are measured in X band using a network analyzer. Numerical results are compared with measured phase, resonant frequencies and signal attenuation for two orientations of the liquid crystal molecules. The resonators are fabricated and the measured characteristics are found to agree very well with the simulated data.

In the last part of the thesis, the behaviour of the hairpin resonator structure used as a reflectarrays element is predicted, based on experimental data. Finally, the radiation patterns of a 301 element LC reflectarray antenna, are presented.

xi

CONDENSÉ

Dans tout système de radar et de communication l'antenne joue un rôle primordial. Cependant, l'incapacité des antennes à s'adapter à de nouveaux scénarios d'opérations limite les performances des systèmes [1]. L'antenne reconfigurable permet d'améliorer ou d'éliminer ces limitations. Théoriquement, les antennes reconfigurables devraient être capables d'ajuster leurs fréquence d'opération, polarisation, impédance, largeurs de bande et diagramme de rayonnement en fonction des exigences du système [1]. La reconfigurabilité peut être obtenus en utilisant des technologies telles que les interrupteurs (par exemple diodes, MEMS), ou le changement de matériaux (par exemple : ferrites, ferroélectriques et liquides).

Les antennes reconfigurables basées sur les changements de matériaux subissent généralement plus de pertes en raison des fuites de courant à travers les lignes de contrôle ou des rayonnements non désirés des circuits utilisés dans les éléments reconfigurables de l'antenne [1]. Il est très important de réduire les pertes en vue d'améliorer les performances de l'élément rayonnant.

Plusieurs tentatives ont été faites pour avoir des antennes reconfigurables. Les diodes à jonction PIN, les MEMS et les ferrites ont un grand potentiel, cependant ils créent certains désavantages: l'usage des diodes semi-conducteurs est limité à la plage des fréquences GHz inférieures (jusqu'à environ 15-20 GHz) en raison de capacités

parasites et de pertes élevées. Les commutateurs MEMS montrent d'excellentes caractéristiques dans la région GHz plus élevée. Cependant les dispositifs utilisant cette technologie ont besoin d'un grand nombre de commutateurs MEMS avec chacun sa propre ligne de polarisation, afin de minimiser les erreurs de phase et d'obtenir une fiabilité et une complexité élevée [11]. D'autre part, en raison de la détérioration des propriétés électromagnétiques à haute fréquence, les coûts de fabrication élevés, une grande consommation de puissance, l'encombrement et probablement de hautes pertes d'insertion; les dispositifs à base de ferrites fonctionnent plus efficacement en dessous de 30 GHz et ont des problèmes d'adaptation pour une opération au-dessus de 30 GHz, et sont particulièrement difficiles à utiliser au delà de 100 GHz [12].

Le cristal liquide est un matériau diélectrique non linéaire et polaire dont la polarisation peut être modifiée en appliquant un champ électrique. Les dispositifs accordables utilisant la technologie des cristaux liquides présentent de nombreux avantages : faible coût de fabrication, faible poids, encombrement réduit, compatibilité avec des circuits hybrides, possibilité de mise en réseau, consommation électrique négligeable et plus spécialement, leurs applications dans des circuits et les antennes reconfigurables. De façon générale, en tenant compte des inconvénients des autres dispositifs accordables mentionné ci-dessus, les matériaux en cristaux liquides semblent supérieurs en termes de coût, de l'intégration et de la facilité de fabrication par rapport aux diodes, MEMS ou ferrites.

Dans ce mémoire, le cristal liquide thermotrope est traité. Un cristal liquide est thermotrope si l'ordre de ses molécules est déterminé ou modifié par la température. En effet dans ces matériaux, les transitions de phases sont induites par des variations de température.

Les différentes phases des cristaux liquides thermotropes (smectique, nématique, cholestérique) ont été découvertes jusqu'aujourd'hui [26]. La caractéristique commune de ces phases est leur stabilité dans la plage de température où le liquide isotrope et la phase solide sont stables.

Ce mémoire examine uniquement le cristal liquide nématique. Les molécules qui constituent la phase nématique sont disposées de telle manière qu'il n'y a pas d'ordre positionnel pour leurs centres de masse, comme dans le liquide isotrope, mais il y a un large ordre d'orientation. Les molécules ont tendance à s'orienter sur la moyenne le long d'une direction privilégiée au sein d'un groupe important de molécules.

Considérons le cas où le cristal liquide est contenu entre deux surfaces solides métalliques à travers lesquelles une tension peut être appliquée. Dans le cas d'un champ électrique nul, les molécules de cristal liquide sont parallèles aux substrats et la permittivité de cristal liquide est $\varepsilon_\perp$. Lorsqu'un champ électrique E_0 est appliqué, les molécules de cristal liquide subissent une rotation de 90°. Dans ce cas, les axes des molécules du cristal liquide sont parallèles à la direction de la tension appliquée et la

permittivité devient $\varepsilon_{\parallel}$. Pour une valeur intermédiaire de champ électrique ($0 \leq E \leq E_0$), la permittivité varie continûment entre $\varepsilon_{\perp}$ et $\varepsilon_{\parallel}$.

La différence entre les valeurs de la constante diélectrique dans les cas parallèle et perpendiculaire i.e. $\Delta\varepsilon = \varepsilon_{\parallel} - \varepsilon_{\perp}$ définit l'anisotropie diélectrique du cristal liquide. La variation de phase réalisée dans un résonateur accordable est fortement liée à la valeur de $\Delta\varepsilon$.

En raison de ce phénomène, il est possible de contrôler avec précision la fréquence de résonance d'un résonateur en appliquant une tension continue, ou alternativement, contrôler la phase de la réponse de réflexion à la fréquence de résonance.

Des cristaux liquides ont été insérés dans de différents dispositifs micro-ondes accordables dont des déphaseurs [12] [14], condensateurs accordables [21], filtres accordables [22] [23], lignes à retards variables [15], antennes réseau-réflecteurs [16] [17] [19] [20], etc. La plupart d'entre eux utilisent une ligne de transmission ou une structure patch ouverte. Des études récentes ont montré que des antennes électroniques reconfigurables à réseau-réflecteur peuvent être créées en plaçant des éléments patch imprimés au-dessus d'un métal soutenu par des cavités remplies de cristal liquide nématique [13] [19]. Dans une antenne réseau-réflecteur à cristal liquide, la phase du signal réfléchi par chaque élément est ajustée en appliquant une tension de polarisation

pour contrôler l'orientation des molécules de cristal liquide. Suite à cet ajustement de phase, un faisceau focalisé est généré.

Les cristaux liquides nématiques utilisés dans cette étude sont des produits commercialisés par la société Merck KGaA avec des propriétés différentes et référencés BL006 [16], K15 [28], [24] et la MDA-05-893 [17]. Leurs données techniques et les fiches de sécurité sont inscrites dans l'Annexe A.

Afin d'atteindre le minimum de perte et le déphasage maximal du coefficient de réflexion et donc la meilleure performance en termes de reconfiguration, quatre types de conceptions : résonateur patch rectangulaire, lignes à retard micro ruban, résonateur demi-onde et résonateur épingle à cheveux sont présentées, et leurs points forts et faiblesses relatives sont comparés. Des simulations ont été effectuées avec des outils de simulation de méthode des éléments finis et de méthode des moments Ansoft - HFSS ® et Ansoft - ® Designer. Toutes les conceptions ont été faites pour une fréquence d'opération proche de 10 GHz.

Ensuite, la forme en épingle à cheveux a été adoptée, choisie pour sa compacité et ses faibles pertes par rayonnement. En effet, la symétrie impaire de la répartition de courant des deux côtés de l'épingle à cheveux conduit à l'annulation des champs rayonnés [18]. Par conséquent, la plus importante perte provient de la dissipation dans les conducteurs et le diélectrique.

Dans cette étude, nous envisagerons un nouveau résonateur accordable composé d'une épingle à cheveux repliée imprimée. Le résonateur et sa ligne d'accès en courant continu sont placés sur la face inférieure d'un substrat d'alumine. Sur la face supérieure sont posées les lignes d'entrée RF et de courant continu. Un via interconnecte les parties supérieure et inférieure de la ligne de courant continu. Une ligne étroite de polarisation à haute impédance a été utilisée pour empêcher les fuites RF dans le réseau de polarisation. La ligne d'alimentation RF est au dessus du cadre de l'alumine et est donc moins affecté par l'état de polarisation des cristaux liquides.

Pour atteindre les meilleures performances possibles, les directives suivantes ont été suivies dans la conception de la structure multicouche:

- Pour augmenter l'accordabilité, le pourcentage de stockage de l'énergie RF du résonateur dans le volume de cristal liquide est maximisé. Ceci est réalisé en mettant l'épingle à cheveux métallique imprimée en contact direct avec le cristal liquide;

- Veiller à ce que l'impédance caractéristique de la ligne d'alimentation du résonateur ne soit pas affectée par le changement de permittivité résultant de la polarisation du cristal liquide, en maintenant un bon couplage entre le résonateur et le port 50-ohm de test;

- Éviter d'avoir les ports de connexion RF et DC en contact avec le récipient de cristal liquide afin d'éviter les fuites et les déversements.

Certaines références consultées [11] - [19] ont indiqué qu'une certaine rugosité du contact sur les surfaces de polarisation est nécessaire afin de favoriser l'alignement des molécules polaires du cristal liquide dans l'état non-polarisé. À cette fin, ces articles recommandent de couvrir les électrodes métalliques de polarisation d'une fine couche de polyimide dont la rugosité est obtenue par le frottement avec un chiffon. Cette procédure supplémentaire n'est pas adoptée par tous les auteurs [20] [24] et n'apparaît donc pas comme essentielle.

Avant de commencer la fabrication de résonateurs, un condensateur à plaques parallèles opérant à basses fréquences a été construit et mesuré afin de vérifier l'accordabilité des cristaux liquides en contact avec les électrodes métalliques avec le procédé de pulvérisation cathodique disponible dans notre laboratoire à Poly-GRAMES. La différence entre $\varepsilon_{\parallel}$ et $\varepsilon_{\perp}$ est la plage d'accordabilité de la capacitance. Les résultats montrent que l'augmentation de la tension de zéro à 32 volts a conduit à une variation significative de la susceptance.

L'ajout de couches de polyimide sur les deux électrodes ne montre pas de différence sensible par rapport au cas sans polyimide. Bien sûr, ce condensateur n'a pas été conçu pour une opération en bande X, cependant le résultat de cette mesure révèle la capacité

de réglage du cristal liquide en contact directe avec les électrodes en or. Il est donc possible d'utiliser ce processus simple dans nos essais sur des résonateurs, selon la description suivante.

Deux structures de résonateurs en épingle à cheveux ont été fabriquées avec deux épaisseurs différentes de la couche supérieure de l'alumine, soit 0.127 mm et 0.254 mm. Le cristal liquide est injecté dans une cavité fermée. Afin d'augmenter l'accordabilité, le résonateur métallique imprimé a été mis directement en contact avec le cristal liquide. Un étalonnage à un port circuit ouvert, court-circuit et charge adaptée avec la plan de référence posé au niveau de la connexion coaxiale du dispositif sous test a été fait. Les résultats numériques calculés par HFSS sont comparés avec les caractéristiques mesurées de phases, fréquences de résonance et des pertes de retour pour les deux orientations des molécules du cristal liquide. Les résultats de cette étude montrent que même une faible tension est suffisante pour moduler la phase d'un signal qui est réfléchi par le résonateur. L'agilité de phase dépend du décalage de la fréquence de résonance de la structure. Pour la tension donnée, la fréquence de résonance est déterminée par l'anisotropie diélectrique des cristaux liquides. Trois cristaux liquides différents (BL006, K15 et MDA-05-893) ont été mesurés et en raison de leur plus grand déphasage et de leur perte minimum, MDA-05-893 et BL006 sont les plus recommandés. Une plage de phase accordable de près de 180° a été atteinte pour les trois types de cristal liquide. Le BL006 avec 0,254 mm d'épaisseur de la couche supérieure d'alumine a un déphasage

maximum de 200° à la fréquence 9,636 GHz. Les niveaux de perte de retour dans les états parallèle et perpendiculaire sont de 15dB (0V) et de 10 dB (32V).

À notre connaissance, aucune des structures basées sur des cristaux liquides BL006 présentées dans la littérature n'a réalisé cette performance en bande X. En effet, avant le résonateur en épingle à cheveux, la meilleure gamme de décalage de phase maximale a été mesurée à environ 200° en utilisant des éléments patch [16] avec des pertes maximales entre 18 et 12dB, tandis que ceux obtenus par la structure en épingle à cheveux sont de 15 dB et 10 dB. Ainsi, les pertes de retour du résonateur à épingle à cheveux sont d'au moins 2 dB inférieurs à celles de la structure patch. Cela est dû au fait que l'épingle métallique imprimée est directement en contact avec le cristal liquide alors que les éléments de patch ont été imprimés sur un substrat de PTFE ($\varepsilon_r = 2,9$, $\tan\delta = 0,0028$). Ainsi, les pertes en PTFE ont été ajoutées à la perte de cristal liquide.

En utilisant un modèle numérique combiné aux caractéristiques d'une cellule résonateur en épingle à cheveux obtenues expérimentalement, il est démontré que l'anisotropie diélectrique des cristaux liquides peut être utilisée pour créer une antenne réseau-réflecteur reconfigurable. Cette application du cristal liquide est montrée dans le mémoire.

Les données expérimentales sont les coefficients de réflexion mesurés à la fréquence d'opération (9,636 GHz) pour la cellule de résonateur en épingle à cheveux avec une

couche d'alumine supérieure de 0,254 mm d'épaisseur, où le BL006 est utilisé comme cristal liquide. L'accord de la phase a été obtenu en faisant varier la tension de polarisation de 0 et 32 volts et la direction du faisceau principal rayonné est contrôlée par l'ajustement des phases de réflexion.

Pour déterminer le diagramme de rayonnement théorique, l'optique géométrique est utilisée pour calculer le champ à l'ouverture de l'antenne. La transformée de Fourier de ce champ donne le diagramme de rayonnement en champ lointain du système. A fin de simplification, l'analyse est faite uniquement pour un réflecteur en 2D.

Dans l'antenne réseau-réflecteur réel, il est nécessaire d'avoir une variation de phase de 360°. Selon les données expérimentales, cette variation n'est pas disponible. Il est possible d'obtenir un circuit avec une variation de phase de 360° en combinant deux cellules à cristaux liquides en série.

Il existe un compromis entre la plage de phases disponible et la perte. Cependant, de nouveaux mélanges de cristaux liquides ont été rapportés [33] qui présentent des pertes diélectriques relativement faibles, puisque la tangente de pertes est de 0,004, ce qui est suffisamment faible pour permettre un gain à l'antenne réseau-réflecteur lorsque ce nouveau type de déphaseur est intégré dans la structure de l'antenne.

TABLE OF CONTENTS

LIST OF TABLES

LIST OF FIGURES

LIST OF ABBREVIATIONS

LC   Liquid Crystal

PIN   P-type intrinsic N-type

RF   Radio Frequency

DC   Direct Current

HFSS   High Frequency Structure Simulator

FoM   Figure of Merit

PTFE   Poly Tetra Fluoro Ethylene

MEMS   Micro-Electro-Mechanical-Systems

CHAPTER 1. INTRODUCTION

Antennas are widely used in radar and communications applications, however, their inability to adjust to new operating scenarios can occasionally limit the system's performance [1]. Reconfigurable antennas can improve or eliminate these limitations. Theoretically, reconfigurable antennas should be able to adjust their operating frequency, polarization, impedance bandwidths and radiation patterns according to operating requirements [1]. Reconfigurability of antennas can be obtained with various technologies such as switches, structural changes, and material changes.

Frequency-reconfigurable antennas are also called tuneable antennas. The most common antennas (e.g. linear antennas, loop antennas, slot antennas, and microstrip antennas) usually operate near resonance. The operating frequency is determined by the effective electrical length of the antenna. For example, in a linear dipole antenna, the first resonance occurs at the frequency where the antenna is approximately a half wavelength long and the resulting current distribution results in a radiation pattern centered on and normal to the antenna axis. To be able to use the antenna at a higher frequency, the antenna should be shortened to the correct length corresponding to a half wavelength at the new frequency. The new radiation pattern will have very similar characteristics to the first one because the current distribution is the same, i.e. it is simply scaled with

respect to the wavelength. The same theory applies to loops, slots, and microstrip antennas also.

1.1 Reconfiguration methods

The change in the effective length of resonant antennas can be created by different reconfiguration methods. The following methods are just some of the many mechanisms which can be used to change the effective length of resonant antennas.

1.1.1 Switches

Different kinds of switching technologies can be used for changing the operating frequency of the antenna. They operate by adding or removing parts of the effective length of the antenna.

1.1.1.1 Diodes

Diodes in reconfigurable antennas have gained in popularity. They are less expensive and require low biasing voltages too. The most common diode switch is based on the PIN diode. Diodes may be placed in series, shunt or shunt-series combinations. The series design favours low insertion loss over a wide frequency range whereas the shunt design provides high isolation. Therefore, a series-shunt configuration of PIN diodes offers a compromise of good isolation and low insertion loss over a broad frequency

range [2]. On the other hand, it is hard to integrate several diodes close to each other and each diode requires a number of passive components around it for biasing and DC isolation. Therefore, it is evident that PIN diode switches occupy a substantial amount of space on the microwave circuits [3].

By the control voltage in PIN diode switches, the stored charge in the intrinsic region is discharged. For instance, Yang et al. [4] used the PIN diode for connecting separate parts of a patch antenna. In this case, a slot is etched in a standard rectangular patch. PIN diodes should be placed at high RF current locations to maximize the obtained frequency shift. Therefore, a switched PIN diode positioned in the center of the slot changes the current paths on the patch more effectively. When the diode switch is open, currents travel around the slot and the antenna operates in a lower frequency. When it is closed, the effective length of the patch is shorter and the antenna operates in a higher frequency. The slot length controls the frequency ratio between the upper and lower operating frequencies. As long as the slot length is not too long, the radiation pattern of the original antenna is largely preserved [1].

1.1.1.2 FETs

The advantages of the field effect transistors (FETs) are simplicity of circuit design using three-terminal devices, high gain, good dynamic range, wide bandwidth, low noise, and easy implementation in monolithic circuits [5]. The switching power of the

FET is very low and because the device has three terminals, isolation between the DC

biasing circuit and the RF path is possible [6]. For example, Kawasaki and Itoh [7]

presented a one wavelength tuneable slot antenna loaded with two one-port reactive FET

components. By changing the bias voltage, the reactances of the FETs were varied,

which in turn changed the effective length of the slot and its operating frequency. The

resonant frequency of the slot shifted over a range of 1 GHz around the center frequency

of 10 GHz (10% tuning range) with negligible changes in the radiation pattern. So

although the radiation pattern properties were preserved in all resonant frequencies, the

tuning range of the resulting antenna was very limited.

1.1.1.3 RF-MEMs

PIN diode or FET switches are not suitable to reduce the radiation efficiency of the

antennas. Furthermore, these devices also exhibit nonlinearities that contribute to

harmonic and intermodulation distortions in the upper GHz range [8]. Switches based on

Radio-frequency and Microwave Microelectromechanical Systems (RF MEMs)

minimize these undesired effects. The monolithic fabrication of RF MEMs with

antennas can reduce parasitic effects, losses and costs. More recently, a microstrip patch

antenna using integrated RF-MEMS capacitors has been proposed [1]. For instance, in

[9], a reconfigurable dual-frequency rectangular slot antenna integrated with MEMS

cantilever type capacitors to tune the operating frequencies is described. The structure

has a dual-frequency behaviour in which both of the resonant frequencies can be

adjusted. By the actuation of MEMS, the lower resonant frequency shifts by 390 MHz, whereas the higher resonant frequency has a shift of 880 MHz without any distortion on the radiation pattern. In this case, approximately 1GHz tuneability for the desired frequencies was achieved. MEMs can have very small losses at RF and microwave frequencies and can handle higher power levels. However, they have some disadvantages including low tuneability, slow switching speed, and high bias voltage (50-100 V) however in more recent design this voltage has been reduced considerably. They require sealed packaging, which is expensive and hard to integrate with other circuits.

1.1.2 Material alterations

This reconfiguration method is making use of controlled alterations in the dielectric or magnetic properties of materials such as ferroelectrics, ferrites and liquid crystals. Reconfigurable antennas based on material alterations usually experience more losses because of the presence of current leakage through control lines or undesired radiation by the circuitry used to enable the antenna's reconfiguration [1].

Generally, the relative permittivity of a ferroelectric or liquid crystal materials can be changed by applying a static electric field, and the relative permeability of a ferrite can be changed by applying a static magnetic field. These alterations in relative permittivity

or permeability are the reasons for the change of the effective electrical length of the antennas, which causes a shift in the operating frequency.

1.1.2.1 Ferrite and Ferroelectric

Ferrites and ferroelectrics can handle large power levels and have faster switching times (few μs to tens of μs) than MEMS. However, the associated circuits may have a large size and mass. They can be used in bulk form, so that planar circuits like coplanar waveguide and microstrip lines can be directly fabricated on them.

As an example, the frequency-tuned performance of a ferrite-based microstrip patch antenna is presented in [10]. A 40% continuous tuning range was achieved by varying the DC magnetic bias field applied to the ferrite. The dimensions of the patch are reduced because of the high dielectric constant of the ferrite substrate. However, the efficiency of the antenna is poor because of losses in the substrate. The external magnet used to apply bias makes it bulky. Finally, factors such as the non-uniform bias fields and the multiple modal field distributions excited in a bulk ferrite substrate may prevent its practical applications [1].

As mentioned, there have been various attempts to make reconfiguration. PIN diodes, MEMS and ferrites have great potential; they also create a series of disadvantages: Semiconductor diodes are limited in use to the lower GHz range (up to about 15-20 GHz) due to their high parasitic and losses. MEMS switches have excellent properties in

the higher GHz region, but the devices with this technology need a large number of MEMS switches, each one with its own bias line, to minimize phase errors and produce reliability and high complexity [11]. On the other hand, due to deteriorating electromagnetic properties at high frequency, high fabrication cost, high power consumption, bulkiness and probable high insertion loss, ferrite-based devices operate efficiently below 30 GHz and have adaptation problems for a satisfying operation above 30 GHz, and are particularly difficult above 100 GHz [12].

1.1.2.2 Liquid crystal

Liquid crystal is a polar nonlinear dielectric material. Its dielectric polarization can be changed by applying an electric field. Due to their light weight, low cost, compact size, and negligible power consumption, tuneable devices based on liquid crystal are receiving an increased attention, in particular in view of their use in reconfigurable circuits and antennas. In a general discussion about the disadvantages of other tuneable devices, as mentioned above, LC materials are superior in terms of cost, integration and ease of fabrication when compared with diode, MEMs or ferrites.

There are several distinct kinds of liquid crystalline phases reported. However, the common characteristic of these phases is that they are stable in a temperature range which is between the temperature ranges where the isotropic liquid and the solid phase are established. The simplest liquid crystal phase is called the nematic phase. It has the

lowest ordering of all the mesophases (the phases of the liquid crystalline compound between the crystalline and the isotropic liquid phase) and precedes the transition to the isotropic liquid, which occurs at the clearing point. When the temperature is increased above the clearing point, the liquid crystal behaves as a simple liquid and it will be as clear as water. The properties of liquid crystal will be described in more details in Chapter 2. Molecules in a nematic phase tend to become ordered along parallel axes.

Various tuneable microwave components with liquid crystals have been proposed, for example, liquid crystal phase shifter [12] [14], tuneable capacitor [21], tuneable filter [22] [23], variable delay-line [15], reflectarray antenna [16] [17] [19] [20], etc. most of them use open transmission line or patch structure. Recent studies have shown that an electronically reconfigurable reflectarray antenna can be created by placing the printed patch elements above a metal backed cavity which is filled with nematic LC [13] [19]. In LC reflectarray antenna, the phase of the reflected signal from the individual patch elements is adjusted by applying a bias voltage to control the orientation of the LC molecules and then by phase adjustment, a focused beam is generated. For example, in [13], the feasibility of using the anisotropic properties of liquid crystal to control the reflection phase of a reflectarray patch antenna in X-band has been demonstrated. A layer of liquid crystal was introduced in the region between the resonant patch array and a conducting ground plane. The geometry of liquid crystal cells is shown in Figure 1.1 [13]. All the units are in millimetre. The liquid crystal molecules are parallel to the

substrate surfaces. By applying an external electric field, the molecules become aligned and are nearly perpendicular to the substrate surface. This molecular orientation of liquid crystal molecules in two states, parallel and perpendicular (or with and without the applied bias voltage), causes changes in the permittivity and hence the electrical size of the individual patches can be changed. Small changes in the electrical size of the patch results in large changes in the phase of the reflected signal at frequencies close to resonance. The difference phases of the reflected signal at resonance between the parallel and perpendicular states can be named dynamic phase range that is close to the 150° for this structure. In Chapter 3, finite element simulations of the structures depicted in this paper will be presented.
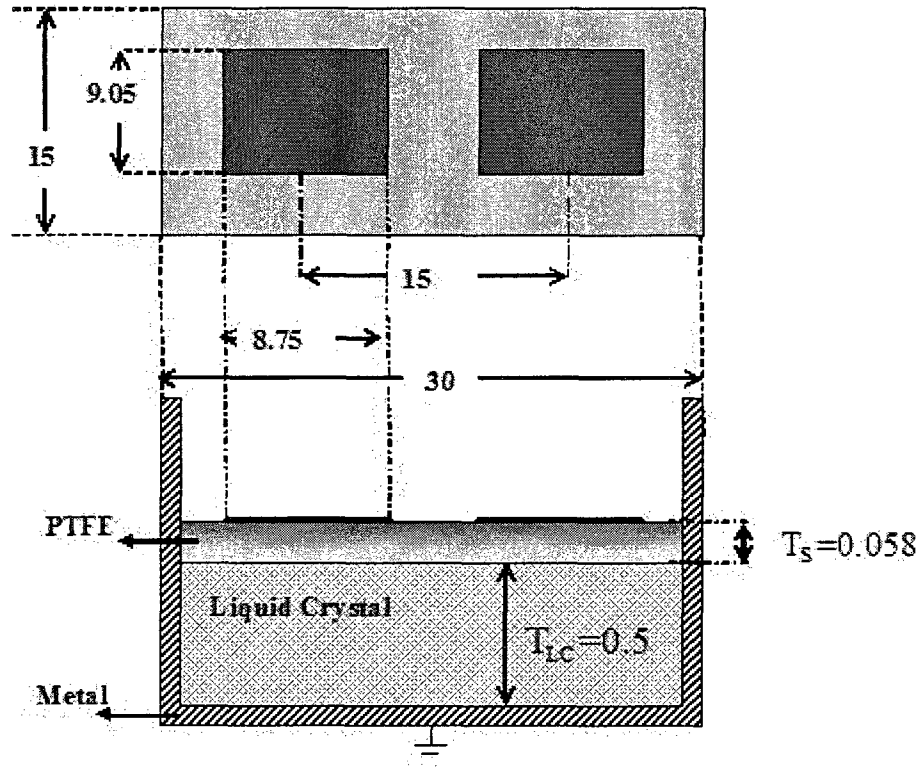
Figure 1.1 Schematic of the two unit cells. All the units are in millimetre.

1.2 Thesis structure and overview

The aim of this thesis is to study the potential of using tuneable resonators in X band using liquid crystal as a dielectric in a reflectarray element. Due to the bias-dependent permittivity of the anisotropic nematic liquid crystal embedded in the resonator's multilayer substrate, a differential phase shift in the reflection coefficient is predicted. Three liquid crystal namely K15, BL006 and MDA-05-893 from Merck KGaA will be tested. This study includes two parts: theory and experiments. In the theoretical part,

design, simulation and optimization of various microstrip resonators are done by finite element modeling (Ansoft-HFSS®). In this study, we will consider a new tuneable resonator consisting of a printed folded hairpin. The hairpin shape was adopted in order to provide compactness and low radiation losses. In fact, the odd symmetry of the current distribution on both sides of the hairpin leads to the cancellation of the radiated fields [18]. Therefore the most significant loss contribution comes from dissipation in conductors and dielectrics.

In the experimental part, the best suited resonator design is fabricated. The structure of the resonator includes multiple layers and the liquid crystal is injected in a closed-cavity. In order to increase tunability, the printed metallic resonator should be as close as possible, and possibly in direct contact, with the liquid crystal. To prevent any leakage and spills, RF and DC connection ports are kept away from the liquid crystal (LC) container. The reflection coefficients (S11) in parallel and perpendicular liquid crystal states are measured in the X band with a network analyzer.

Finally, experimental and predicted data are compared. Consistency between these results provides confidence that the employed design and fabrication are accurate.

The outline of this master's thesis is as follows: after the introduction of reconfigurable antenna concepts in Chapter 1, the basic concepts to understand liquid crystal as a polar dielectric material, such as the structure interaction, molecular orientations and physical

characteristics is described in Chapter 2. In addition, dielectric tunability, phase shift per mm and figure-of-merit of liquid crystals of the three different type of liquid crystal, used in the project are calculated.

To achieve the minimum loss and maximum phase shift in the reflection coefficient and hence the best possible reconfigurability performance, many kinds of microstrip resonators and filters are studied and are simulated in Chapter 3. The best-suited resonator design has been selected and fabricated. The direct comparison between properties obtained from simulation with those found from experimental measurements is made in Chapter 4.

Besides, an experimental setup used to observe the experiments is described. Chapter 5 predicts the behaviour of the hairpin resonator structure as a reflectarray. The last chapter, Chapter 6, includes the conclusion and suggests avenues for future work.

CHAPTER 2. LIQUID CRYSTALS

"Liquid crystals are a mesophase emerging between liquid and crystalline phases and have fluidity of liquid and anisotropy of crystal,"[25]. Mesophase is given from the Greek word mesos meaning middle and is referred to any of the phases of a liquid crystal which is intermediate between liquid and solid. In this thesis, we will be concerned with only the thermotropic liquid crystal. A liquid crystal is thermotropic if the order of its molecules is determined or changed by temperature.

The various thermotropic liquid crystal phases (smectic, nematic, cholesteric) have been discovered still now [26]. The common characteristic of these phases is that they are stable in a temperature range, which is between the temperature ranges where the isotropic liquid and the solid phase are stable. This is depicted in Figure 2.1. In this phase, the liquid crystal molecules are aligned parallel to each other but are able to rotate about their long axes. *"Liquid crystals of the nematic type are of by far the greatest importance technically speaking,"* [26]. On 1922 Friedel [27] assigned *"the name nematic from the Greek word nema, meaning thread, because of the thread-like discontinuities which can be observed under the polarizing microscope for this phase,"*.

The molecules making up the nematic phase are arranged in such a manner that there is no positional order for their mass centers, like in the isotropic liquid, but there is a long-

range orientational order. The molecules tend to orient on the average along a preferred direction within a large cluster of molecules, called the director $\vec{n}$.

Within a sufficiently large electric field, however, all the local directors will be either parallel or perpendicular to the magnetic field depending on the sign of the molecular magnetic susceptibility anisotropy of the molecules. This thesis examines only the nematic mesophase.

Cooling ← ——— **Heating** ————→

Crystal phase
Centers and
directions both
aligned

Nematic
(liquid crystal)phase
Centers random,
directions approximately
aligned

Isotropic
(liquid)phase
Centers and
directions both
random
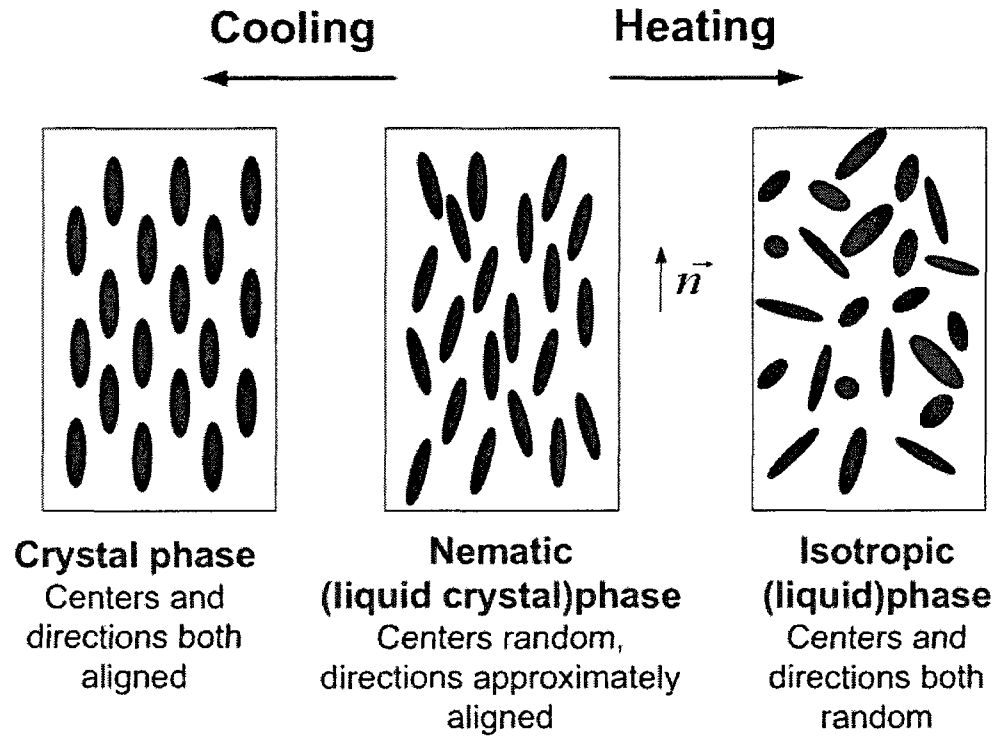
Figure 2.1 Molecular order dependence on temperature.

2.1 Resonant performance of liquid crystal

Liquid crystal, as a nonlinear dielectric, is a polar dielectric material whose internal dielectric polarizability can be changed by applying an external electric field. This is illustrated in Figure 2.2. Consider the case where the liquid crystal is contained between two solid metallic surfaces across which a voltage can be applied. Without electric field the liquid crystal molecules are parallel to the substrates and liquid crystal permittivity is $\varepsilon_\perp$. When an electric field E_0 is applied, the LC molecules rotate by 90°. In this case,

the axis of LC molecules become parallel to the direction of the applied E-field and the permittivity becomes $\varepsilon_{\parallel}$. For an intermediate value of electric field ($0 \leq E \leq E_0$), the permittivity varies continuously between $\varepsilon_{\perp}$ and $\varepsilon_{\parallel}$.

Due to this phenomenon, it becomes possible to control precisely the resonance frequency of a resonator with an applied DC voltage, or alternatively, to control the phase of the reflection response at the resonant frequency.

No applied field   Applied electric field
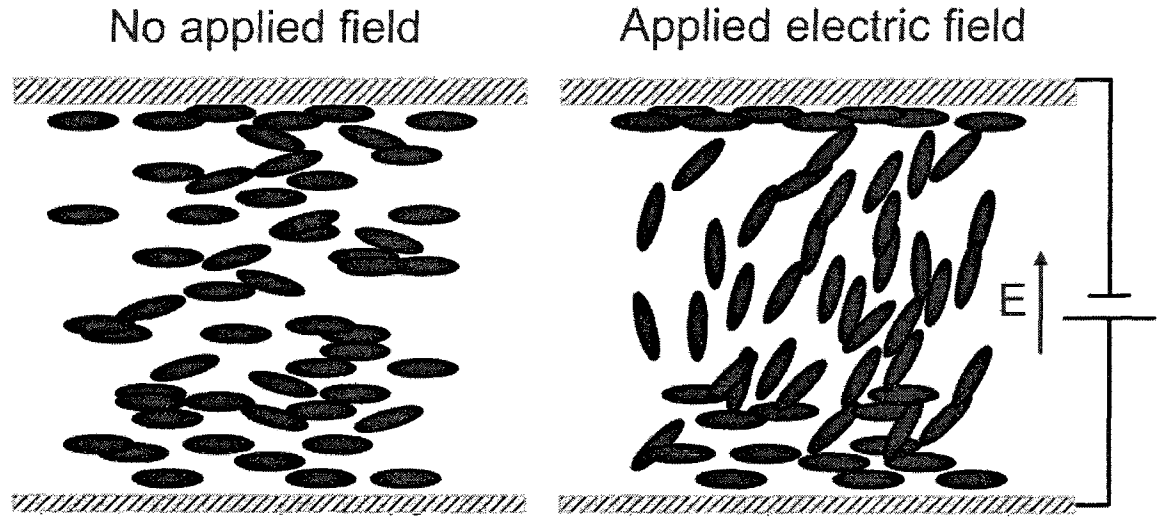
Figure 2.2 Polarizability of nematic liquid crystals.

The difference between the parallel and perpendicular dielectric constant defines the LC

dielectric anisotropy, i.e. $\Delta\varepsilon=\varepsilon_{\parallel}-\varepsilon_{\perp}$. The phase variation achieved in a tuneable

resonator is strongly related to $\Delta\varepsilon$.

The tuning range and the resonance bandwidth are related to the intrinsic dielectric

tuneability τ, the phase shift per unit length $\Delta\Phi'$ and figure-of-merit (FoM) defined in

[28]. $\Delta\Phi'$ corresponds to the achievable phase variation for a plane wave travelling over

1mm of LC, whereas FoM is the ratio of the achievable phase variation over the wave

attenuation due to the losses in the LC.

$$\tau = \frac{\varepsilon_{\parallel} - \varepsilon_{\perp}}{\varepsilon_{\parallel}} \qquad (2.1)$$

$$\Delta\Phi' = \frac{360^{\circ}.f}{1000c_0} \cdot \left(\sqrt{\varepsilon_{\parallel}} - \sqrt{\varepsilon_{\perp}}\right) \quad \left[\frac{\deg}{mm}\right] \qquad (2.2)$$

Where c_0 (speed of light) is 3×10^8 m/sec.

$$FoM = \frac{360^{\circ}}{8.686.\pi} \frac{\sqrt{\varepsilon_{\parallel}} - \sqrt{\varepsilon_{\perp}}}{\sqrt{\varepsilon_{\perp}}.\tan\delta_{\perp}} \quad \left[\frac{\deg}{dB}\right] \qquad (2.3)$$

2.2 Liquid crystal materials

With a single liquid crystal it is not possible to control all optimization aspects such as temperature range, viscosity, tuning voltage and dielectric anisotropy. Only a mixture of liquid crystal that may include up to twenty (20) types of liquid crystal can meet all the desired specifications [28]. For this study, three different nematic liquid crystal mixtures with various properties, namely BL006 [16], K15 [28], [24] and MDA-05-893[17] from Merck KGaA have been used. Their technical data and safety sheets are included in Appendix A.

The melting and clearing point temperatures are used to describe the properties of liquid crystals. At the melting point, the material transforms between a solid phase and a liquid crystal (LC) phase. At a temperature below the melting point, the liquid crystal will be in the solid state. At a temperature above the clearing point, it will enter the isotropic liquid state. Normally liquid crystal is milky white below its clearing point but is as clear as water above its clearing point. These temperature points are given in appendix A. Comparison between LCs shows that their melting points are below 23°C and K15 has the lowest clearing point (35°C). Therefore, in room temperature (26°C) all of them will be in the liquid crystal state. MDA-05-893, due to its large temperature range (20°C-110°C) is the most suitable LC for operation at room temperature.

The characteristics of the LCs at room temperature in both perpendicular and parallel modes [16] [17] [24] [28] are summarized in Table 2-1. The values of $\varepsilon_{\parallel}$ and $\tan\delta_{\parallel}$ correspond to the case where a bias voltage is applied to LCs. The table shows that the dielectric anisotropy of BL006 at 10 GHz is greater than that of K15. Unfortunately, the dielectric properties of MDA-05-893 at 10GHz are not available in the literature.

Table 2-1 Dielectric properties of liquid crystals

LC	f (GHz)	$\varepsilon_\perp$	$\tan \delta_\perp$	$\varepsilon_\parallel$	$\tan \delta_\parallel$
BL006	10	2.51	0.032	2.7	0.026
K15	10	2.6	0.025	2.77	0.043
MDA-05-893	35	2.3	0.025	2.65	0.01

By using Table 2-1 and formulas (2.1)-(2.3) dielectric tuneability, phase shift per mm and figure-of-merit of liquid crystals can be calculated. The results are given in Table 2-2.

MDA-05-893 used at 35 GHz has a higher tuneability percentage and figure of merit. However, we should consider that LCs have high losses in the lower frequency range, so its FoM could be smaller at 10GHz.

Table 2-2 Dielectric tuneability, phase shift and figure-of-merit

LC	f (GHz)	$\tau\left[\%\right]$	$_{\Delta}\Phi'\left[\dfrac{\deg}{mm}\right]$	$FoM\left[\dfrac{\deg}{dB}\right]$
BL006	10	7.04	2.47	15.32
K15	10	6.14	0.62	16.97
MDA-05-893	35	13.21	4.67	38.73

CHAPTER 3. FULL WAVE ANALYSIS

In this chapter, four different types of designs: rectangular patch resonator, microstrip delay line, half wave resonator and hairpin resonator are presented along with the relative strengths and weaknesses. Simulations were done with commercial finite-element and method-of-moments simulation tools, namely Ansoft – HFSS® and Ansoft – Designer®. All the designs were done for the operation frequency around 10 GHz.

3.1 Patch antenna

This structure was presented by Hu et al. [24]. The reason for the re-simulation of their structure is to assess the feasibility of using the anisotropic properties of the LC to control the reflection phase of a reflectarray unit cell. The permittivity of the LC substrate and hence the electrical size of the individual patches can be controlled by varying the applied DC bias.

Figure 3.1 shows the dimensions of two unit cells. All the dimensions are in millimetre. The patches are separated from the ground plane by a 58.42 μm thick dielectric layer with $\varepsilon_r = 2.9$, $\tan\delta = 0.0028$, and a 500.38 μm thick K15 liquid crystal. The patches were printed on 42×27 mm PTFE material. They show a predicted shift in the resonant frequency from 9.44 GHz to 9.18 GHz for permittivity values corresponding to the

parallel and perpendicular orientation of the LC molecules. At the centre design frequency of 9.30 GHz, the phase of the individual reflectarray cells can be continuously varied over a range of 183°. The reflection loss is predicted to vary from -13 to -18dB.
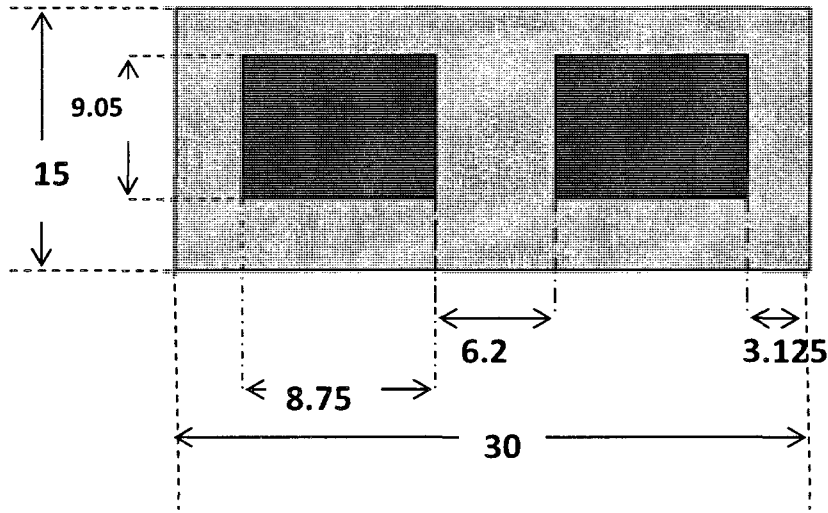
Figure 3.1 Top view of patch reflectarray cell geometry (Hu et al. [24],

©Electronics Letter 2006) ; (LC:K15). All the dimensions are in millimetre.

In our simulations, phase characterization is carried out by using the waveguide simulator approach, which eliminates the need for larger arrays for the element design. The virtual waveguide simulator is created using Agilent HFSS. The results are similar to those obtain in [24].The results depicted in Figure 3.2(a) shows that the return loss vary in the range of 15-19 dB. Figure 3.2(b) and (c) show that the maximum voltage

controlled phase range is 210° at 9.4 GHz. The purpose of this simulation is to quantify

the voltage effect on the LC molecules.
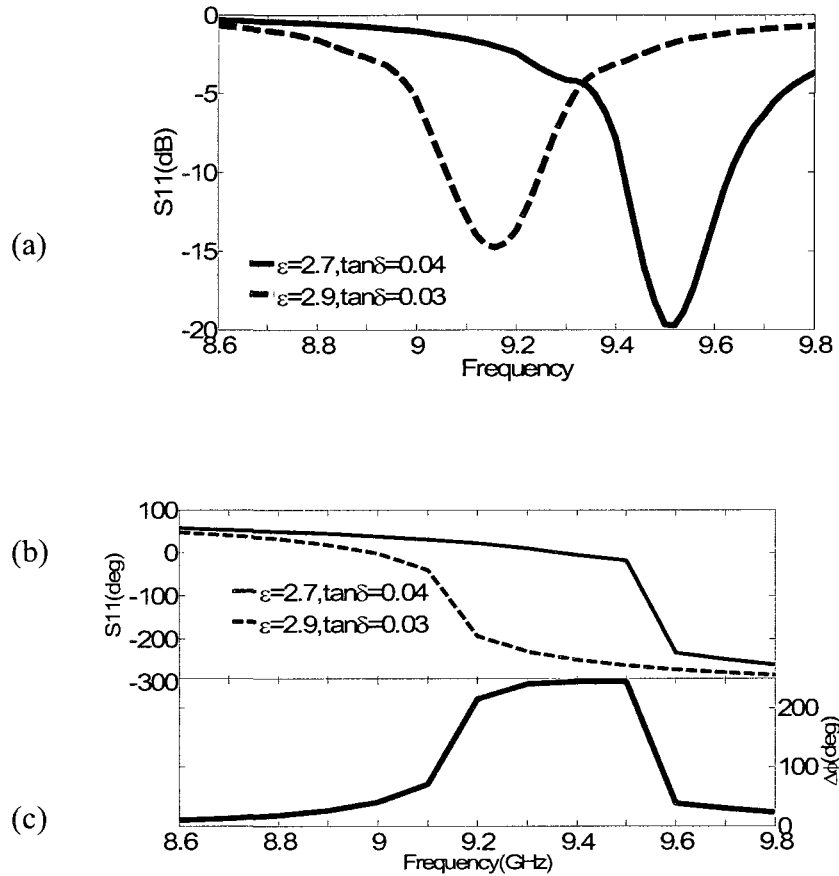
Figure 3.2 Patch structure simulation. (a) Return Loss; (b) Reflection phase; (c) Bias-induced phase difference, (LC:K15).

3.2 Microstrip variable delay line

The liquid crystal voltage-variable delay line is designed with two cases of the phase

difference; one with a bias voltage applied to the LC layer and the other without bias

[15]. By applying a bias voltage between microstrip conductor and ground metal, the permittivity and thereby the transmission characteristics of the microstrip line, including delay time can be controlled. In this section, we want to simulate its implementation in microstrip implementation using Ansoft – HFSS®. The structure is shown in Figure 3.3. The liquid crystal layer has a thickness of 0.254 mm and serves as the substrate of the microstrip line. A strip conductor is plated on an alumina ($\varepsilon_r = 9.9$ and $\tan\delta = 0.0001$) with thickness of 0.254 mm. The width of microstrip line W is 406.4 μm and the characteristic impedance is approximately 50Ω. Dimension K is 11.684 mm and structure is simulated for two different values of length of microstrip line L, 11.684 mm and 17.78 mm respectively.

(a)   (b)
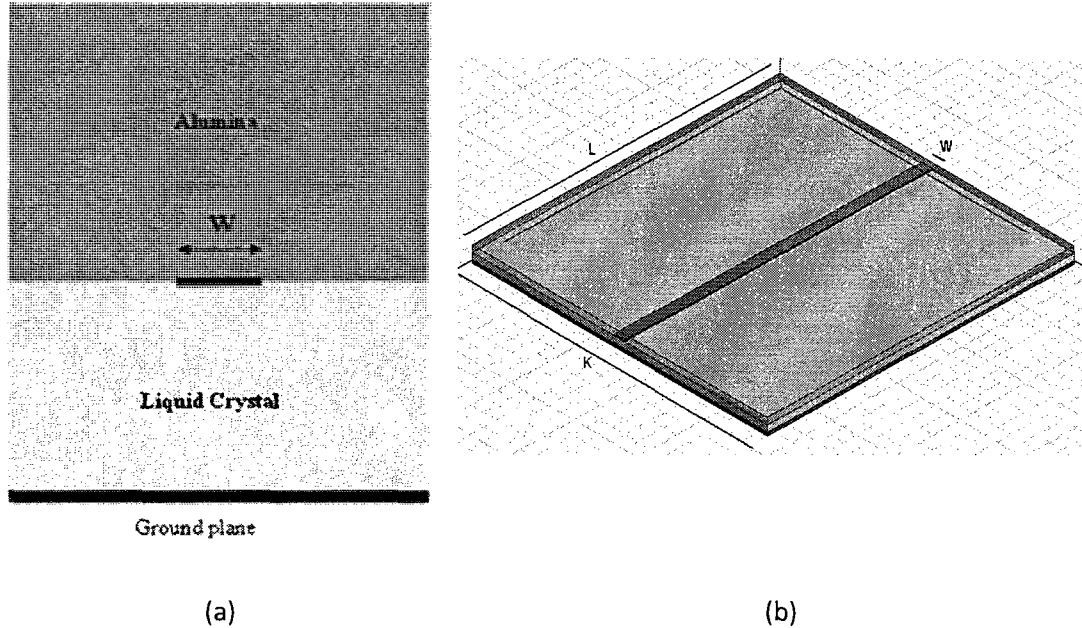
Figure 3.3 Geometry of microstrip line cell (a) side view (b) 3D view.

Simulations were done with the parallel and perpendicular dielectric properties of the LC. Table 3-1 shows that the material-induced phase changes are small and increase by only 3 degrees when the length of microstrip is increased from 11.684 mm to 17.78 mml. This is a direct consequence of the small variation of permittivity (only few percents), which is an intrinsic limitation of the material. If we want to make a delay line, it is not likely to be acceptable because the device will become very long and not suitable for practical applications.

Table 3-1 Differential phase at 10 GHz for two different lengths of microstrip; (LC:K15)

Length of Microstrip	$\angle S21_{10GHz}$		$\Delta \angle S21 = \angle S21_{\parallel} - \angle S21_{\perp}$
	$K15_{\perp}$	$K15_{\parallel}$	
11.684 mm	91.10(deg)	85.08(deg)	6.02(deg)
17.78 mm	-48.09(deg)	-57.01(deg)	8.92(deg)

Table 3-2 gives a comparison between the phase changes for three types of liquid crystals at 10 GHz, for a 11.684 mmmicrostrip line length. For example, it can be seen that for K15, the phase change is 0.51 degrees per mm. So changing the phase by 360 degree would require a line of about 700 mm. This is clearly impractical. By comparing these results with those obtained with the patch resonator, it can be concluded that a possible practical benefit of LC in these conditions is maybe in a resonator.

Table 3-2 Differential phase at 10 GHz for three types of LC for microstrip delay line

Liquid Crystal	∠S21(deg)		$\Delta \angle S21 = \angle S21_{\parallel} - \angle S21_{\perp}$	Phase Change (deg/mm)
	Perpendicular	Parallel		
BL006	93.9	81.29	12.61	1.079
MDA-05-893	104.28	92.95	11.33	0.969
K15	91.10	85.08	6.02	0.51

3.3 Half-wave resonator

In the last section, it was concluded that the controllable phase shift in a LC based resonant device is greater. In this section, we are proposing a novel coupled open-circuit half-wave microstrip resonator, as illustrated in Figure 3.4. In order to increase the sensitivity of the resonance frequency with respect to the variation in permittivity of the LC, the resonator is put directly in contact with a tuneable material. As will be discussed in the next chapters, this leads to some practical difficulties in the fabrication, in order to have a sealed LC container in which a circuit has to be somehow coupled with a leak-free excitation mechanism. The coupling scheme proposed here to address this issue is

to use electromagnetic coupling from a simple feeding line printed on a different metal layer, so that it is not in contact with the LC. As shown in Figure 3.4 (a) and (b), L1 and Lv are the dimensions of the outer feeding line. L2 is the length of the half-wave resonator. L2 and the DC bias line are embedded between 0.508 mm liquid crystal and 0.127 mm alumina layers. BL006 is used as liquid crystal. The length L2 determines the resonance frequency of the structure. The distance between lines (S), L1, W1 and W2 are optimized for maximum phase change and minimum return loss (dB). The resonator section is connected to a narrow DC bias line. Since the structure is planar, Ansoft Designer, based on the method of moment technique was employed.

(a)

(b)
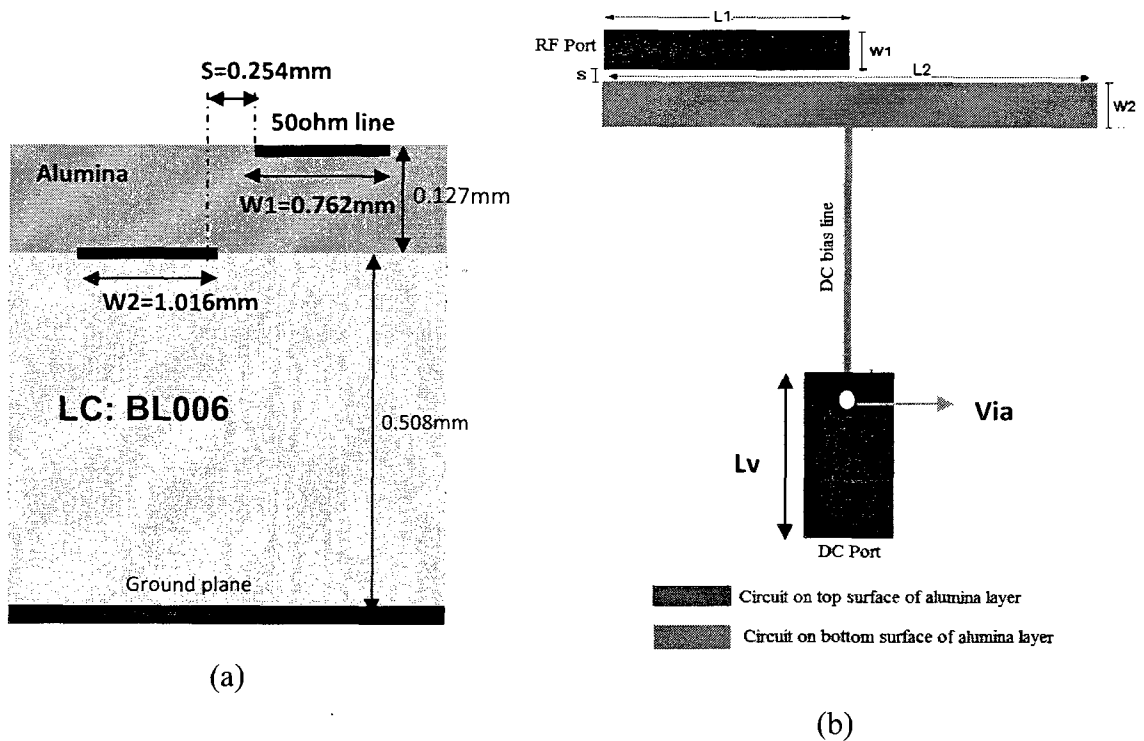
Figure 3.4 Geometry of half-wave resonator cell (a) side view; (b) top view.

The layout of the structure on both faces of the alumina layer is shown in Figure 3.5. All the dimensions are in millimetre.The length of the DC bias line is fixed at λg/4 for the design frequency so that it behaves as an open circuit for the RF signal. In addition, the width of the bias line is 0.127 mm. The DC bias pad is connected to the outer surface of alumina by a via. Because of the soldering of the DC connector, the outer DC bias pad is larger than the inner one.

(a)   (b)
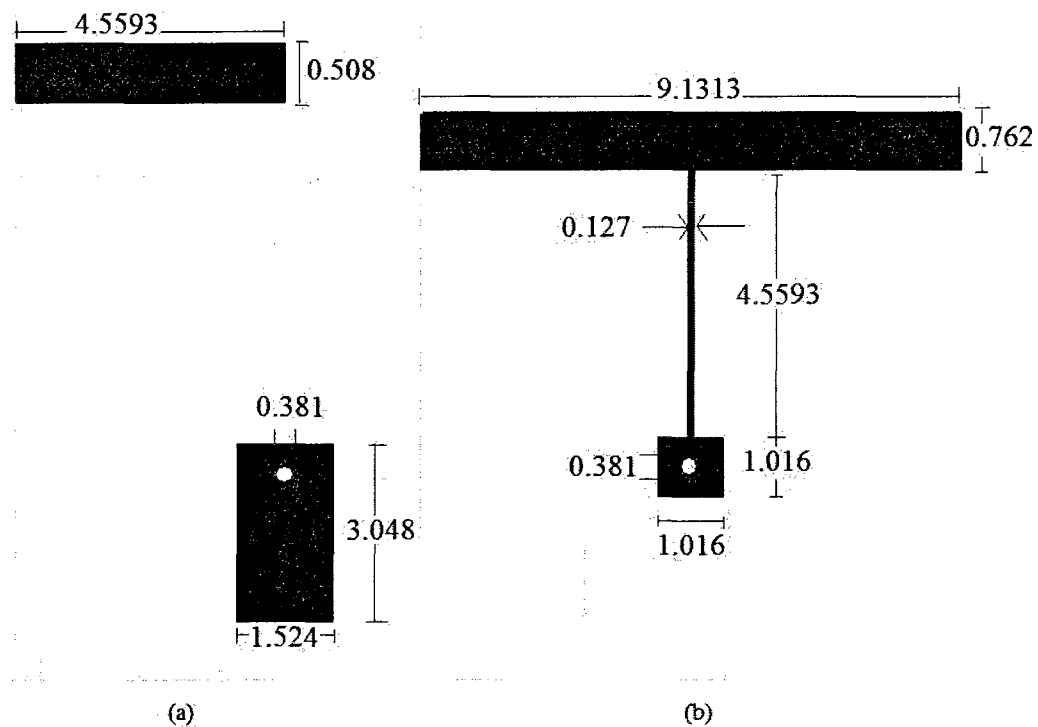
Figure 3.5 Microstrip dimensions of a half-wave resonator on the alumina layer. (a) Top surface; (b) Bottom surface. All the dimensions are in millimetre.

Figure 3.6 presents simulated results of the half-wavelength resonator. The maximum values of return loss are 14 and 17 dB in the parallel and perpendicular states

respectively. It is also shown that the predicted shift in the resonant frequency is from

9.25 to 9 GHz. Figures 3.6(b) and (c) show that the maximum voltage-controlled phase

range is 180.3 degrees, at a frequency of 9.144 GHz.
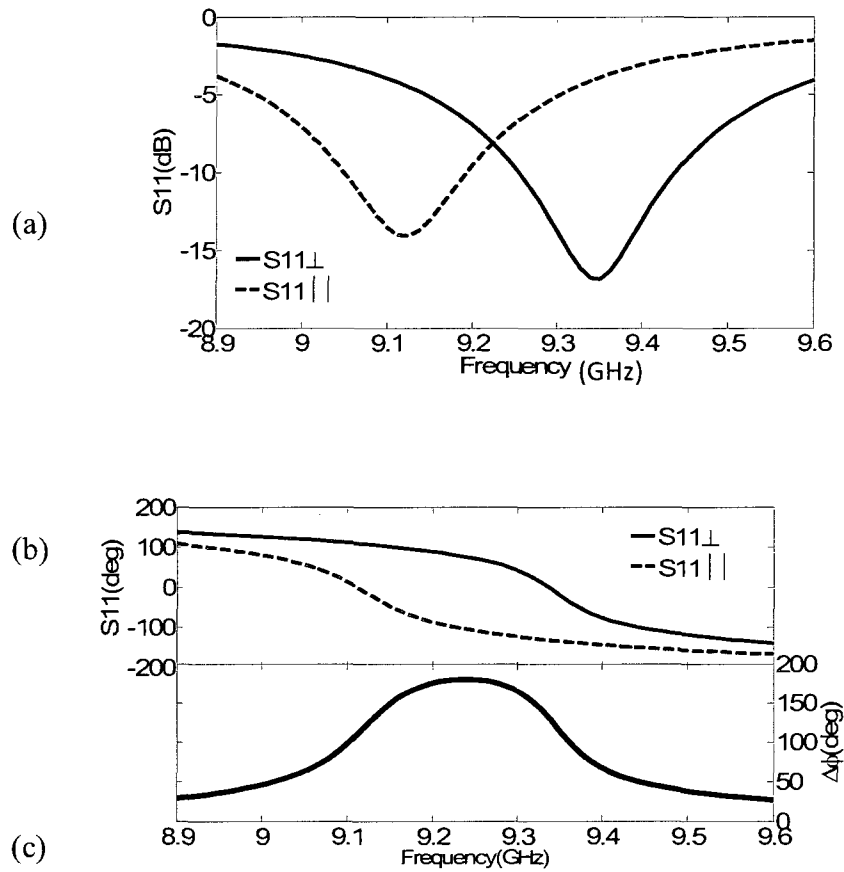
Figure 3.6 Half wave resonator simulation. (a) Return loss; (b)

Reflection phase; (c) Bias-induced phase difference, (LC:BL006).

The model was re-simulated by considering lossless dielectrics (i.e. $\tan \delta$ set to 0) and

metals taken as perfect electric conductors. All the layout dimensions were left

unchanged. This resulted in a decrease of the controlled phase range to 143 degrees. The

worst case S11, in perpendicular and parallel modes, increased to substantially to -2.8dB

and -2.9dB respectively. These remaining losses can only be due to radiation or surface

waves in the substrate.

While this form of resonator has the advantages of compactness and convenient

fabrication, the radiation represents a limitation on the Q factor and the expected surface

waves or radiation may enhance unwanted coupling between parts of a microwave

integrated circuit module. Therefore, a resonator which has the advantages of the half-

wavelength open-circuit type, but with much reduced radiation, is quite desirable. So,

another open-circuit half-wavelength resonant structure is considered next. This

resonator has a hairpin shape, which provides a high degree of cancellation of the

radiation fields, as the two parallel arms of the hairpin carry equal and opposed currents

[18].

3.4 Reduction of radiation losses

To prove the effect of decrease of radiation loss resulting from the hairpin shape, it is

interesting to compare its performance with those of the unfolded resonator. Figure 3.7

depicts a schematic of the two types of resonator in top and side views. Simulations are

done using Ansoft – Designer ®.

Unfolded coupled-line resonator   **Hairpin resonator**
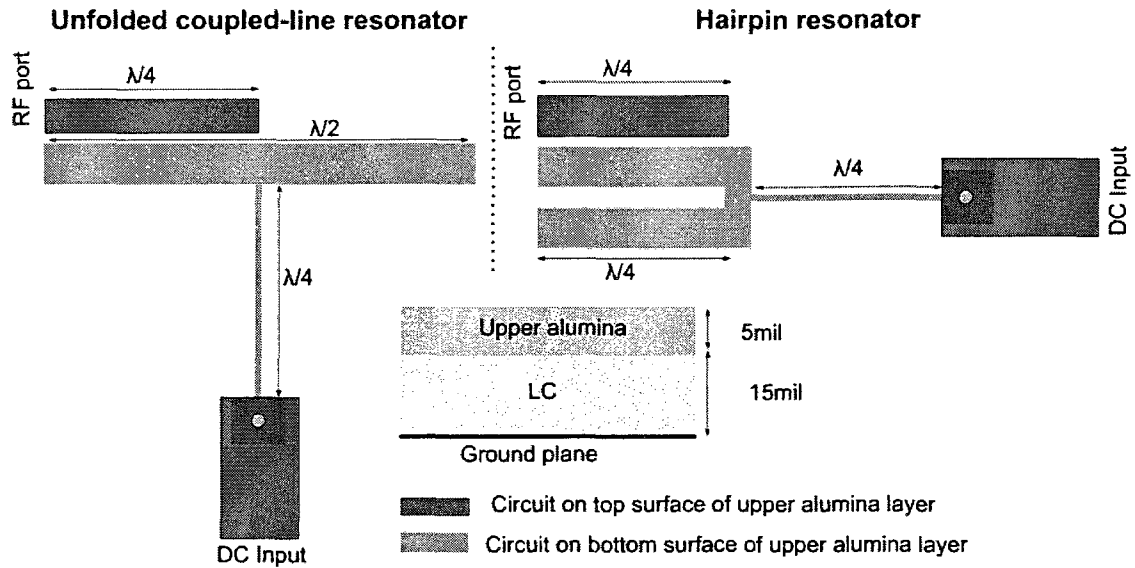
Figure 3.7 Top and side views of unfolded and folded coupled-line resonator structures.

Figure 3.8(a) shows that the simulated return loss in an unfolded half-wave coupled-line resonator as resonance changes is between 15dB and 18.5dB. These values decrease to 13dB and 15dB in the hairpin resonator, as shown in Figure3.8(b). Thus, folding the resonator to reduce radiation and surface wave losses led to an improvement of 2 to 3.5 dB.
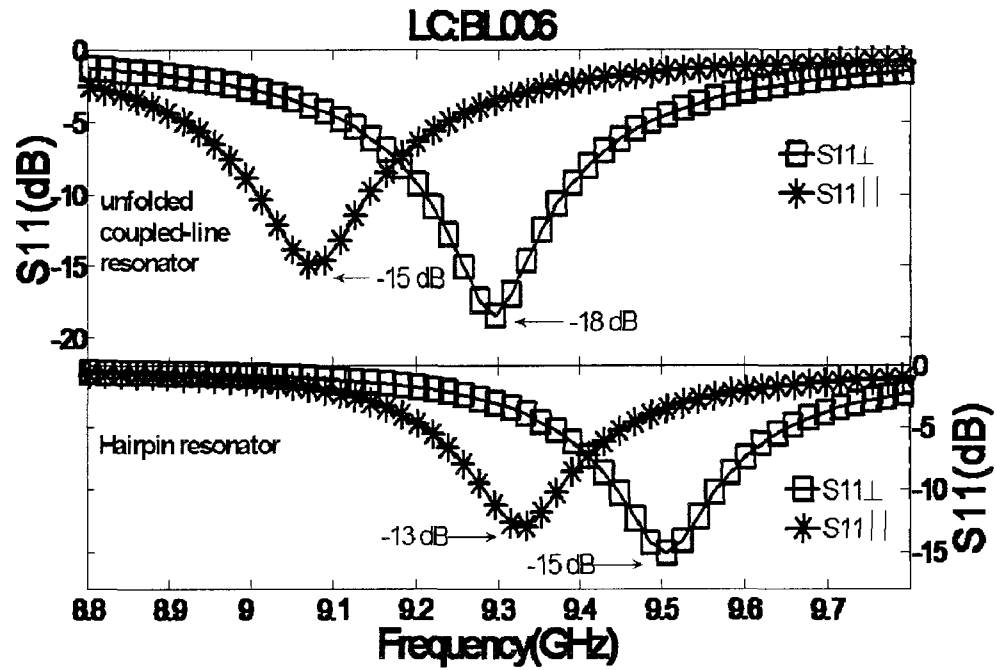
Figure 3.8 Simulated return loss (a) Half-wave coupled-line circuit; (b) Hairpin circuit.

On the other hand, by removing all losses in dielectrics and using perfect conductors in place of metal, losses in perpendicular and parallel modes are changed to 0.13dB and 0.135dB. These amounts are significantly less than those obtained with the unfolded resonator in similar conditions.

3.5 Hairpin resonator design

The adopted configuration is illustrated in Figure 3.9. The resonator and its DC bias line are settled on the bottom face of an alumina substrate (h_{Al}), which also has the RF input line and the DC biasing line and pad on its top surface. A via hole interconnects the top and bottom sections of the biasing line. A high-impedance narrow bias line (width of 101.6μm) was used to prevent RF leakage in the bias network. The RF feed line is above the alumina frame and is therefore less affected by the bias state of the LC. The thickness of LC (h_{LC}) is 381μm.
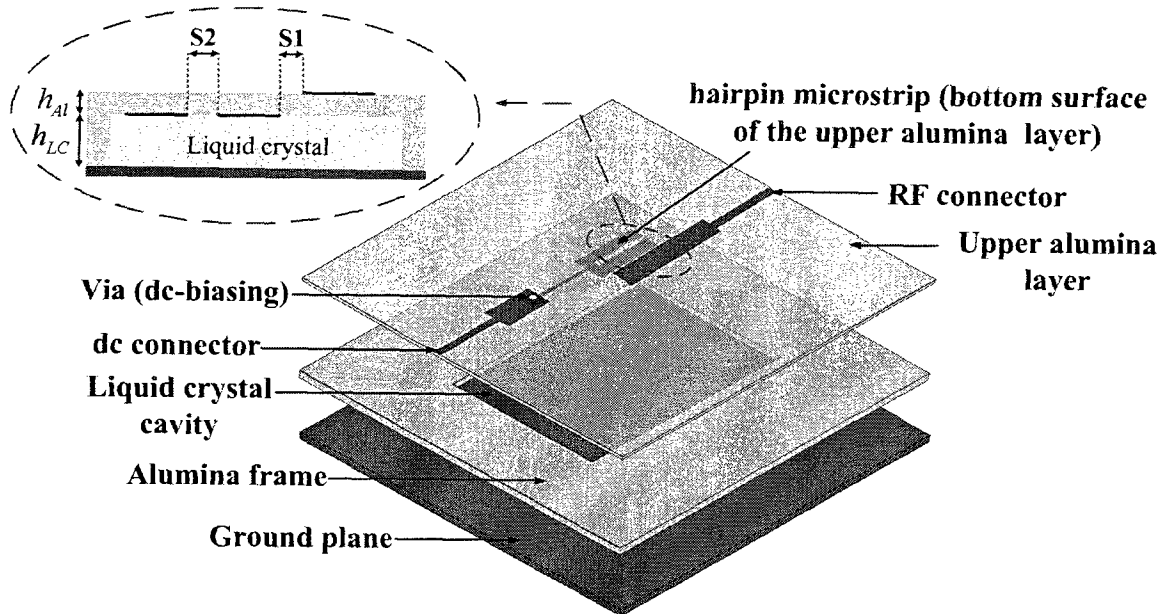
Figure 3.9 The structure of the hairpin resonator backed with a liquid crystal cavity.

In order to achieve the best possible performance, the following guidelines were followed in the design of the multilayer structure:

> To increase tuneability, the percentage of the resonator's RF energy storage in the liquid crystal (LC) volume is maximized. This is achieved by having the printed metallic hairpin directly in contact with the LC;

> To ensure that the characteristic impedance of the line feeding the resonator is not affected by the change of permittivity resulting from LC biasing, a good coupling between the resonator and the 50-ohm testing port should be maintained;

> To avoid having RF and DC connection ports in contact with the LC container to prevent leakage and spills.

The magnitude and phase variations of the reflection coefficient measured at the RF port depend critically on values of the coupling gaps S1 and S2. These parameters were optimized by simulation using Ansoft-HFSS®. Two different simulation were done for two different thicknesses of upper alumina layer (h_{Al}), i.e. 0.127 mm and 0.254 mm respectively.

3.5.1 Results for a 0.127-mm thick upper alumina layer

The coupling gaps S1 (0.254 mm) and S2 (0.381mm) for this thickness were optimized by simulation. The layouts of the structure on both faces of the upper alumina layer are shown in Figure 3.10. All the dimensions are in units of micrometer. We will now present the results obtained with the three types of liquid crystal previously used.

(a)

(b)
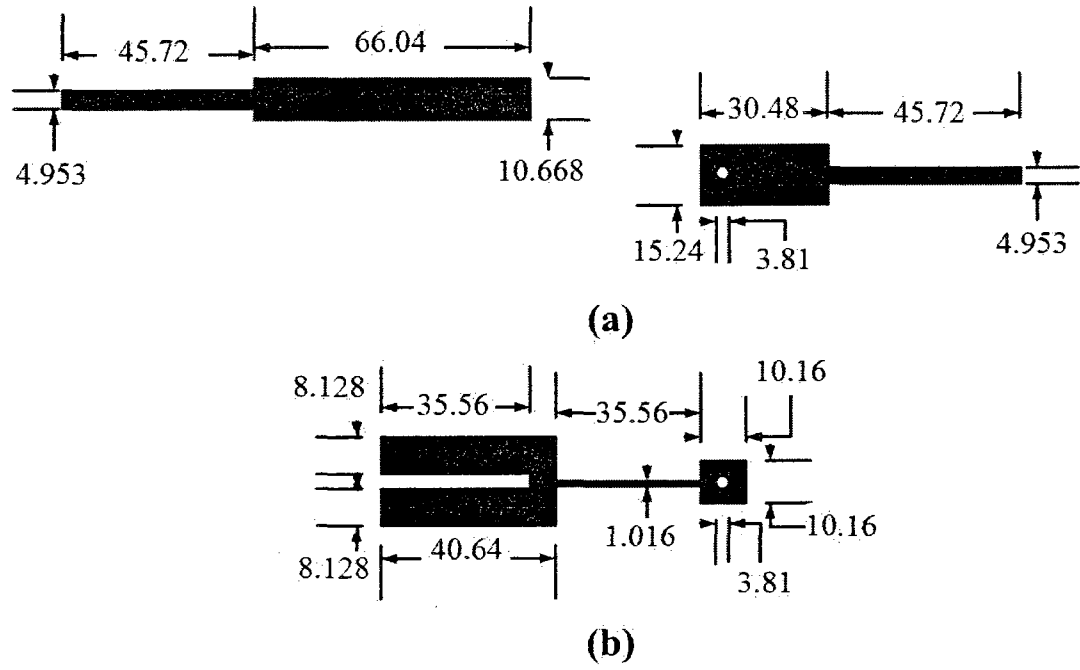
Figure 3.10 Dimensions of microstrip on the upper alumina layer (a) Top surface; (b)

Bottom surface; (h_{Al} =0.127 mm). All the dimensions are in units of micrometer.

3.5.1.1 K15

Figure 3.11 shows that the resonant frequency of a hairpin resonator structure filled by K15 decreases from 9.54 to 9.38GHz and gives a peak reflection phase variation of 174° at a frequency of 9.48GHz. The return loss at the resonance varies between 24.5 and 13dB.
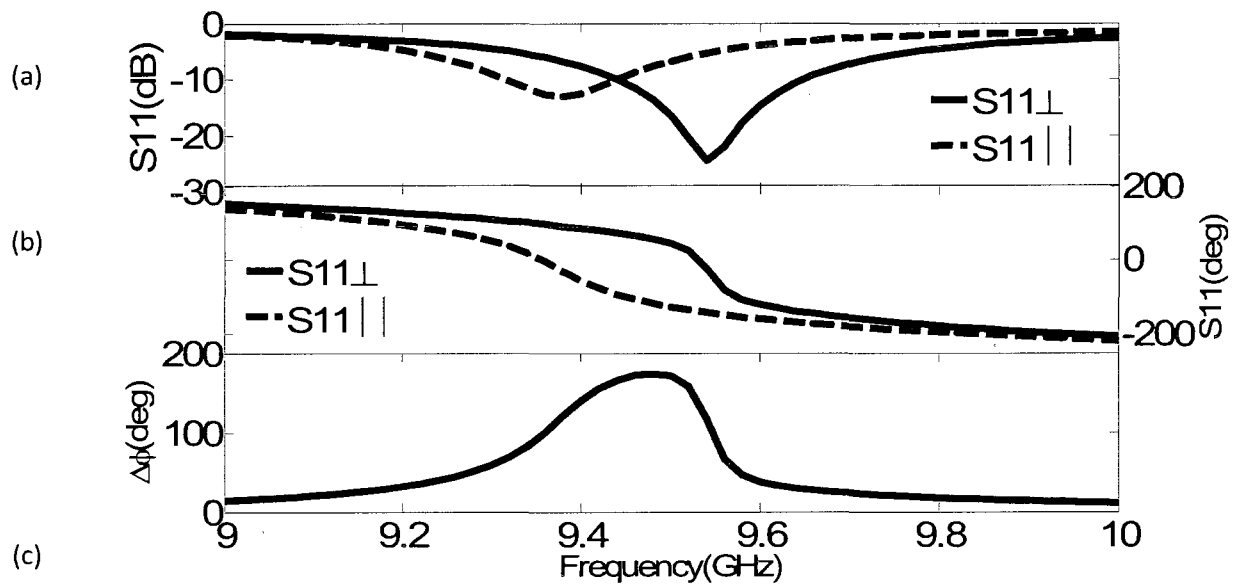
Figure 3.11 Hairpin simulation. (a) Return Loss; (b) Reflection phase; (c) Phase difference, LC: K15, h_{Al} =0.127 mm.

3.5.1.2 MDA-05-893

The calculated reflection phase plots of the hairpin resonator are shown in Figure 3.12. The resonant frequency is shown to shift from 9.85 to 9.42 GHz. The reflection losses are 10.5 and 6dB at the two resonances. The maximum dynamic phase range is 222.5 °at 9.65 GHz.
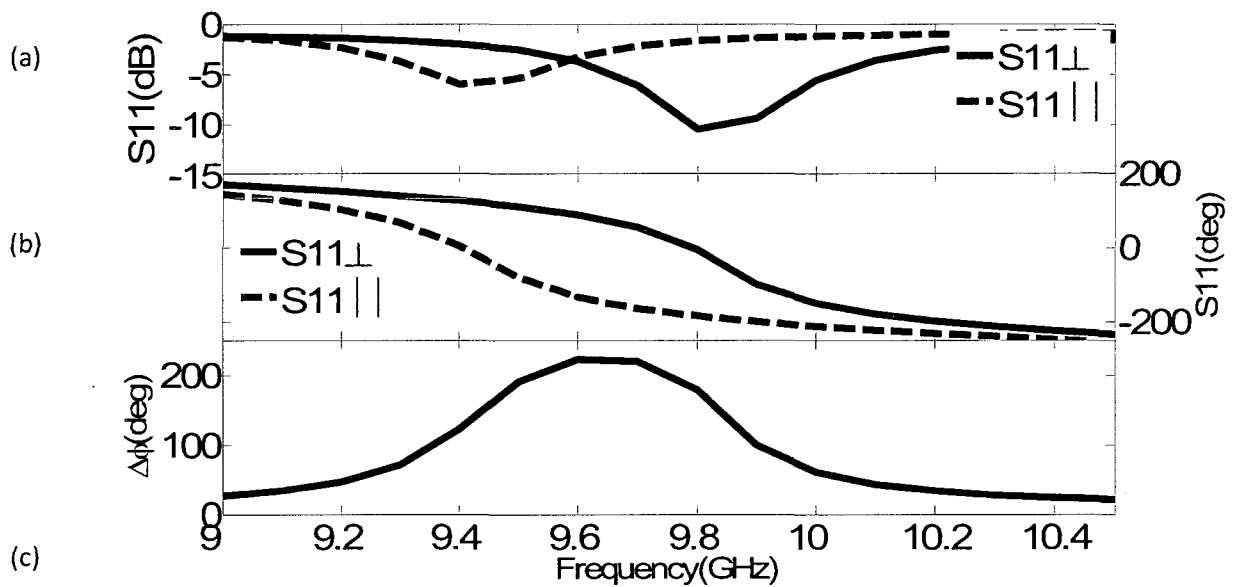
Figure 3.12 Hairpin simulation. (a) Return loss; (b) Reflection phase; (c) Phase difference, LC:MDA-05-893, h_{Al}=0.127 mm.

3.5.1.3 BL006

Figure 3.13 shows that the resonant frequency decreases from 9.6 to 9.4 GHz when the LC is biased. The maximum phase shift is 156.5° and it occurs close to 9.5 GHz. The maximum losses at resonance are 15 and 13dB.
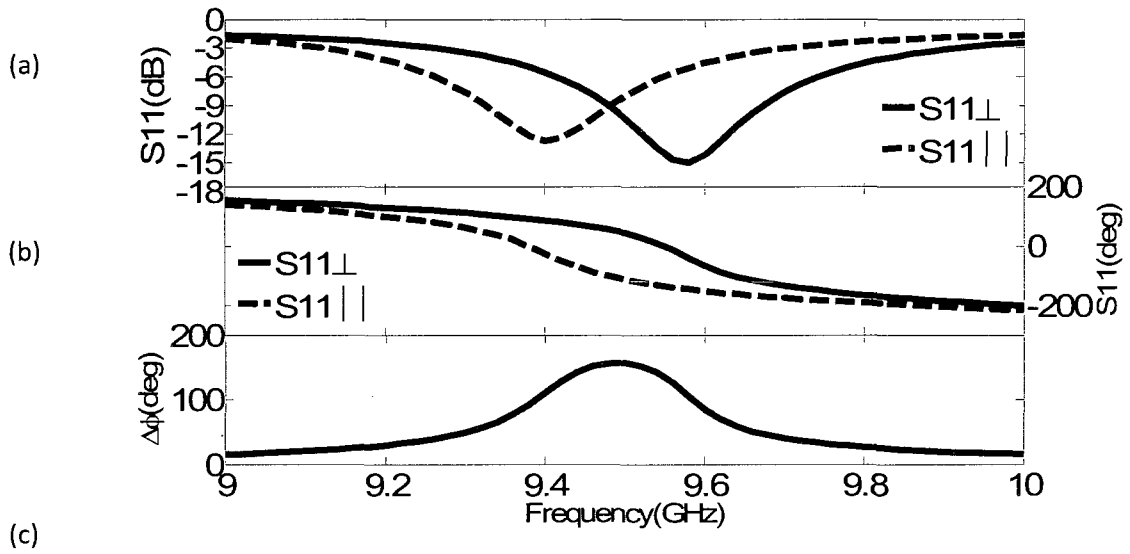
Figure 3.13 Hairpin simulations. (a) Return loss; (b) Reflection phase; (c) Phase difference, LC:MDA-05-893, h_{Al} =0.127 mm.

3.5.2 Results for a 0.254-mm thick upper alumina layer

The 0.127 mm thick substrate is quite fragile. So the thickness of upper alumina was changed from 0.127 mm to 0.254 mm. To achieve to same frequency as for the 0.127-mm case, S1, S2 and the dimensions of microstrips on both top and bottom surfaces of

upper alumina layer were changed. In the new structure S1and is S2 are 0.2921 mm and

0.3429 mm. The layouts of the new structure on both faces of the upper alumina layer

are shown in Figure 3.14. All the dimensions are in units of micrometer.

(a)

(b)
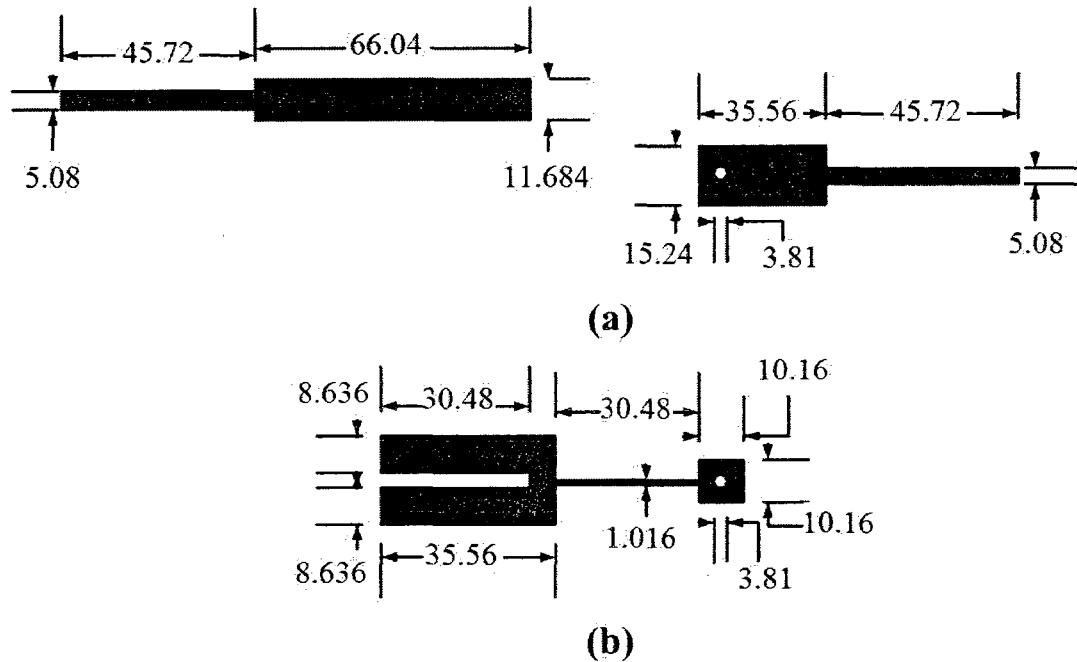
Figure 3.14 Dimensions of microstrips on the upper alumina layer. (a) Top surface; (b)

Bottom surface, (h_{Al} =0.254 mm). All the dimensions are in units of micrometer.

The results for each of the three considered liquid crystals are given in the following

sections.

3.5.2.1 K15

Figure 3.15 shows that when the permittivity changes from the parallel to perpendicular states, the maximum signal losses at resonance are 13 and 21dB respectively. The shift in resonance frequency occurs from 9.8 to 9.7 GHz and the maximum dynamic phase range is 154°.
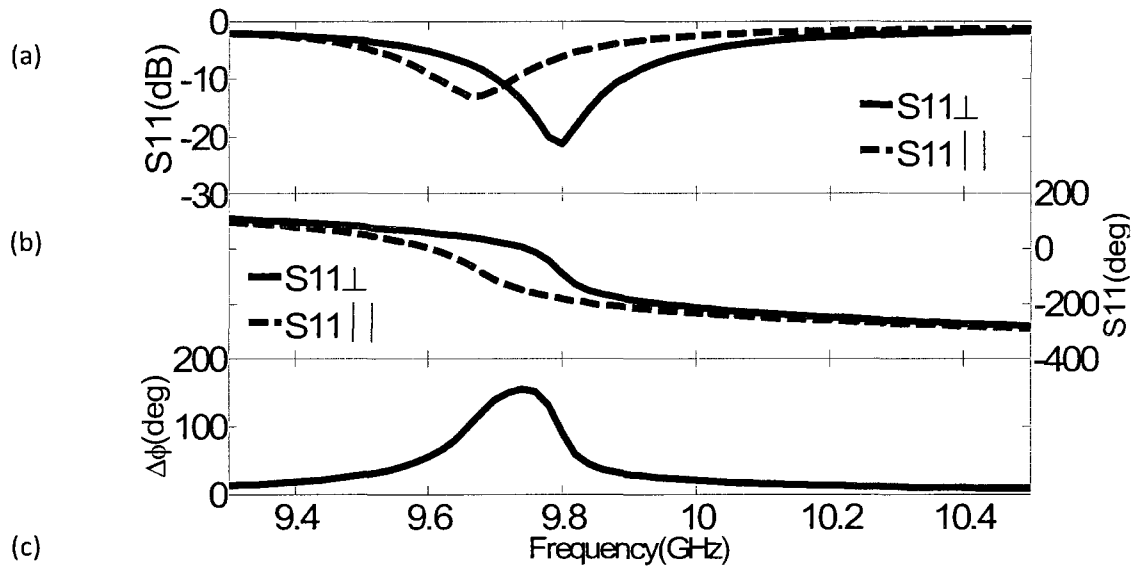
Figure 3.15 Hairpin simulation (a) Return loss; (b) Reflection phase; (c) Phase difference, LC:K15, h_{Al} =0.254 mm.

3.5.2.2 MDA-05-893

Figure 3.16 demonstrates the computed resonant frequency shifts from 10.05 to 9.75 GHz, while the return loss level varies from 11.5 to 7.5dB. The maximum phase shift (203°) takes place at 9.9 GHz.
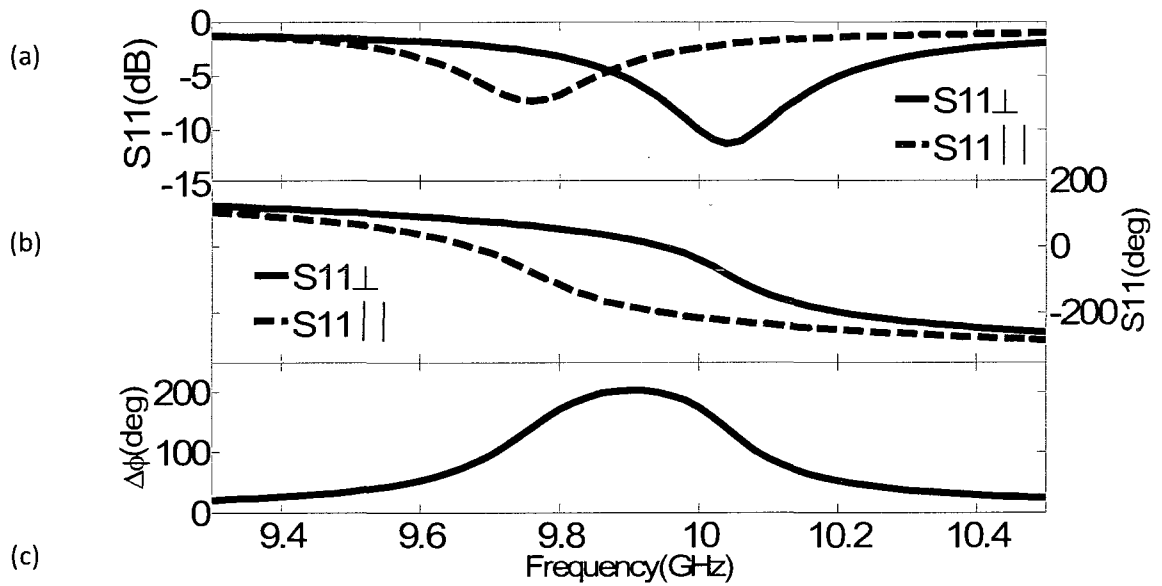
Figure 3.16 Hairpin simulation. (a) Return loss; (b) Reflection phase; (c) Phase difference, LC:MDA-05-893, h_{Al}=0.254 mm.

3.5.2.3 BL006

Figure 3.17 shows the simulated S-parameter of the hairpin resonator. It can be recognized that the maximum phase shift (147.6°) happens at 9.8 GHz. The return loss at resonance frequencies of 9.85 GHz and 9.73 GHz is varying from 14.6 to 13dB.
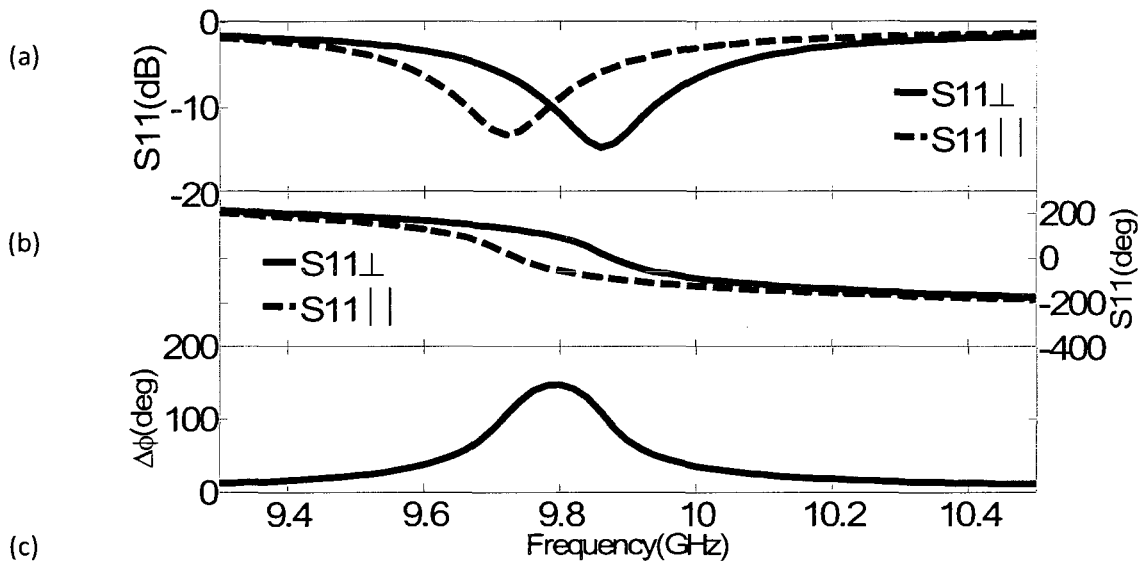
Figure 3.17 Hairpin simulation. (a) Return loss; (b) Reflection phase; (c) Phase difference, LC:BL006, h_{Al} =0.254 mm.

3.5.3 Comparison between structures

Phase range and reflection losses for the two values of the upper alumina layer thickness, using K15, MDA-05-893 and BL006, are summarized in Table 3-3. It can be seen that for the structure with 0.127-mm thickness, the maximum phase shift for each

LC is higher than that in the other structure. By changing the thickness of alumina layer, reflection losses are not changed so much. Due to its maximum phase shift and minimum losses, MDA-05-893 appears the most suitable of the three liquid crystals for tuneable circuit and antenna applications.

Table 3-3 Computed data for two hairpin structures

h_{Al} LC	0.127 mm			0.254 mm		
	$S_{\perp}(dB)$	$S_{\parallel}(dB)$	$\Delta\phi$(deg)	$S_{\perp}(dB)$	$S_{\parallel}(dB)$	$\Delta\phi$(deg)
K15	-24.5	-13	174.1	-21.3	-13	154.2
MDA-05-893	-10.5	-6	222.5	-11.4	-7.5	203.5
BL006	-15	-12.7	156.5	-14.63	-13.1	147.6

CHAPTER 4. EXPERIMENTAL VALIDATIONS

In the previous chapter, four basic designs (patch, microstrip, half-wave resonator and hairpin resonator) were analyzed using simulations. This chapter will only focus on the hairpin resonator design as it appeared to be the most promising in terms of losses and phase tuneability.

Prior to manufacturing the resonator structures, a simple parallel plate capacitor operating at low frequencies was built and tested in order to verify the tuneability of the LC materials in contact with the metal electrodes fabricated with the sputtering process available in our laboratory. In fact, some of the references consulted [11]-[19] indicated that a certain roughness of the contact on the biasing surfaces was required in order to favour the alignment of the LC polar molecules in the non-biased (perpendicular) state. For this purpose, theses papers recommend to cover the biasing metal electrodes with a thin layer of polyimide dielectric, whose roughness is obtained by rubbing with a simple cloth. This extra procedure is not done by all authors [20] [24] and therefore doesn't appear as essential. Our tests with the capacitor served to validate this conjecture.

4.1 Capacitor

As a first experimental step to prove the tuneability effect of the liquid crystal, a tuneable capacitor was fabricated on alumina substrates with conductive electrodes coated with gold. In this structure, a thin layer of a liquid crystal can modulate the propagating RF signal with its birefringence. A source of RF signal generator is electrically connected to the capacitor. The effective dielectric constant of the liquid crystal layer is modulated by applying a DC voltage. The capacitance can thus be changed by varying the effective dielectric constant of the liquid crystal medium.

Figure 4.1(a) and (b) show the schematic of tuneable capacitor. The bottom of the cavity is a metallic ground plane and the sides consist of the inner edges of a 0.254 mm-thick (h_{LC}) micro-machined alumina frame. The liquid crystal is injected into the cavity between the upper alumina layer and lower conductor layer. The thickness of upper alumina (h_{AL}) is 0.254 mm. The control voltage signal is superimposed on the RF signal through a bias tee to vary the capacitance. The layout of the structure on the upper alumina layer is shown in Figure 4.1(c). A view of the fabricated capacitor is shown in Figure 4.2.

(a).
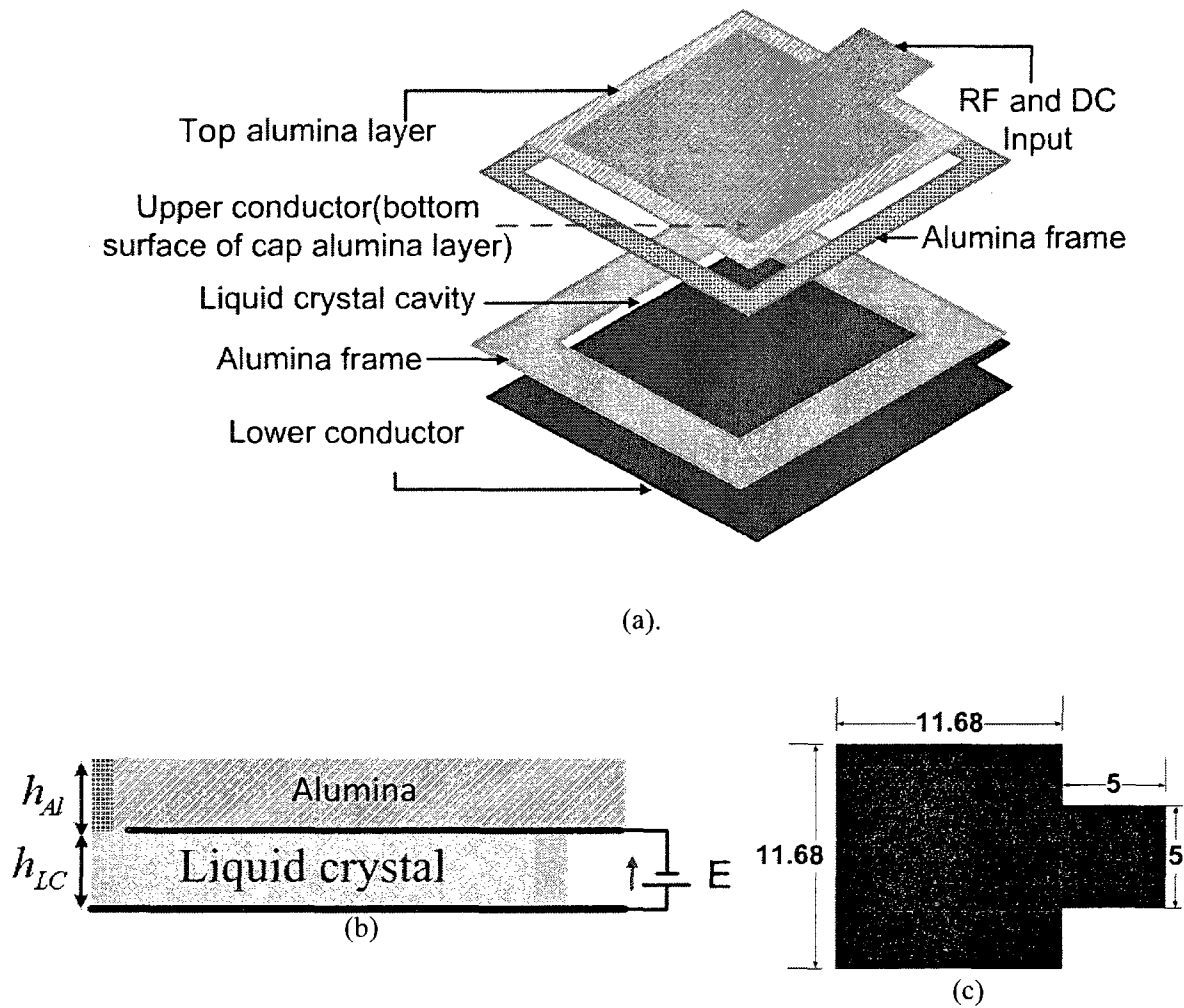
Figure 4.1 (a) Schematic; (b) Side view; (c) Dimensions of LC tuneable capacitor. All the dimension are indicated in millimeters.
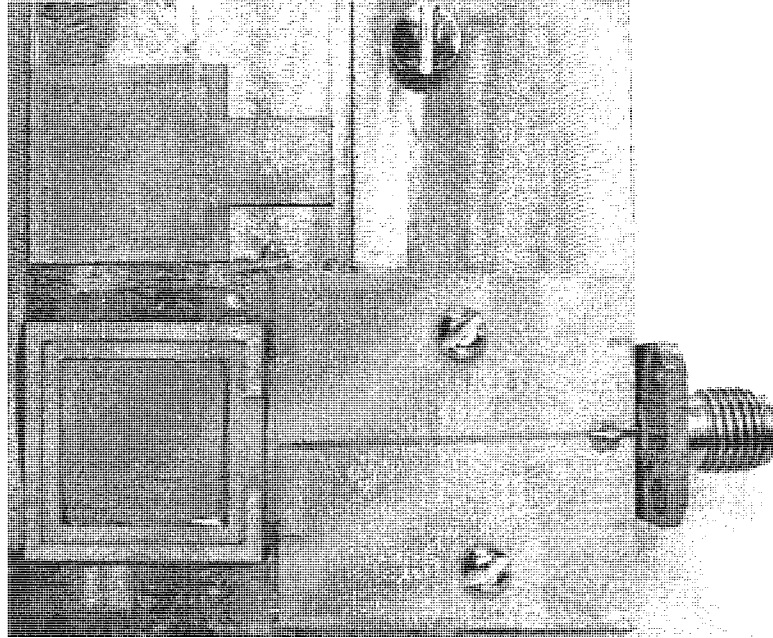
Figure 4.2 View of the fabricated capacitor.

In the first step, the capacitor was tested with olive oil as a dielectric ($\varepsilon_r = 3.1$). At 1

MHz, the measured susceptance was 110×10^{-6} Siemens. However, in the experimental

data, besides the capacitance of the cavity, there is an additional capacitor formed

between the "RF and DC input port" (as shown in Figure 4.1(a) and (c)) and the ground

plane of dimension of $5 \text{mm} \times 5 \text{mm}$, with 0.254 mm PCB as a dielectric ($\varepsilon_r = 2.9$). This

capacitance should be subtracted from the experimental data. Therefore

$$A_{\text{PCB}} = 0.005 \times 0.005 = 0.000025(m^2), d_{\text{PCB}} = 0.01 \times 2.54 \times 10^{-2} = 0.000254(m)$$

$$\varepsilon_0 = 8.85 \times 10^{-12} \, F/m, \quad \varepsilon_{r\_\text{PCB}} = 2.9$$

$$C_{PCB} = \frac{\varepsilon_0 \varepsilon_{r\_\text{PCB}} A_{\text{PCB}}}{d_{\text{PCB}}} = 2.5 \times 10^{-12} = 2.5 pF$$

The admittance can be calculated by :

$$|Y| = |j\omega C| = 110 \times 10^6 \Rightarrow C = 17.6 pF = C_{\text{Olive oil}} + C_{PCB} \Rightarrow C_{\text{Olive oil\_experimental}} = 15.1 pF$$

According to the tabulated value of olive oil, we should obtain a capacitance of 14.8 pF, as indicated below.

$$A = (11.68 \times 10^{-3})^2 = 0.0001365(m^2), d = 0.01 \times 2.54 \times 10^{-2} = 0.000254(m)$$

$$\varepsilon_0 = 8.85 \times 10^{-12} \, F/m, \quad \varepsilon_{r\_\text{Olive oil}} = 3.1$$

$$C_{\text{Olive oil\_theory}} = \frac{\varepsilon_0 \varepsilon_{r\_\text{Olive oil}} A}{d} = 14.78 pF$$

The values of capacitance calculated in theory and obtained in the experiment are found to be very close. It shows that the capacitor structure works correctly. It should be noted that the capacitance formula used does not account for the fringing fields at the edges of the metal traces, which should contribute to a small capacitance increase. This effect was omitted here, as its consideration would have no effect on the validation we want to achieve on the LC contact effectiveness.

In the next step, the structure was tested without adding polyimide layer. The cavity was filled with liquid crystal (BL006). As the DC control voltage (i.e., electric field

intensity) increases, liquid crystal molecules are forced to align more parallel to electric field.
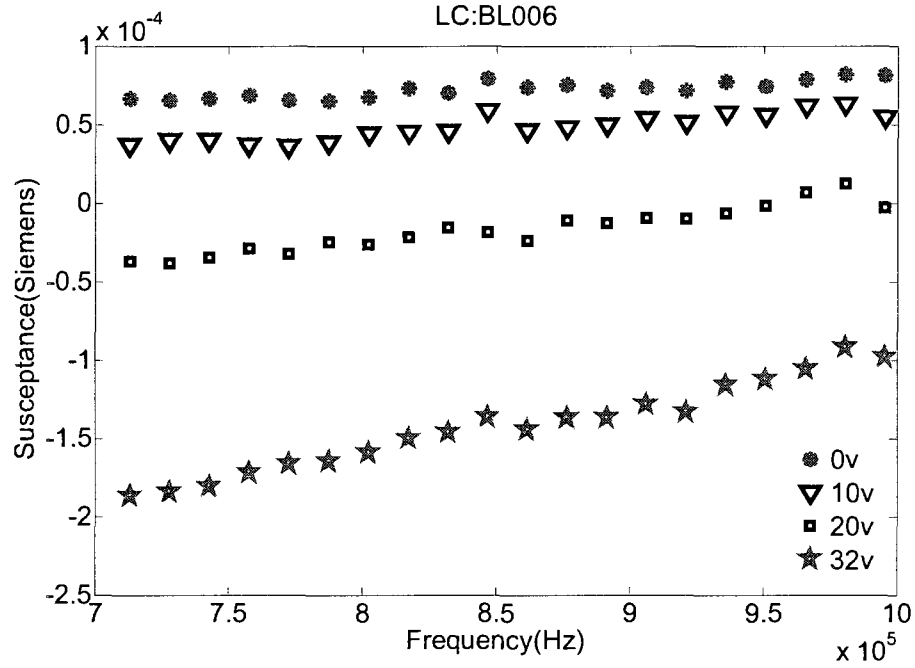
Figure 4.3 Susceptance of tuneable capacitor.

Hence, the dielectric constants of the liquid crystal change continuously from $\varepsilon_\perp$ to $\varepsilon_\parallel$.

The difference between $\varepsilon_\parallel$ and $\varepsilon_\perp$ is the tuning ranges of capacitance. This phenomenon is visible in Figure 4.3. As can be seen, increasing the bias voltage from zero to 32 volts led to a significant variation of the susceptance. The negative value of the susceptance is due to inductive effect of DC and RF transmission line.

Also this structure was tested with adding the polyimide layers to pre-align the LC molecules almost perpendicular to the RF-field. The 2μm-thick polyimide films were

spin coated on the upper surface of the lower conductor and the lower surface of the top

alumina layer, between which the liquid crystal layer is placed. The rubbing process was

also applied. No appreciable difference was observed compared to the case without

polyimide.

Of course, this capacitor was not designed for operation in X-band but the result of this

test nevertheless reveals the capability of tuning the LC by having it directly in contact

with the gold electrodes fabricated in house. It is thus possible to use this simple process

in our tests on resonators as described next.

4.2 Hairpin resonator

As shown in Figure 3.9, the bottom of the LC container is a metallic ground plane and

the sides consist of the inner edges of a 0.381mm-thick (h_{LC}) micro-machined alumina

frame. The resonator and its DC bias line are sputter-coated on the bottom face of an

alumina substrate (h_{Al}), which also has the RF input line and the DC biasing line and

pad on its top surface. A via interconnects the top and bottom sections of the biasing

line. A high-impedance narrow bias line (width of 101.6μm) was used to prevent RF

leakage in the bias network. The RF feed line is above the alumina frame and it is

therefore less affected by the bias state of the LC.

The effective dielectric constant of the liquid crystal layer is modulated by applying a DC voltage on the bias port, i.e. between the bias line and the metal ground plane. The ground plane was mechanically rubbed to favour the alignment of the liquid crystal molecules perpendicular to the RF electric field in the 0-volt bias state. However, no extra layer of polyimide was used, as in [11]-[19].

Figure 4.4 shows a photograph of this resonator. LC is inserted in the cavity via using the injection holes. Two different prototypes using two different thicknesses of the upper alumina layer (h_{Al} = 0.127 mm and 0.254 mm) were fabricated.
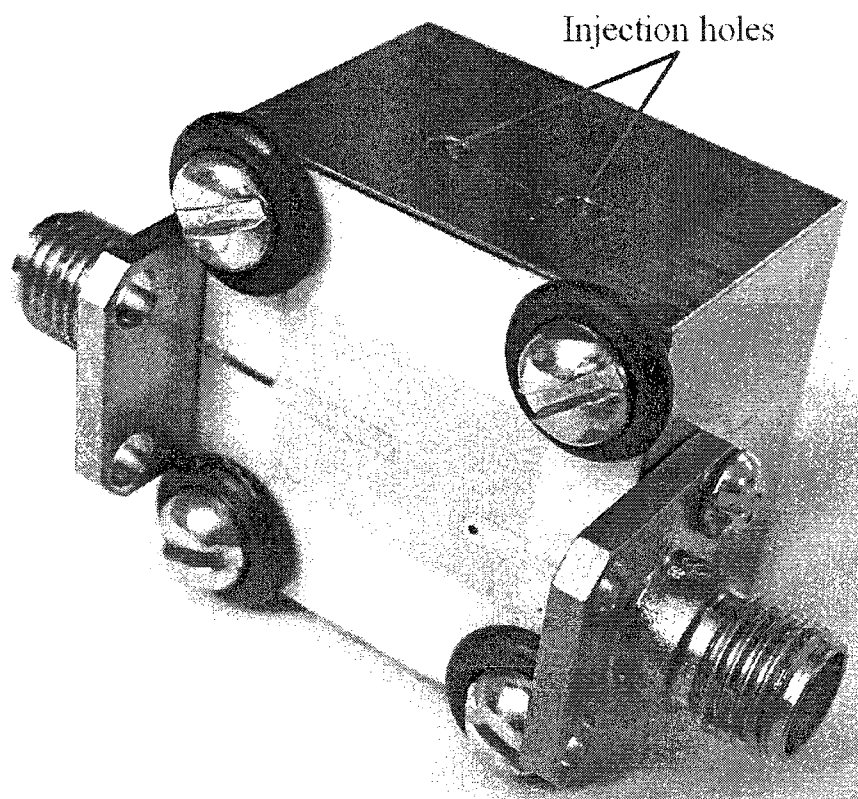
Figure 4.4 Photograph of the 10 GHz hairpin resonator.

4.2.1 Liquid crystal and applied field polarizations

When the RF input transmission line is excited, power couples to the hairpin resonator on the bottom surface of the upper alumina layer and the RF electric field is polarized vertically between hairpin microstrip and ground plane. With a 0-volt bias, the RF electric field is orthogonal to the axis of liquid crystal molecules and liquid crystal

permittivity becomes $\varepsilon_\perp$. On the other hand, the LC molecules can rotate up to 90° in a region surrounding the resonator when a DC voltage (E_0) is applied. In this case, the axis of the LC molecules becomes parallel to the direction of the excited RF E-field and the permittivity becomes $\varepsilon_\parallel$. For an intermediate value of electric field of the applied DC voltage ($0 \leq E \leq E_0$), the permittivity varies continuously between $\varepsilon_\perp$ and $\varepsilon_\parallel$. Due to this phenomenon, it becomes possible to control precisely the resonance frequency of the hairpin with the applied DC voltage, or alternatively, control the phase of the reflection response at a fixed frequency.

4.2.2 Analysis and measurement results

Finite element modelling of the proposed structure was done using Ansoft-HFSS® in the previous chapter and these results are now compared with the measurements. The measurement setup is shown in Figure 4.5. The DC voltage is applied to the hairpin resonator through a bias-T. Principally, the use of such a component in RF circuits prevents coupling of the RF signal to the DC supply and decreases the losses associated with.

The reflection coefficients (S11) in parallel and perpendicular LC states have been measured in the frequency range 9-10.5 GHz with an Anritsu 37369D network analyzer.

A one-port short-open-load calibration was done prior to measurement, with the reference plane at the DUT's coaxial connector level.
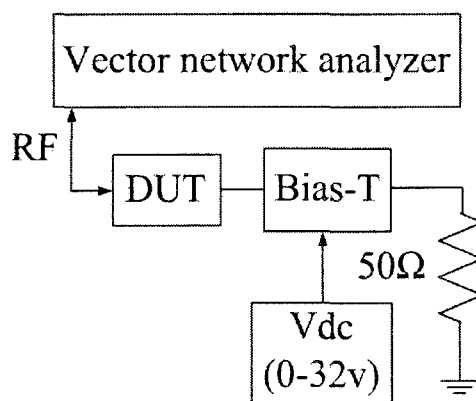
Figure 4.5 Measurement setup

4.2.2.1 Results for a 0.127-mm alumina layer

Figure 4.6 represents the simulated and measured return loss at the coaxial input port over the frequency range of interest. It can be seen that the resonant frequency changes from 9.327 GHz (0V) to 9.154 GHz (32V). In the experiments, the resonant frequencies in both 0V and 32V states have shifted by about 250 MHz in comparison with the HFSS predictions. The measured return loss levels at resonance are however in very good agreement with predictions in both states.
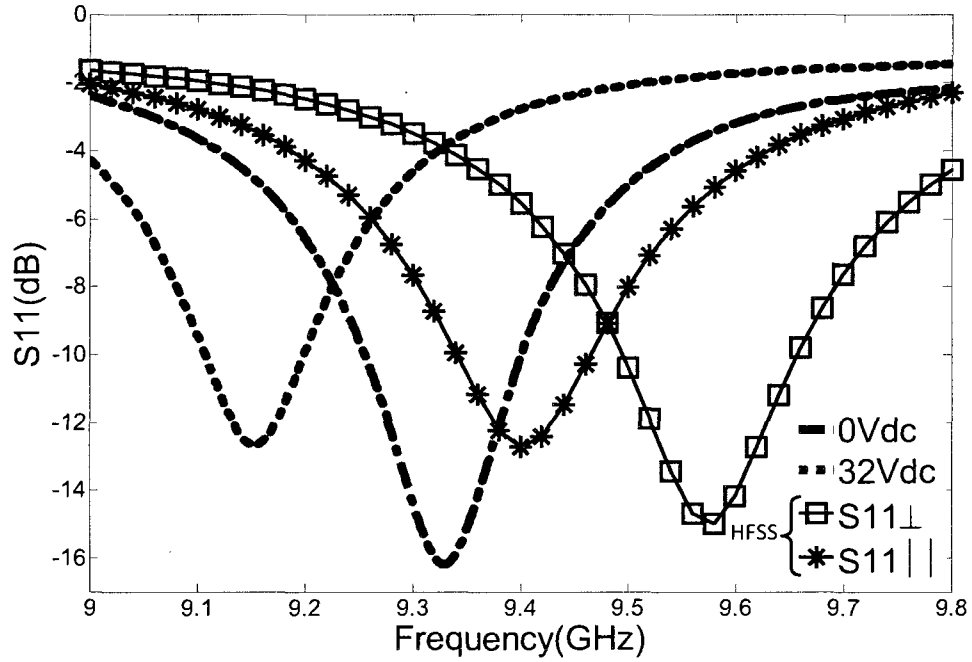
Figure 4.6 Experimental and predicted return loss (h_{Al} =0.127 mm, LC: BL006).

Figure 4.7(a) illustrates the reflection coefficient phase results. The phase transition exhibits a nonlinear behaviour near the resonance. Bias-induced phase differences are shown in Figure 4.7(b). In the experiments, the maximum phase change (177°) occurs at 9.24 GHz. A good agreement between the measurement and simulation result can be observed despite the fact that the liquid crystal permittivity is not known accurately.
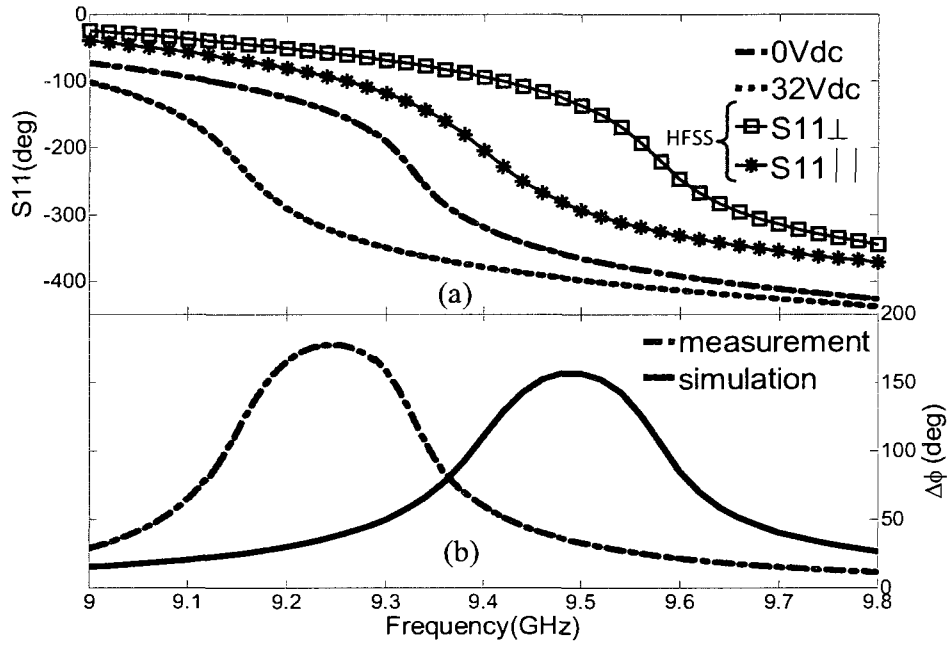
Figure 4.7 a) Measured and simulated reflection phase; b) Measured and simulated bias-induced phase difference, h_{AL}=0.127 mm, LC: BL006.

The 0.127-mm substrate layer was very fragile and it was accidentally broken during cleaning after the first measurement with BL006.Therefore, there is only measurement data with BL006 for this structure.

4.2.2.2 Results for the 0.254-mm thick upper alumina layer

The measurements using three different liquid crystals BL006, K15 and MDA-05-893 were done and the experimental data and simulation data are now compared.

4.2.2.2.1 K15

Figure 4.8(a) shows experimental and measured return losses over the frequency range of 9.3 GHz to 10.1 GHz and change of the resonant frequency from 9.79 GHz (0V) to 9.65 GHz (32V). Figure 4.8(b) illustrates the reflection coefficient phase results. In the experiments, the maximum phase change of 183° as it is shown in figure 4.8(c) occurs at 9.744 GHz.
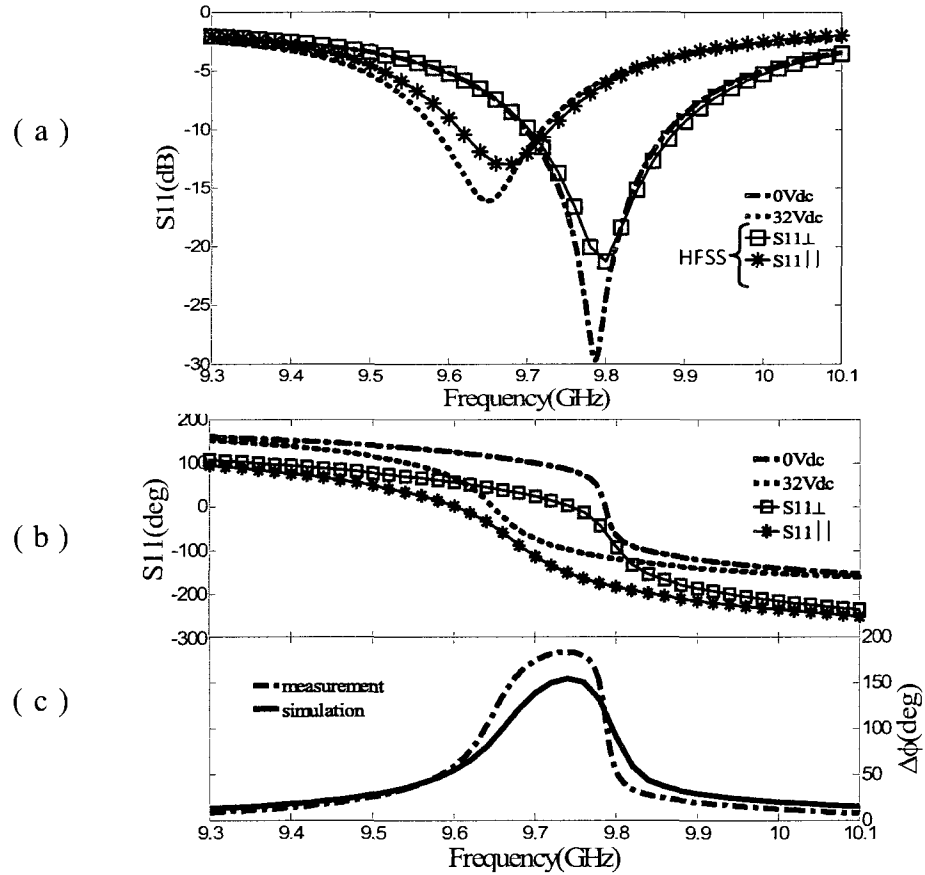
Figure 4.8 Measured and simulated results. (a) Return loss; (b) Reflection phase; (c) Bias-induced phase difference, h_{Al} =0.254 mm, LC:K15.

4.2.2.2.2 MDA-05-893

First of all, it should be considered that the only available permittivity values in the literature for the MDA-05-893 mixture were for a frequency of 35 GHz. Since our tests are done near 10 GHz, some discrepancies are to be expected. This is visible in Figure 4.9 where the resonant frequencies in both 0V and 32V states have shifted and more losses are measured in comparison with the HFSS predictions.
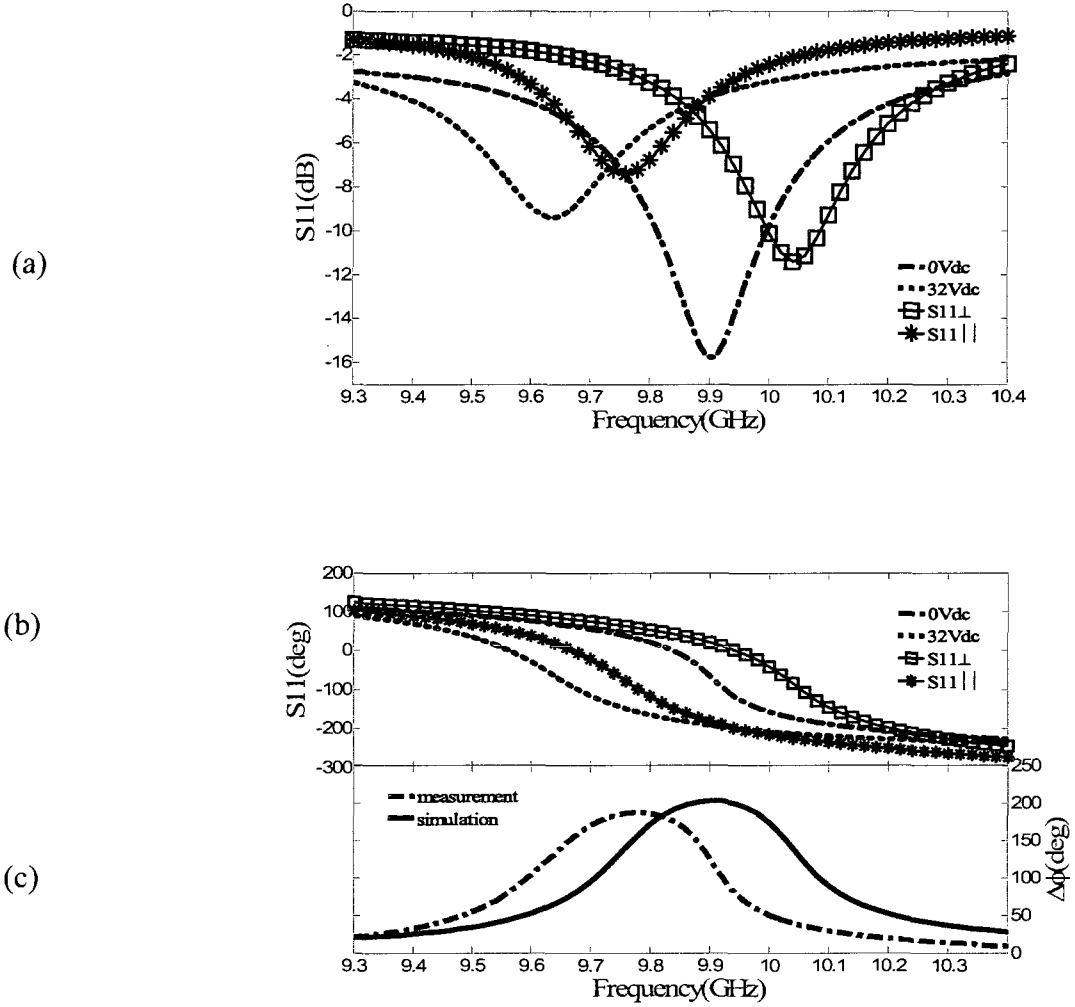
Figure 4.9 Measured and simulated. (a) Return loss; (b) Reflection phase; (c) Bias-induced phase difference, h_{Al} =0.254 mm, LC: MDA-05-893.

Figure 4.9(a) shows experimental and predicted return loss over the frequency range of 9.3 GHz to 10.5 GHz and the shift of the resonant frequency from 9.91 GHz (0V) to 9.64 GHz (32V). The reflection coefficient phase results are shown in Figure 4.9(b).The

maximum voltage controlled phase range, as it is shown in Figure 4.9(c), is 187.4° at 9.784 GHz.

4.2.2.2.3 BL006

Simulated and measured return losses over the frequency range of interest are represented in Figure 4.10(a). It can be seen that the resonant frequency changes from 9.804 GHz (0V) to 9.52 GHz (32V). The reflection coefficient phase results are shown in Figure 4.10(b). Figure 4.10(c) illustrates that the maximum phase shift is 200° at 9.636 GHz. The experimental data of this section will be used in the next chapter to predict the performance of a reflectarray based on tuneable LC cells.
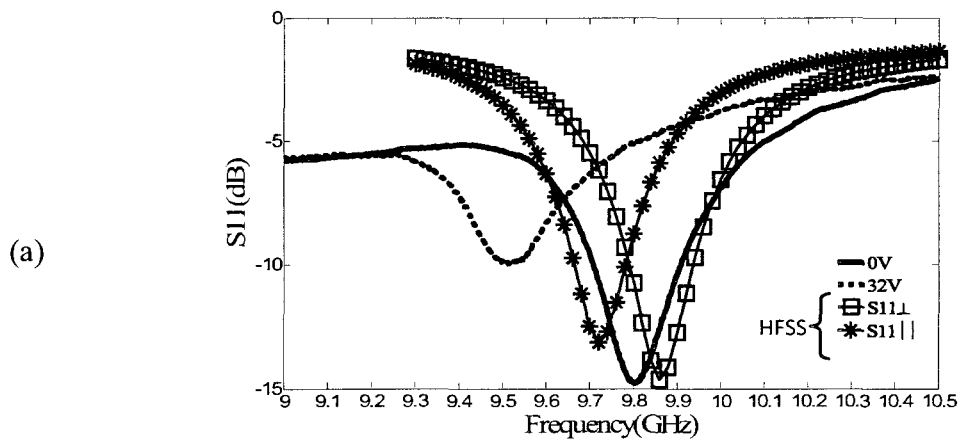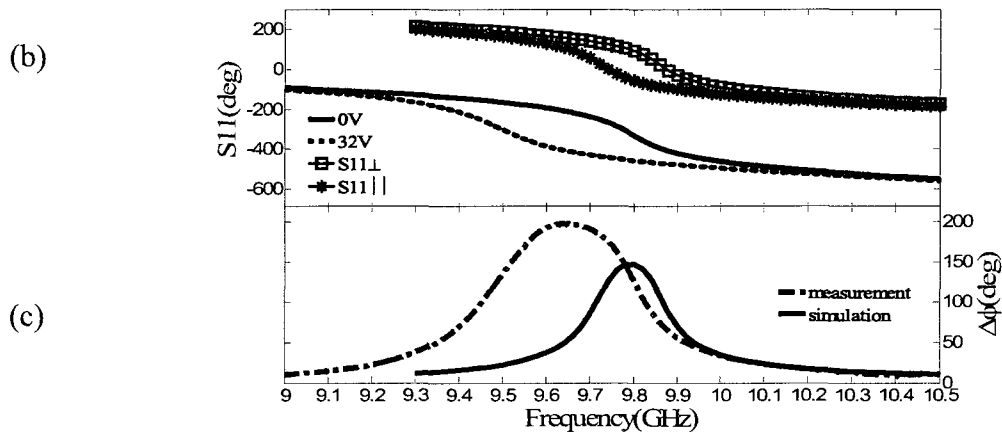
(a)

Figure 4.10 Measrued and simulated. (a) Return loss; (b) Reflection phase; (c) bias-induced phase difference, h_{Al} =0.254 mm, LC: BL006.

The magnitude and the phase of the complex reflection coefficient of the measured hairpin resonator cell are shown in Figure 4.11 for finer tuning voltage steps, as it will be required in the reflectarray design procedure.
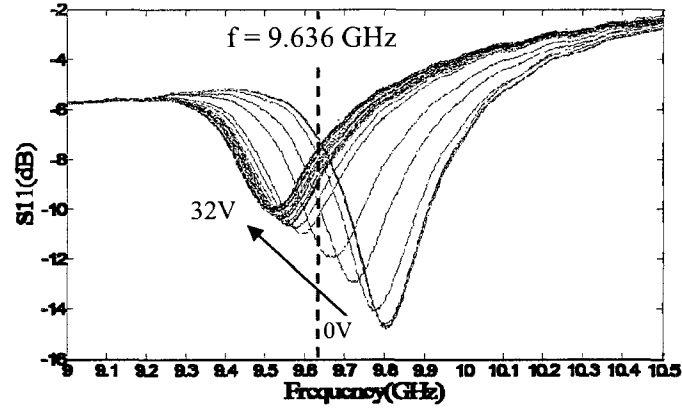
(a)
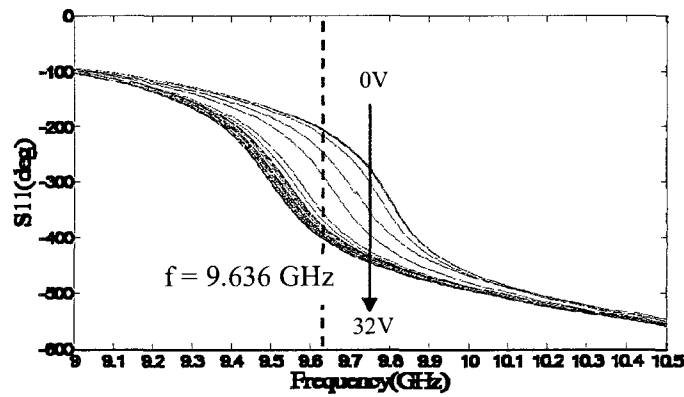
(b)

Figure 4.11 (a) Magnitude and (b) phase of the reflection obtained when the control voltage is swept from 0 to 32V with the step of 1V, h_{Al}=0.254 mm, LC: BL006.

The distribution of S11 at the operating frequency of 9.636GHz in a polar diagram is shown in Figure 4.12. This figure illustrates how the biasing voltage determines the angle of reflection coefficient S11. The biasing voltage is varied between 0 and 32V for this figure.
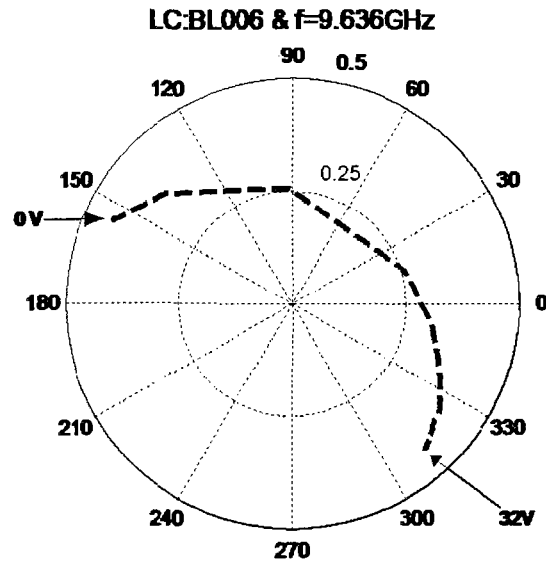
Figure 4.12 Polar diagram of S11; h_{Al} =0.254 mm, LC: BL006

This data is presented in Cartesian magnitude and phase formats in Figure 4.13. It can be observed that the tuneable phase range is approximately 203 degrees. It is apparent that the return loss due to dielectric and conductors are expected to be about 12dB in the worst case scenario.
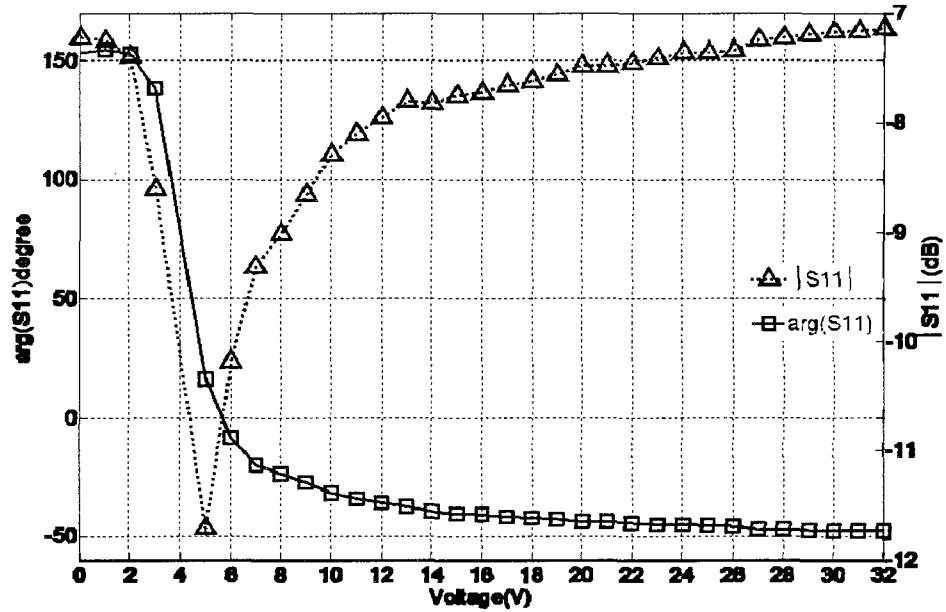
Figure 4.13 Extracted magnitude and phase of the free standing LC hairpin resonator when the DC control is varied between 0-32V; f=9.636 GHz, h_{Al} =0.254 mm, LC: BL006.

4.2.2.2.4 Comparison between LCs

The summary of experimental results of two structures is presented in Table 4-1. In this table, the maximum voltage-controlled phase range and the maximum return loss at resonant frequency when the control voltage is zero and 32V, of each type of LCs are shown. Due to maximum phase shift and minimum losses obtained, MDA-05-893 and BL006 are thus recommended. Achievement of phase differences greater than 180° for three types of LCs can be seen in this table.

Table 4-1 Comparison between measured characteristics of the three resonators filled with

three different LCs

h_{AL}	LCs	Maximum phase shift (degree)	Maximum Loss (dB)	
			0 V	32 V
0.127 mm	BL006	177	-16	-12.5
0.254 mm	BL006	200	-14.8	-10
	K15	183	-29.5	-16
	MDA-05-893	187.4	-15.8	-9.4

4.2.2.2.5 Comparison with the patch structure

In this subsection, the results of the hairpin resonator are compared with the patch structure of [16]. Both of them are filled by BL006. The patch elements were printed on a 125μm thick glass reinforced PFTE substrate (ε_r =2.9, tanδ=0.0028) which is mounted on a 500μm cavity containing the LC. Patch elements were biased from zero to 20V.

The maximum phase shift and the maximum magnitudes of reflection coefficient at operating frequencies, when the control voltage is switched between zero and Vmax, for each type of structures are summarized in Table 4-2.

It can be seen that hairpin with h_{AL}=0.254 mm and patch structure has the same maximum phase shift (200°) but the return loss of the hairpin is at least 2dB less than the patch structure. This is possibly due to the fact that the printed metallic hairpin is directly in contact with the LC whereas the printed patch elements were separated from the LC by a PFTE substrate (ε_r =2.9, tanδ=0.0028). So, PTFE losses were added to LC losses.

Table 4-2 Comparison between the characteristics of the patch and hairpin resonators.

LC: BL006		Maximum phase shift (degree)	Maximum Loss (dB)	
			0 V	Vmax
Patch		200	-18.3	-12
Hairpin	h_{AL} = 0.127 mm	177	-16	-12.5
	h_{AL} =0.254 mm	200	-14.8	-10

CHAPTER 5. REFLECTARRAY DESIGN BASED

ON A TUNEABLE LC CELL

For space applications, the low-cost, low-mass, deployable antennas with large surface area that can be rolled-up or folded for launch and then deployed in space are needed. For such applications, a reflectarray based on LC is suitable model. *"A reflectarray is made up of an array of radiating elements that provide a preadjusted phasing to form a focused beam when it is illuminated by a feed. Printed reflectarrays combine certain advantages of reflector antennas and phased arrays. They are manufactured on a planar substrate using printed circuit technology and offer the possibility of beam steering as phased arrays; on the other hand, the feeding mechanism (as in a reflector antenna) eliminates the complexity and losses of the feeding network used in planar arrays, thus providing a higher efficiency. Recently, some potential applications of reflectarrays in space have been researched, such as contoured beam antennas for Direct Broadcast Satellites and very large inflatable antennas."* [29]

Reflectarrays typically use variable-length patches [30], patches with tuning stubs [31], or CP patches [32] with rotations to achieve required reflection phases. A flat array of microstrip patches is excited by a feed antenna and the reflection phase from each element leads to a planar reflected phase front. The radiation pattern is subsequently due to the fields scattered by each patch.

In this work, we consider the design of a reflectarray using a tuning voltage to control the reflection phases of the unit cells. It can be modelled (and designed) by considering reflection from patch elements which are printed on LC cells. Reflectarray alters the scattered EM field to form a radiation maximum in a desired direction. The reflection phase of the individual array elements (LC cells) is thus modified to form the desired scattered beam pattern. In the case presented here, each unit cell is designed at 9.636 GHz with an adjustable phase range of nearly 180°. The direction of the radiated main beam is controlled by adjusting reflection phases. The goal of this chapter is to predict the performance of a reflectarray based on the proposed tuneable hairpin resonator structure used as a reflectarray cell. This implies that a radiating element, such as a patch or a dipole, is used to couple the incident and scattered waves to the input port of the resonator. The design of this radiating element has not been addressed, as it is usually not a limiting factor in previously realized reflectarrays. It is assumed that each resonator is coupled to a broadband radiating element (e.g. patch on a thick substrate) laid on the reflector's surface. By following the standard reflectarray design process, the total reflection phase of a given LC cell can be determined. The experimental data is the reflection coefficient at the operating frequency of 9.636 GHz for the hairpin resonator designed with a thickness of 0.254 mms for the upper alumina substrate and the LC cavity is filled by BL006 as the liquid crystal.

To determine the theoretical radiation pattern, geometrical optics is used to calculate the field at the aperture of the antenna. This field is then Fourier transformed to obtain the far-field radiation pattern of the system. For simplicity, the analysis is done for a 2D reflector only.

5.1 Analysis process

The analysis process can be summarized in the following steps. First, the desirable reflectarray is created by getting a minimum of two samples per wavelength to prevent grating lobes. The number of samples determines the size of the reflector. Then by using experimental data and the desired reflection coefficients of the reflectarray, the achievable reflectarray is synthesized. The feed pattern and spreading losses are taken into account in this perfect reflectarray design. Finally by using the achievable reflections coefficients for the LC resonator together with the perfect reflectarray design, the real reflectarray based ono the hairpin resonator is designed.

5.1.1 Geometry considerations for the reflectarray synthesis

Figure 5.1 shows the geometry used in the synthesis process. Suppose $F = 100\lambda$, $R = 50\lambda$ and $0 \leq x \leq R$. It will be assumed that ray l_0 incident in the center of the reflector has a specular reflection that is parallel with the direction of the desired main beam of the reflector. So its angle of incidence is equal the angle of reflection (

$\theta_r = \theta_i = \dfrac{\theta_0}{2}$). The three angles in the triangle (AOC) must add up to 180 degrees,

therefore $\alpha = \dfrac{\theta_0}{2}$. On the other hand, $\Delta1 = x_0 \cot(\theta_0) = x_0 \cot(2\alpha)$ and $\Delta2 = x_0 \tan(\alpha)$

also $\Delta1 + \Delta2 = F$ thus

$$\theta_0 = \arcsin\left(\frac{x_0}{F}\right), x_0 = \frac{R}{2} \qquad (5.1)$$

$$\alpha = \frac{1}{2}\arcsin\left(\frac{R}{2F}\right) \qquad (5.2)$$
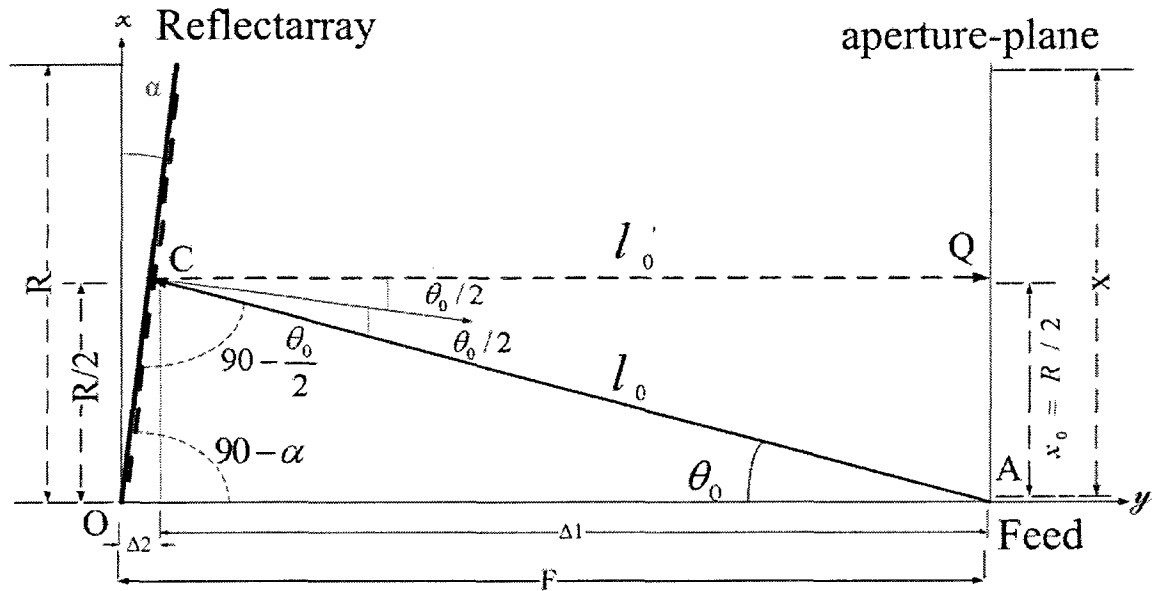
Figure 5.1 Central beam geometry.

If $\overline{A}=(0,F)$, $\overline{C}=(x_0,x_0\tan(\alpha))$ and $\overline{Q}=(x_0,F)$ by using vector geometry, $l_0=\overline{AC}$

and $l_0'=\overline{CQ}$ can be calculated as follow,

$$l_0'=\left|F-x_0\times\tan\alpha\right| \tag{5.3}$$

$$l_0=\sqrt{x_0{}^2+\left(l_0'\right)^2} \tag{5.4}$$

The phase obtained on aperture plane has to be uniform and thus is equal to

$$\Delta\varphi_0=-\beta\left(l_0+l_0'\right)+\varphi_0,\quad \varphi_0=k\pi \tag{5.5}$$

5.1.2 Desirable reflectarray

In order to have a planar phase front, the phase of all the rays in the aperture plane should be equal as depicted in Figure 5.2.

$$\Delta\varphi_0=\Delta\varphi_1=\Delta\varphi_2=...=\Delta\varphi_{(i)} \tag{5.6}$$

Consequently, for each element in the array, the reflection phase $\varphi_{(i)}$ is computed by the following formula.

$$\Delta\varphi_0 = -\beta\left(l_1 + l_1'\right) + \varphi_1 = ... = -\beta\left(l_i + l_i'\right) + \varphi_{(i)}$$

$$\Rightarrow \varphi_{(i)} = \Delta\varphi_0 + \beta\left(l_i + l_i'\right) + 2k\pi \tag{5.7}$$

Where each ray path l_i and l_i' can be described by using vector geometry; i.e.

$l_i' = \left|F - x_i \tan\alpha\right|$ and $l_i = \sqrt{x_i^2 + \left(l_i'\right)^2}$. For a perfect reflector, the magnitude of the reflection coefficient should be unity. So reflection coefficients on each cell of the desirable reflectarray are given by:

$$\Gamma_{(i)des} = \Gamma_{(i)} e^{i\varphi_{(i)}} = e^{i\varphi_{(i)}} \tag{5.8}$$
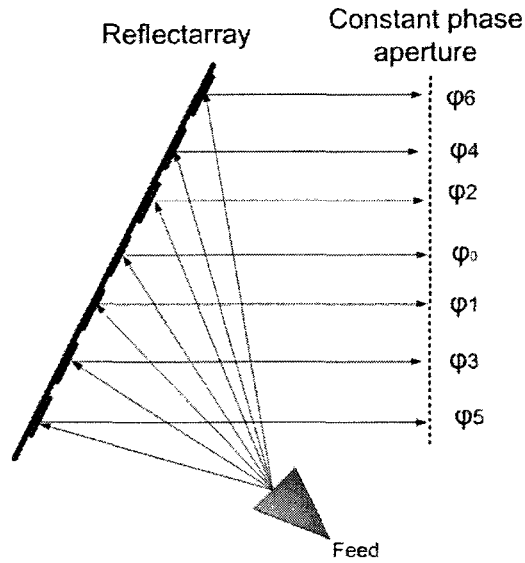
Figure 5.2 Phase demonstration of a reflectarray with arbitrary antenna element.

5.1.3 Achievable reflectarray

Synthesizing the reflectarray with the LC elements requires finding among the various LC state cells those who give the closest reflection phases to those predicted with the perfect reflectarray design. In other words, for a given cell of the perfect reflectarray requiring a desired reflection coefficient Γ_{des}, the achievable value Γ_{ach} is among the set of reflection coefficients Γ_{exp} obtained experimentally that is closest in phases to Γ_{des}. Thus, for each cell we have:

$$\Gamma_{ach} = \min_{\Gamma_{exp}}(\angle\Gamma_{des} - \angle\Gamma_{exp}) \qquad (5.9)$$

5.1.4 Perfect reflectarray

The feed pattern and spreading losses are taken into account in the perfect reflectarray design. As shown in Figure 5.3, we suppose that ray l_0 is in main lobe direction of the feed.
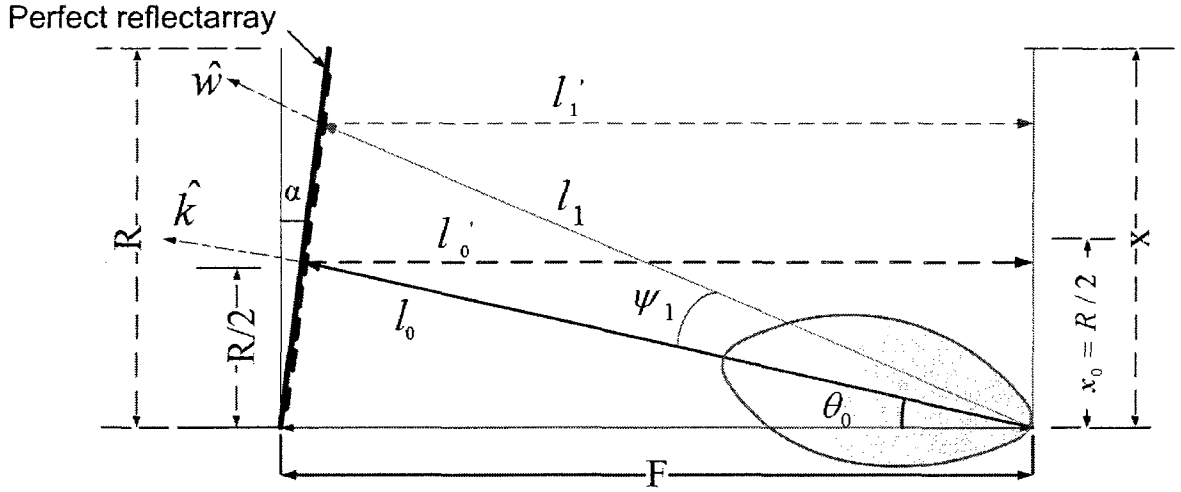
Figure 5.3 Scheme of the design of the perfect reflectarray.

$$\cos(\psi_1) = \hat{k} \times \hat{w} = \frac{\bar{k}.\bar{w}}{\|\bar{k}\|.\|\bar{w}\|} = \frac{x_0 x_1 + (x_0 \tan\alpha - F)(x_1 \tan\alpha - F)}{\sqrt{x_0^2 + (x_0 \tan\alpha - F)^2} \times \sqrt{x_1^2 + (x_1 \tan\alpha - F)^2}}$$

$$= \frac{x_0 x_1 + (x_0 \tan\alpha - F)(x_1 \tan\alpha - F)}{l_0 \times l_1}$$

(5.10)

Feed pattern and spreading loss can be taken in consideration by applying the following factor to the incident field.

$$|v_{(i)}| = \left| \frac{\cos^q (\psi_i)}{l_i + l_i'} \right|$$

(5.11)

Where q is the exponent of the feed pattern. In [35], q (feed beamwidth) has a value of 10.5. Here due to some practical considerations the selected q=12 which a little bit deviates from optimal.

The propagation phase is calculated by

Figure 5.4 Polar diagram of calculated reflectarray.

5.2 Providing 360° phase variation

It is possible to obtain a circuit with a phase variation 360° simply by combining two liquid crystal cells in series as it is shown in Figure 5.5. By looking at the reflection plot of the experimental results, it is noticed that there is a need for phase compensation at each element.

Adding two pieces of transmission line with different lengths L1 and L2 followed by two LC cells, provides reflections Γ_1 and Γ_2 that are approximately different by 180-degree in phase. Such different is a rotation in the polar diagram illustrated in Figure 5.6.

It is worth to mention that due to practical considerations, we added a common transmission line segments to both phase shifter in advance (0.2π).

$$\Gamma_1 = \Gamma_{exp} e^{j0.2\pi} \qquad (5.15)$$

$$\Gamma_2 = \Gamma_{exp} e^{j1.118\pi} \qquad (5.16)$$

Curves of Γ_1 and Γ_2 are represented in Figure 5.6(a) and (b). And the impedances Z_1 and Z_2 are connected in series to form a total impedance Z_{total}.

$$Z_1 = \frac{1 + \Gamma_1}{1 - \Gamma_1} \qquad (5.17)$$

$$Z_2 = \frac{1 + \Gamma_2}{1 - \Gamma_2} \qquad (5.18)$$

$$Z_{total} = Z_1 + Z_2 \qquad (5.19)$$
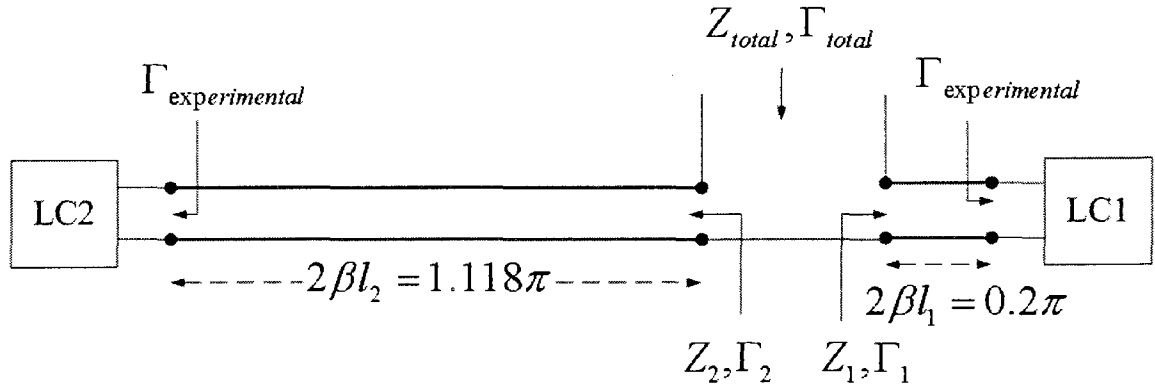
Figure 5.5 Schematic of two LC cells in series.

The reflection coefficient of Z_{total} makes a full rotation of the polar diagram. Since this circle is not centered in the Smith chart, it causes large variations of the magnitude on the reflectarray surface. This can be alleviated by using an impedance transformer which renormalizes the impedance, so that the circle is better centered in the smith chart. An impedance renormalization of 2.2 (i.e. use of a characteristic impedance of 110 ohms) gave a good compromise on the magnitude uniformity. Thus, we have:

$$\Gamma_{total} = \frac{Z_{total} - 2.2}{Z_{total} + 2.2}$$
(5.20)

Finally as shown in Figure5.7(c) a variation of phase 360° of Γ_{total} is obtained. Such a variation allows for a maximum in-phase contribution of all elements in the desired main beam direction, and thus for any desired beam angle.

(a)   **(b)**   **(c)**
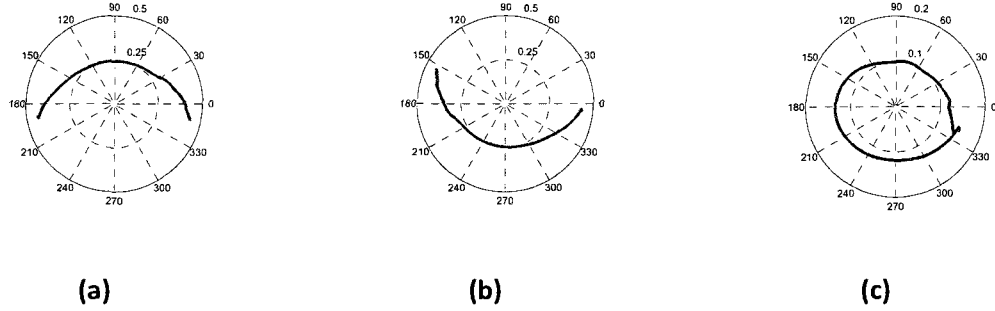
Figure 5.6 Curves   **(a)** Γ_1 **vs voltage; (b)** Γ_2 **vs voltage; (c)** Γ_{total} **vs voltage.**

5.3 Predicting the radiation pattern

To find the radiation patterns, all the analysis steps are done again using Γ_{total} instead of

experimental data (Γ_{exp}). So $\Gamma_{(i)ach}$ is changed to $\Gamma_{(i)ach\_2LC}$.

$$\Gamma_{(i)ach\_2LC} = \min(\varDelta\Gamma_{(i)des} - \varDelta\Gamma_{total})$$ (5.21)

First, the radiation pattern of each element of reflectarray is calculated as define in

equation 5.22.

$$E_i(x) = v_{(i)}\Gamma_{(i)ach\_2LC}$$ (5.22)

Then the total radiation pattern of the designed reflectarray consist of 301 identical

elements is obtained using equation 5.23.

$$E(\theta) = \sum_i E_i(x)e^{(j\beta x\cos(\theta))}, \frac{-\pi}{4} \le \theta \le \frac{\pi}{4} \qquad (5.23)$$

Figure 5.7 (a) shows a normalized radiation pattern of a 301- element reflectarray antenna. The antenna was simulated using the approach presented in the previous section. Figure 5.7(b) shows a closer view of the main beam and its first side lobes. The pattern of LC reflectarray compared with the pattern of a perfect reflectarray antenna. This figure shows that the main beams of LC reflectarray and perfect reflectarray are basically in the same direction. This means that the phase distributions of two antennas are similar. Moreover they also have the same beamwidth. The comparison between the two radiation patterns also shows that the sidelobe level is 1 dB higher for the LC reflectarray (LC reflectarray:-14.6dB, perfect reflectarray: -15.6dB). The lower level of the maximum is due to loss in the LC resonators, whereas the highest sidelobe is attributed to the modulation in the aperture field magnitude coming from the non circular shape of the LC element characteristics (see Figure 5.6(c)).
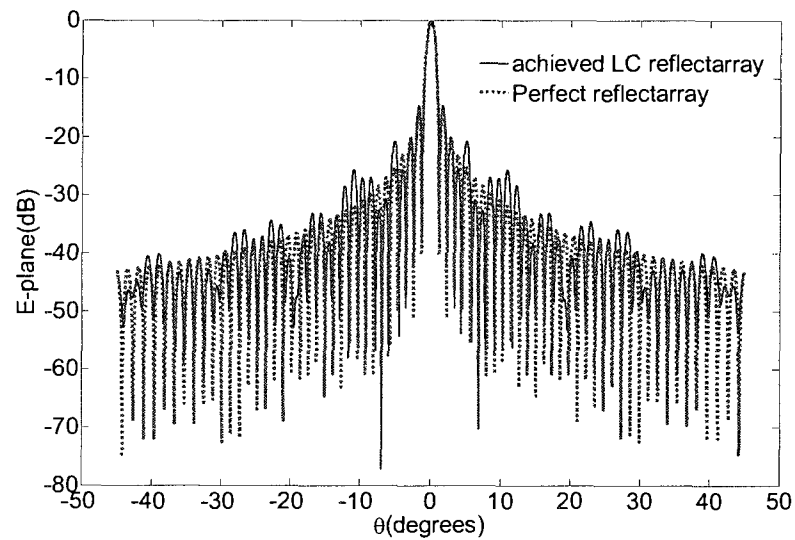
(a)
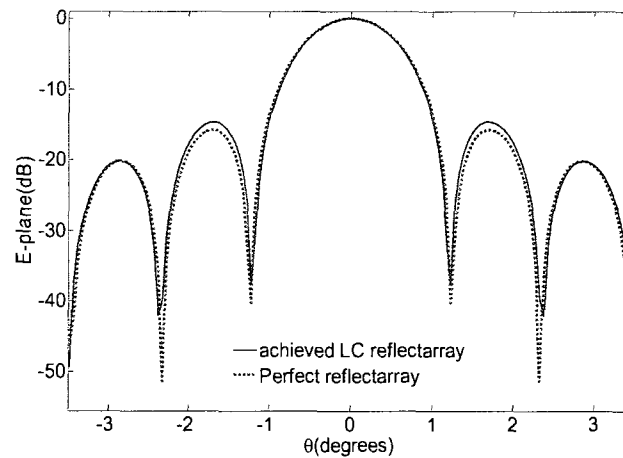
(b)

Figure 5.7 Radiation patterns of the perfect and LC-based reflectarray designs. (a) $-50° \leq \theta \leq 50°$; (b) Closer view of the main beam and the first sidelobes.

Figure 5.8 (a) shows the comparison between the aperture fields of the LC-based and perfect reflectarray. As it is shown, there are some ripples in LC reflectarray diagram in

both magnitude and angle. Figure 5.8(b) demonstrates that the discrepancies between the achieved and expected phase of the aperture field are less than 0.01 radians. This expected low level of phase error is only limited by the numerical accuracy of the minimum search function used to implement equation 5.21.

The Matlab codes (m-file) which have been developed to calculate the required parameters are provided in Appendix B.

(a)

(b)
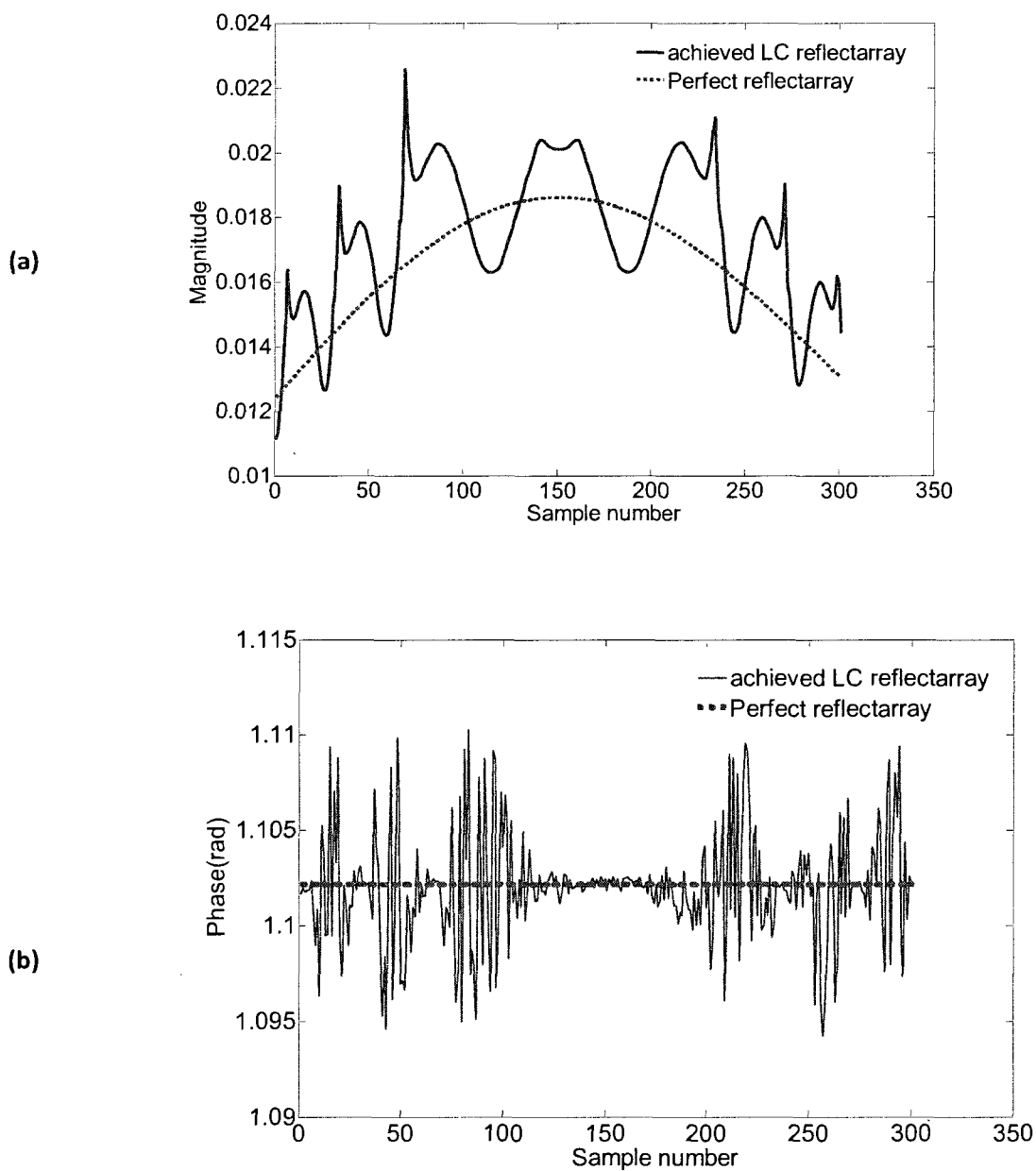
Figure 5.8 Comparison between the aperture field distribution of perfect and LC-

based reflectarray designs. (a) Magnitude; (b) Phase (radian).

CHAPTER 6.CONCLUSION

6.1 Outcomes

This M.A.Sc. thesis addressed the feasibility of using a reconfigurable resonator based on liquid crystal for use in a reflectarray antenna. A new tuneable hairpin resonator implemented with a nematic liquid crystal for an operating frequency around 10 GHz was proposed. Reduction of the radiation losses using a folded hairpin shape was demonstrated. Two hairpin resonator structures were fabricated with two different thicknesses of upper alumina layer, i.e. 0.127 mm and 0.254 mm. In order to increase the tuneability, the printed metallic resonator was put directly in contact with the liquid crystal. A one-port short-open-load calibration was done, with the reference plane at the DUT's coaxial connector level. Numerical results using Ansoft HFSS were compared with the measured phase characteristics, resonant frequencies and return losses for two orientations of the liquid crystal molecules. The results of this study show that even a small voltage is sufficient to modulate the phase of a signal that is reflected from the resonator. The phase agility is dependent on the shift in the resonant frequency of the structure. For the given voltage, the resonant frequency is determined by the dielectric anisotropy of the liquid crystals. Three different liquid crystals (BL006, K15 and MDA-05-893) were measured and due to maximum phase shift and minimum losses, MDA-05-893 and BL006 are the most recommended. A tuneable phase range of almost 180°

was achieved for the three types of LC. Compound BL006 with 0.254 mm thickness of upper alumina layer exhibited the maximum phase shift, 200°, at a frequency of 9.636 GHz. The return loss levels in biased and unbiased states were obtained to be 15dB (0V) and 10dB (32V).

To our knowledge, no other structure based on liquid crystal presented in literature achieved this performance with BL006 in X band. Indeed, before the hairpin resonator, the best range of maximum phase shift was measured to be about 200° using patch elements [16] with its maximum losses between 18 and 12dB; while those obtained by hairpin structure are 15 dB and 10dB. So, return loss of hairpin is at least 2dB less than those of the patch structure. This is due to the fact that the printed metallic hairpin is directly in contact with the LC whereas the patch elements were printed on a PTFE substrate (ε_r =2.9, tan δ =0.0028). So, PTFE losses were added to LC loss.

By using a numerical model combined with experimentally obtained characteristics of a hairpin resonator cell, it is demonstrated that the dielectric anisotropy property of liquid crystals can be used to create a reconfigurable reflectarray antenna and this application of the LC is demonstrated in the thesis. The experimental data is the reflection coefficient at operating frequency (9.636 GHz) for the measured hairpin resonator cell with an upper alumina layer of 0.254 mm and BL006 used as liquid crystal. Phase tuning was obtained by varying the biasing voltage between 0 and 32 volts. There is a trade-off between the phase range and the loss, however new liquid crystal mixtures have been

reported [33] that have loss tangent values of around 0.004 which is sufficiently low to give a reflectarray gain when this novel type of phase shifter is integrated into the antenna structure.

6.2 Future works

The results of the extensive study on the liquid crystal and its applications in microwave engineering demonstrate its promising future in this field. It can be used in very high frequency applications at 35 GHz or 60 GHz due to its lower loss behaviour.

Response time is a critical concern for a liquid crystal device. The phase transition exhibits a nonlinear behaviour near the resonance. The transient response between the states is mainly predicted by the relaxation time of the LC's molecules. By using the transient nematic effect [34] the phase transition can be accelerated. A short response time results in a better performance for the LC device. Future works is however considered on reducing the response time and providing a fast switch liquid crystal.

REFERENCES

[1] Bernhard J.T. "Reconfigurable antennas (Synthesis Lectures on Antennas and Propagation)" 2006. Publ. by Morgan & Claypool. Pages:120

[2] Varadan V. K., Kalarickaparambil Joseph Vinoy and K. A. Jose, "RF MEMS and their applications," 2003. Publ by John Wiley and Sons. Pages:394

[3] Rebeiz G. M. "RF MEMS: Theory, Design, and Technology " 2003,Publ by Wiley-IEEE, Pages:512

[4] Yang F. and Y. Rahmat-Samii, "Patch antenna with switchable slot (PASS): dual-frequency operation", *Microwave and Opt. Tech. Lett.,* Vol. 31, Nov. 2001, pp. 165-168.

[5] W. Chew and H. Fetterman, "Millimeter-Wave imaging using FET detectors integrated with printed circuit antennas," *International Journal of Infrared and Millimeter Waves* ,vol. 10 No. 5 May 1989, pp. 565-578.

[6] Kato, T., Tanaka. Y., Ueda. H., Kano, H., Hashimoto, M., "L-band phase shifter with switching FETs for phased array antenna", *in Proceedings of IEEE MTT-S International Microwave symposium 1992,IEEE,* Washington, DC,1527-1530

[7] S. Kawasaki and T. Itoh, "A Slot Antenna with Electronically Tunable Length", *in IEEE Antennas and Propagation Society International Symposium*, June 1991,vol. 1, pp. 130–133.

[8] Sung-Hoon Oh, James T. Aberle, Sree Anantharaman, Kentaro Arai, Han L. Chong, and Seng C. Koay, "Electronically Tunable Antenna Pair And Novel RF Front-End Architecture For Software-Defined Radios," *EURASIP JASP* 2005:16 (2005) 2701-2707.

[9] K. Topalli, E. Erdil, and Ö Aydin Civi, "Reconfigurable Antenna Structures Using MEMS Technology," 28th *General Assembly of URSI,* 23-29 October 2005, New Delhi-India.

[10] Pozar, DM, and V. Sanchez, Magnetic Tuning of a Microstrip Antenna on a Ferrite Substrate, Electronics Letters, Vol. 24, June 1988, pp. 729-731

[11] A. Moessinger, R. Marin, J. Freese, S. Mueller, A. Manabe, and R. Jakoby, "Investigations on 77 GHz tunable reflectarray unit cells with liquid crystal," *EuCAP 2006*, Nice, France.

[12] K.C. Lim , J.D. Margerum, and A.M. Lackner, "Liquid crystal millimeter wave electronic phase shifter," *Applied Physics Letters*, vol. 62(10), March 1993, pp. 1065-1067

[13] Hu, W. Ismail, M. Y. Cahill, R. Gamble, H.S. Dickie, R. Fusco, D Linton, SP Rea and N Grant N, "Phase Control of Reflectarray Patches Using Liquid Crystal Substrate," *EUCAP* 2006, Nice, France

[14] Weil, C., G. Luessem and R. Jakoby, "Tunable inverted-microstrip phase shifter device using nematic liquid crystals," *IEEE MTT-S Int. Micro. Symp. Dig.* 2002, Seattle, WA, USA, pp. 367–370, June 2002.

[15] Kuki, T., H. Fjikake and T. Nomoto, "Microwave variable delay line using dual-frequency switching-mode liquid crystal," *IEEE Trans. Microwave Theory Tec.*, Vol. 50, No. 11, pp. 2604- 2609, 2002.

[16] Hu, W. , M.Y. Ismail , R. Cahill, J.A. Encinar , V.F. Fusco , H.S. Gamble , D. Linton , R. Dickie , N. Grant and S.P. Rea, "Electronically Reconfigurable Monopulse Reflectarray Antenna with Liquid Crystal Substrate, " *in The Second European Conference on Antennas and Propagation(EuCAP 2007)* , EICC, Edinburgh, UK, November 2007,1-6.

[17] A. Moessinger, R. Marin, D. Eicher, H. Schlaak, and R. Jakoby, "Liquid Crystal Reflectarray with Electronic 2D-Reconfiguration Capability," *29th ESA Antenna Workshop,* Noordwijk, the Netherlands, April 2007 .

[18] Roberts, R.J. and B. Easter," Microstrip resonators having reduced radiation loss, " *Electronic Letters*, Vol. 7, No. 8, 191-192, 1971.

[19] A. Moessinger, R. Marin, S. Mueller, J. Freese, and R. Jakoby, "Electronically reconfigurable reflectarrays with nematic liquid crystals," *Electronics Letters*, vol. 42, no. 16, pp. 899–900, 2006.

[20] W. Hu, M. Y. Ismail, R. Cahill, et al., "Liquid-crystal-based reflectarray antenna with electronically switchable monopulse patterns," *Electronics Letters*, vol. 43, no. 14, pp. 744–745, 2007.

[21] Yeh, J.A.; Chang, C.A.; Chih-Cheng Cheng; Jing-Yi Huang; Hsu, S.S.H., "Microwave characteristics of liquid-crystal tuneable capacitors" *Electron Device Letters, IEEE* Volume 26, Issue 7, July 2005 Page(s): 451 - 453

[22] K. Hirabayashi, H. Tsuda, and T. Kurokawa, "New structure of tunable wavelength-selective filters with a liquid crystal for FDM systems," *IEEE Photon. Technol. Lett.* 3, 741-743 (1992).

[23] A. Sneh and K. M. Johnson, "High-speed continuously tunable liquid crystal filter for WDMnetworks," *J. Lightwave Technol.* 14, 1067-1080 (1996).

[24] W. Hu , M. Y. Ismail , R. Cahill , H. S. Gamble , R. Dickie , V. F. Fusco , D. Linton , S. P. Rea, N. Grant, "Tunable liquid crystal reflectarray patch element", *IEE Electronics Letters*, April 2006, Vol. 42, Issue 9, p. 509-511

[25] http://www.op.titech.ac.jp/lab/Take-Ishi/English/Research/overview.html

[26] P. J. Collings, M. Hird, "Introduction to Liquid Crystals: Chemistry and Physics".1997. London, UK: *Publ by Taylor and Francis*. Pages:298

[27] G. Friedel, "The mesomorphic states of matter". Ann. Phys. 18, 273-474. 1922. Paris.France.

[28] S. Mueller, A. Penirschke, C. Damm, P. Scheele, M. Wittek, C. Weil, and R. Jakoby, "Broad-band microwave characterization of liquid crystals using a temperature-controlled coaxial transmission line", IEEE *Trans. Microwave Theory Tec.* Vol. 53, No. 6, pp. 1937- 1945, 2005.

[29] John Huang, Jose Antonio Encinar "Reflectarray Antennas" *Wiley-IEEE Press* (Nov. 2007) 216 pages

[30] D. M. Pozar, S. D. Targonski, and H. D. Syrigos, "Design of Millimeter Wave Microstrip Reflectarrays", *IEEE Trans. Antennas and Propagation.* vol. 45, pp. 287-295, February 1997.

[31] Park, I.; Mittra, R.; Aksun, I. "Analysis of microstrip patch antennas with tuning stubs using the closed-form Green's function" *Antennas and Propagation Society International Symposium,* vol.3, pp. 1442-1445, 1993

[32] Malik, D.P.S. Eskell, J.M. Skeen, M.H "Microstrip patch array antennas for space application" *Satellite Antenna Technology in the 21st Century, IEE Colloquium on*, pp.9/1-9/5,1991

[33] A. Penirschke, S. Muller, P. Scheele, C. Weil, M. Wittek, C. Hock and R.Jacoby, "Cavity pertubation method for characterization of liquid crystals up to 35 GHz" , *34th European Microwave Conference*, Amsterdam pp545-548, 2004.

[34] Wu, S. T. and C. S. Wu, "Small angle relaxation of highly deformed nematic liquid," *Appl. Phys. Lett.,* Vol. 53, No. 19, pp. 1794-1796, 1988.

[35] W. A. Imbriale "Spaceborne Antennas for Planetary Exploration," John Wiley & Sons, ISBN: 978-0-470-05150-4, 592 pages, June 2006.

APPENDIX A – TECHNICAL DATA AND SAFETY

SHEETS OF LIQUID CRYSTALS

Technical Data Sheet

LCG K15

Licristal® LC Mixture

Product No. 058300   preliminary
data sheet
Cyanobiphenyl Compound

Properties:

Melting Point		23 °C
Clearing Point		35 °C
Rotational Viscosity at 20 °C (extrapolated)		58 mPa s
Flow Viscosity 20 °C (extrapolated) 0 °C mm²s⁻¹		20 mm^2s^{-1} 56
Dielectric anisotropy $\Delta\varepsilon$ 20.1		+
(20 °C, 1 kHz) $\varepsilon_{||}$		26.1
$\varepsilon_{\perp}$		6.0
Optical anisotropy Δn		0.212
(20 °C, 589 nm) n_e		1.742
n_o		1.530
Molecular Mass		249.4
Vapor Pressure 20 °C mbar		5×10^{-7}
100 °C		4 x

EMD

Technical Data Sheet

10^{-3} mbar

EMD

Material Safety Data Sheet

EMD

Section 1. Product and Company Identification

Product Name	LCG K15 Licristal® LC Mixture	**Product Code**	058300

Manufacturer	EMD Chemicals Inc. Pigments Division 7 Skyline Drive Hawthorne, NY 10532	**Effective Date**	3/8/2006
		Print Date	3/8/2006

For More Information Call	**In Case of Emergency Call**
(914) 592-4660 M-F, 9AM-4:30 PM EST	800-424-9300 CHEMTREC (USA) 613-996-6666 (Canada) 24 Hours/Day: 7 Days/Week

Material Uses	Electronics Displays
Chemical Family	Organic Liquid Crystal Mixture

Section 2. Composition and Information on Ingredients

Component	CAS #	% by Weight
LCG K15 Licristal® LC Mixture	Mixture (LC)*	100

*Chemical identity withheld as a Trade Secret under the OSHA Hazard Communication Standard, 29CFR 1910.1200 (i) (1).

Section 3. Hazards Identification

Physical State and Appearance	Liquid. (Odorless, milky-white free flowing organic liquid.)
Emergency Overview	MAY BE HARMFUL IF INHALED, ABSORBED THROUGH SKIN OR SWALLOWED. MAY CAUSE RESPIRATORY TRACT, EYE AND SKIN IRRITATION. MAY CAUSE ALLERGIC RESPIRATORY AND SKIN REACTION.

Routes of Entry	Dermal contact. Eye contact. Inhalation. Ingestion.

Potential Acute Health Effects

Eyes May be hazardous in case of eye contact (irritant).

Skin May be hazardous in case of skin contact (permeator, irritant, sensitizer). Skin inflammation is characterized by itching, scaling, reddening, or, occasionally, blistering.

Inhalation May be hazardous in case of inhalation (lung irritant, lung sensitizer).

Ingestion May be hazardous in case of ingestion.

Potential Chronic Health Effects

Carcinogenic Effects This material is not known to cause cancer in animals or humans.

Additional information See Toxicological Information (section 11)

Medical Conditions Aggravated by Overexposure:	Repeated or prolonged inhalation of vapors may aggravate respiratory medical conditions.

99

LCG K15 Licristal® LC Mixture	058300	Page: 2/6

Section 4. First Aid Measures

Eye Contact	Check for and remove any contact lenses. In case of contact, immediately flush eyes with plenty of water for at least 15 minutes. Get medical attention.
Skin Contact	In case of contact, immediately flush skin with plenty of water for at least 15 minutes while removing contaminated clothing and shoes. Cover the irritated skin with an emollient. Wash clothing before reuse. Thoroughly clean shoes before reuse. Get medical attention.
Inhalation	If inhaled, remove to fresh air. If not breathing, give artificial respiration. If breathing is difficult, give oxygen. Get medical attention.
Ingestion	Do NOT induce vomiting unless directed to do so by medical personnel. Never give anything by mouth to an unconscious person. If large quantities of this material are swallowed, call a physician immediately. Loosen tight clothing such as a collar, tie, belt or waistband.

Section 5. Fire Fighting Measures

Flammability of the Product	May be combustible at high temperature.
Auto-ignition Temperature	Not available.
Flash Points	Closed cup: 113°C (235.4°F).
Flammable Limits	Not available.
Products of Combustion	These products are carbon oxides (CO, CO_2), nitrogen oxides (NO, NO_2...).
Fire Hazards in Presence of Various Substances	Flammable in presence of open flames, sparks and static discharge, of shocks, of heat.
Explosion Hazards in Presence of Various Substances	**Risks of explosion of the product in presence of static discharge:** Flammable in presence of open flames, sparks and static discharge. **Risks of explosion of the product in presence of mechanical impact:** Flammable in presence of shocks.
Fire Fighting Media and Instructions	In case of fire, use water spray (fog), foam, dry chemical, or CO2.
Protective Clothing (Fire)	Wear self-contained breathing apparatus and full protective clothing.
Special Remarks on Fire Hazards	Keep away from heat and flame.
Special Remarks on Explosion Hazards	Keep away from sources of ignition.

Section 6. Accidental Release Measures

Small Spill and Leak	Use a tool to scoop up solid or absorbed material and place into appropriate labeled waste container.Finish cleaning by spreading water on the contaminated surface and dispose of according to local and regional authority requirements.
Large Spill and Leak	Use appropriate tools to put the spilled material into a labeled waste disposal container. Finish cleaning by spreading water on the contaminated surface and dispose of according to local and regional regulatory requirements. Check TLV- Section 8 of MSDS.
Spill Kit Information	No specific spill kit required for this product.

LCG K15 Licristaf® LC Mixture   **058300**   *Page: 3/6*

Section 7. Handling and Storage

Handling	Do not ingest. Avoid contact with eyes, skin and clothing. Avoid breathing vapors or spray mists. Avoid breathing dust. Use with adequate ventilation. Wash thoroughly after handling.
Storage	Keep container tightly closed Keep container in a cool, well-ventilated area. Store between 10 to 30°C (50 to 86°F).

Section 8. Exposure Controls/Personal Protection

Engineering Controls	Provide exhaust ventilation or other engineering controls to keep the airborne concentrations of vapors below their respective occupational exposure limits. Ensure that eyewash stations and safety showers are proximal to the work-station location.

Personal Protection

Eyes	Splash goggles.
Body	Lab coat.
Respiratory	Vapor respirator. Be sure to use a MSHA/NIOSH approved respirator or equivalent.
Hands	Nitrile gloves.
Feet	Not applicable.

Protective Clothing (Pictograms)	

Personal Protection in Case of a Large Spill	Splash goggles. Synthetic apron. Nitrile gloves. Wear MSHA/NIOSH approved self-contained breathing apparatus or equivalent and full protective gear.

Product Name	Exposure Limits
LCG K15 Licristaf® LC Mixture	Not available.

Section 9. Physical and Chemical Properties

Odor	Odorless.
Color	Milky-white
Physical State and Appearance	Liquid. (Odorless, milky-white free flowing organic liquid.)
Molecular Weight	549.4 g/mol
Molecular Formula	Not applicable.
pH	Not available.
Boiling/Condensation Point	140 to 150°C (284 to 302°F)
Melting/Freezing Point	22 to 25°C (71.6 to 77°F)
Specific Gravity	Not available.
Vapor Pressure	Not available.
Vapor Density	Not available.
Odor Threshold	Not available.
Evaporation Rate	Not available.
Log K$_{ow}$	Not available.

LCG K15 Licristal® LC Mixture	058300	Page: 4/6

Solubility   Insoluble in water.

Section 10. Stability and Reactivity

Stability and Reactivity	Stable under recommended storage and handling conditions (see section 7).
Conditions of Instability	Avoid excessive heat.
Incompatibility with Various Substances	Reactive with oxidizing agents, moisture.
Hazardous Decomposition Products	These products are carbon oxides (CO, CO_2), nitrogen oxides (NO, NO_2...)
Hazardous Polymerization	Will not occur.

Section 11. Toxicological Information

RTECS Number:	LCG K15 Licristal® LC Mixture Not available.
Toxicity	Acute oral toxicity (LD_{50}): 4090 mg/kg [Rat]. Acute dermal toxicity (LD_{50}): >4000 mg/kg [Rat].
Chronic Effects on Humans	CARCINOGENIC EFFECTS: Not available. MUTAGENIC EFFECTS: Not available. TERATOGENIC EFFECTS: Not available. DEVELOPMENTAL TOXICITY: Not available. Repeated or prolonged inhalation of dust may lead to chronic respiratory irritation.
Acute Effects on Humans	May be hazardous in case of eye contact (irritant). May be hazardous in case of skin contact (permeator, irritant, sensitizer). Skin inflammation is characterized by itching, scaling, reddening, or, occasionally, blistering. May be hazardous in case of inhalation (lung irritant, lung sensitizer). May be hazardous in case of ingestion.
Synergetic Products (Toxicologically)	Not available.
Irritancy	Draize Test: Not available.
Sensitization	Repeated or prolonged exposure to the substance at concentrations above the exposure limits may cause respiratory tract and skin sensitization.
Carcinogenic Effects	This material is not known to cause cancer in animals or humans.
Toxicity to Reproductive System	Not available.
Teratogenic Effects	Not available.
Mutagenic Effects	Not available.

Section 12. Ecological Information

Ecotoxicity	Harmful to aquatic organisms, may cause long-term adverse effects in the aquatic environment.
BOD5 and COD	Not available.

Section 13. Disposal Considerations

EPA Waste Number	Non-hazardous chemical waste.
Treatment	Dispose of according to all federal, state and local regulations.

LCG K15 Licristal® LC Mixture   058300   *Page: 5/6*

Section 14. Transport Information

DOT Classification   Not regulated.

TDG Classification   Not regulated.

IMO/IMDG Classification   Not regulated.

ICAO/IATA Classification   Not regulated.

Section 15. Regulatory Information

U.S. Federal Regulations   TSCA 8(b) inventory: LCG K15 Licristal® LC Mixture
SARA 302/304/311/312 extremely hazardous substances: No products were found.
SARA 302/304 emergency planning and notification: No products were found
SARA 302/304/311/312 hazardous chemicals: No products were found.
SARA 311/312 MSDS distribution - chemical inventory - hazard identification: No products were found.
SARA 313 Form R Reporting Requirements-No products were found.
SARA 313 Supplier Notification- No products were found.
Clean Water Act (CWA) 307: No products were found.
Clean Water Act (CWA) 311: No products were found.
Clean air act (CAA) 112 accidental release prevention: No products were found.
Clean air act (CAA) 112 regulated flammable substances: No products were found.
Clean air act (CAA) 112 regulated toxic substances: No products were found.

WHMIS (Canada)   Class D-2A: Material causing other toxic effects (VERY TOXIC).

CEPA NDSL: LCG K15 Licristal® LC Mixture

This product has been classified in accordance with the hazard criteria of the Controlled Product Regulations and the MSDS contains all required information.

International Regulations

EINECS   LCG K15 Licristal® LC Mixture   255-093-2

DSCL (EEC)   This product is not classified according to the EU regulations.

International Lists   Australia (NICNAS): LCG K15 Licristal® LC Mixture

Korea (TCCL): LCG K15 Licristal® LC Mixture

Philippines (RA6969): LCG K15 Licristal® LC Mixture

State Regulations   No products were found.
California prop. 65: No products were found.

Section 16. Other Information

National Fire Protection Association (U.S.A.)

Fire Hazard 1
Health 2
Reactivity 0
Specific Hazard

Other Special Considerations   Warning - this preparation contains a substance not yet tested completely.

LCG K15 Licristal® LC Mixture	058300	Page: 6/6
Changed Since Last Revision		

Notice to Reader

The statements contained herein are based upon technical data that EMD Chemicals Inc. believes to be reliable, are offered for information purposes only and as a guide to the appropriate precautionary and emergency handling of the material by a properly trained person having the necessary technical skills. Users should consider these data only as a supplement to other information gathered by them and must make independent determinations of suitability and completeness of information from all sources to assure proper use, storage and disposal of these materials and the safety and health of employees and customers and the protection of the environment. EMD CHEMICALS INC. MAKES NO REPRESENTATION OR WARRANTY OF ANY KIND, EXPRESS OR IMPLIED, INCLUDING MERCHANTABILITY OR FITNESS FOR A PARTICULAR USE, WITH RESPECT TO THE INFORMATION HEREIN OR THE PRODUCT TO WHICH THE INFORMATION REFERS.

Technical Data Sheet

LCG BL006 Licristal LC Mixture

Product No. 200216

preliminary data sheet

PDLC Fluid

Properties

Clearing Point °C			113
Flow Viscosity at	20 °C		71 mm^2s^{-1}
Dielectric anisotropy 17.3	$\Delta\varepsilon$		-
(20 °C, 1 kHz)	$\varepsilon_{\parallel}$		22.8
	$\varepsilon_{\perp}$		5.5
Optical anisotropy	Δn		0.2860
(20 °C, 589 nm)	n_e		1.8160
	n_o		1.5300
Elastic constants (20 °C) k_{11} pN			17.9
	k_{33}		33.5 pN
Threshold Voltage V_{10} at 20 °C V			1.77

EMD

Technical Data Sheet

Saturation Voltage V_{90} at 20 °C   2.42
V

(n.b.   voltages measured in a 90° twist cell)

EMD

Technical data sheet

The data found on this sheet may be subject to change without prior notice.

Licristal®

				MDA-05-893	
Physical Properties					
Clearing Point				109.5	°C
Rotational Viscosity	γ_1		+20 °C	237	m Pa s
Optical Anisotropy	Δn	589.3 nm	+20 °C	0.2679	
	n_e	589.3 nm	+20 °C	1.7834	
	n_o	589.3 nm	+20 °C	1.5155	
Dielectric Anisotropy	$\Delta\varepsilon$	1.0 kHz	+20 °C	5.3	
	$\varepsilon_\parallel$	1.0 kHz	+20 °C	8.8	
	$\varepsilon_\perp$	1.0 kHz	+20 °C	3.6	
Elastic Constants	K_1		+20 °C	12.9	pN
	K_3		+20 °C	17.7	pN
	K_3/K_1		+20 °C	1.37	
Low Temp. Storage (Cells)			-20 °C	Passed	
Low Temp. Storage (Cells)			-30 °C	Passed	
Low Temp. Storage (Cells)			-40 °C	Passed	
Low Temp. Storage (Bulk)			+8 °C	Passed	
HTP Dopant: S-811			+20 °C	-11.8	μm^{-1}
Electro-Optical Properties					
Twist Angle				240	°
	d*Δn			0.85	µm
d/p				0.53	
Polyimide Type					
Threshold Voltage	$V_{10, \varphi=0}$		+20 °C		V
Saturation Voltage	$V_{90, \varphi=0}$		+20 °C		V
Steepness			+20 °C		%

Technical data sheet

The data found on this sheet may be subject to change without prior notice.

Licristal®

MERCK

Merck KGaA Germany · Frankfurter Str.250 64293 Darmstadt

Date	13.02.2002
Division/Dept.	LC V/M+S
Care of	H.-J. Lemp
Phone	+49(0)6151/72-30 26
Fax	+49(0)6151/72-31 32
E-Mail	hans-juergen.lemp@merck.de
Your letter	
Your ref.	

Storage Conditions and Minimum Shelf Life

Dear

This is to answer your request for information about the storage conditions and the minimum shelf life of our liquid crystal mixtures.

1. Storage Conditions

Merck liquid crystal mixtures should be stored in unopened original primary packaging (aluminium bottles). Storage in original secondary packaging (inserts and cartons) provides additional protection against damage by external impact.

Unopened bottles should be stored in an area which does not experience large changes in temperature or humidity and where the temperature and humidity are within the following limits:

Temperature:	20° C ± 10° C
Relative Humidity:	50% ± 20%.

2. Minimum Shelf Life

Based on the above specified storage condition the minimum shelf life is 12 months for STN and TN mixtures. For dye-doped liquid crystal mixtures the minimum shelf life is 6 months.

We hope that this information is useful for you.

With best regards,
Merck KGaA

i.A.

Dr. Göbmann   Stenzel

'ıı¦ıMERCK

Safety Data Sheet

According to EC Directive 91/155/EEC

Date of issue: 19.01.2006

1. Identification of the substance/preparation and of the company/undertaking

Identification of the product

Catalogue No.: 136493

Product name: MDA-05-893 Licristal®

Use of the substance/preparation

Liquid-crystal display technology

Company/undertaking identification

Company: Merck KGaA * 64271 Darmstadt * Germany * Phone: +49 6151 72-0

Emergency telephone No.: Please contact the regional Merck representation in your country.

2. Composition/information on ingredients

Mixture of liquid crystals.

Hazardous ingredients:

Name according to EC Directives:

CAS-No.	EC No.	EC-Index-No.	Classification	Content:
4-(4-trans-Vinyl-[1,1'-bicyclohexyl]-4'-trans-yl)-1,2-difluo robenzene				
142400-92-8	430-860-6		R53	1 - < 10 %
4-ethylcyclohexyl-4'-cyanobenzene				
72928-54-2	277-084-2		Xn, R22	≧10 - < 25 %
2',2'',4''-Trifluoro-4-propyl-1,1':4',1''-terphenyl				
154346-21-1			R53	10 - < 25 %
4-((4-Ethyl-2,6-difluorophenyl)-ethinyl)-4'-propylbiphenyl				
221526-72-3			R53	≧10 - < 25 %

(Full text of R-Phrases in heading 16)

3. Hazards identification

May cause long-term adverse effects in the aquatic environment.

Attention - this preparation contains a substance which has not been fully tested so far.

The test results available so far do not permit a complete evaluation. Further risks cannot be excluded if the product is handled inappropriately.

Merck Safety Data Sheet

According to EC Directive 91/155/EEC

Catalogue No.:	136493
Product name:	MDA-05-893 Licristal

4. First aid measures

After inhalation: fresh air. Consult doctor if feeling unwell.
After skin contact: wash off with plenty of water. Remove contaminated clothing. Consult doctor in the event of any complaints.
After eye contact: rinse out with plenty of water with the eyelid held wide open. Call in ophtalmologist if necessary.
After swallowing: immediately make victim drink plenty of water. Call in physician.

5. Fire-fighting measures

Suitable extinguishing media:
CO_2, foam, powder.

Special risks:
Combustible. Development of hazardous combustion gases or vapours possible in the event of fire. The following may develop in event of fire: hydrogen fluoride, nitrogen oxides.

Special protective equipment for fire fighting:
Do not stay in dangerous zone without self-contained breathing apparatus. In order to avoid contact with skin, keep a safety distance and wear suitable protective clothing.

Other information:
Contain escaping vapours with water. Prevent fire-fighting water from entering surface water or groundwater.

6. Accidental release measures

Person-related precautionary measures:
Avoid substance contact. Do not inhale vapours/aerosols. Ensure supply of fresh air in enclosed rooms.

Environmental-protection measures:
Do not allow to enter sewerage system.

Procedures for cleaning / absorption:
Take up with liquid-absorbent material (e.g. Chemizorb®). Forward for disposal. Clean up affected area.

7. Handling and storage

Handling:

Store tightly closed in a cool dry place.

Storage:

Tightly closed. Storage temperature: no restrictions.

8. Exposure controls/personal protection

Personal protective equipment:

Protective clothing should be selected specifically for the working place, depending on concentration and quantity of the hazardous substances handled. The resistance of the protective clothing to chemicals should be ascertained with the respective supplier.

Merck Safety Data Sheet
According to EC Directive 91/155/EEC

Catalogue No.:	136493
Product name:	MDA-05-893 Licristal

Respiratory protection:	required when vapours/aerosols are generated.
Eye protection:	required
Hand protection:	In full contact:

In full contact:
Glove material:	nitrile rubber
Layer thickness:	0.11 mm
Breakthrough time:	> 480 Min.

In splash contact:
Glove material:	nitrile rubber
Layer thickness:	0.11 mm
Breakthrough time:	> 480 Min.

The protective gloves to be used must comply with the specifications of EC directive 89/686/EEC and the resultant standard EN374, for example KCL 741 Dermatril® L (full contact), 741 Dermatril® L (splash contact).
This recommendation applies only to the product stated in the safety data sheet and supplied by us as well as to the purpose specified by us. When dissolving in or mixing with other substances and under conditions deviating from those stated in EN374 please contact the supplier of CE-approved gloves (e.g. KCL GmbH, D-36124 Eichenzell, Internet: www.kcl.de).

Industrial hygiene:
Change contaminated clothing. Application of skin- protective barrier cream recommended. Wash hands after working with substance.

9. Physical and chemical properties

Form:	liquid	
Colour:	milky-white	
Odour:	almost odourless	
pH value		not available
Melting point		not available
Boiling point		not available
Ignition temperature		not available
Flash point		not available
Explosion limits	lower	not available
	upper	not available
Density	(20 °C)	0.97-1.00 g/cm^3
Solubility in Water		not available

10. Stability and reactivity

Conditions to be avoided
no information available

Substances to be avoided

no information available

Hazardous decomposition products
in the event of fire: See chapter 5.

Merck Safety Data Sheet

According to EC Directive 91/155/EEC

Catalogue No.:	136493
Product name:	MDA-05-893 Licristal®

11. Toxicological information

Acute toxicity

Quantitative data on the toxicity of this product are not available.

Further toxicological information

Hazardous properties cannot be excluded.

Further data

The product should be handled with the care usual when dealing with chemicals.

12. Ecological information

Ecotoxic effects:
Quantitative data on the ecological effect of this product are not available.

Biological effects:
May cause long-term adverse effects in the aquatic environment.

Further ecologic data:
Do not allow to enter waters, waste water, or soil!

13. Disposal considerations

Product:

Chemicals must be disposed of in compliance with the respective national regulations. Under www.retrologistik.de you will find country- and substance-specific information as well as contact partners.

Packaging:

Merck product packaging must be disposed of in compliance with the country-specific regulations or must be passed to a packaging return system. Under www.retrologistik.de you will find special information on the respective national conditions as well as contact partners.

14. Transport information

Not subject to transport regulations.

15. Regulatory information

Labelling according to EC Directives

Symbol:	---	
R-phrases:	53	May cause long-term adverse effects in the aquatic environment.
S-phrases:	61	Avoid release to the environment. Refer to special instructions/Safety data sheets.
Additional labelling	Attention - this preparation contains a substance which has not been fully tested so far.	

Merck Safety Data Sheet

According to EC Directive 91/155/EEC

Catalogue No.:	136493
Product name:	MDA-05-893 Licristal®

Reduced labelling (1999/45/EC.Art.10,4)

Symbol:	xxx	
R-phrases:	53	May cause long-term adverse effects in the aquatic environment.
S-phrases:	---	

16. Other information

Text of any R phrases referred to under heading 2:

22	Harmful if swallowed.
53	May cause long-term adverse effects in the aquatic environment.

Regional representation:

This information is given on the authorised Safety Data Sheet
for your country.

The information contained herein is based on the present state of our knowledge. It characterizes the product with regard to the appropriate safety precautions. It does not represent a guarantee of the properties of the product.

APPENDIX B – MATLAB CODES

Work1.m

```
clear;
clc;
load VC00.txt;load VC1.txt;load VC2.txt;
load VC3.txt;load VC4.txt;
load VC5.txt;load VC6.txt;load VC7.txt;
load VC8.txt;load VC9.txt;load VC10.txt;load VC11.txt;
load VC12.txt;load VC13.txt;load VC14.txt;load VC15.txt;load VC16.txt;
load VC17.txt;load VC18.txt;load VC19.txt;load VC20.txt;load VC21.txt;
load VC22.txt;load VC23.txt;load VC24.txt;load VC25.txt;load VC26.txt;
load VC27.txt;load VC28.txt;load VC29.txt;load VC30.txt;
load VC31.txt;load VC32.txt;

z0=complex(VC00(340,5),VC00(340,6));
r0 = abs(z0);theta0 = atan2(imag(z0),real(z0));


z1=complex(VC1(340,5),VC1(340,6));
r1 = abs(z1);theta1 = atan2(imag(z1),real(z1));


z2=complex(VC2(340,5),VC2(340,6));
r2 = abs(z2);theta2 = atan2(imag(z2),real(z2));


z3=complex(VC3(340,5),VC3(340,6));
r3 = abs(z3);theta3 = atan2(imag(z3),real(z3));


z4=complex(VC4(340,5),VC4(340,6));
r4 = abs(z4);theta4 = atan2(imag(z4),real(z4));


z5=complex(VC5(340,5),VC5(340,6));
r5 = abs(z5);theta5 = atan2(imag(z5),real(z5));


z6=complex(VC6(340,5),VC6(340,6));
r6 = abs(z6);theta6 = atan2(imag(z6),real(z6));


z7=complex(VC7(340,5),VC7(340,6));
r7 = abs(z7);theta7 = atan2(imag(z7),real(z7));


z8=complex(VC8(340,5),VC8(340,6));
r8 = abs(z8);theta8 = atan2(imag(z8),real(z8));


z9=complex(VC9(340,5),VC9(340,6));
r9 = abs(z9);theta9 = atan2(imag(z9),real(z9));


z10=complex(VC10(340,5),VC10(340,6));
r10 = abs(z10);theta10 = atan2(imag(z10),real(z10));


z11=complex(VC11(340,5),VC11(340,6));
```

```
r11 = abs(z11);theta11 = atan2(imag(z11),real(z11));

z12=complex(VC12(340,5),VC12(340,6));
r12 = abs(z12);theta12 = atan2(imag(z12),real(z12));

z13=complex(VC13(340,5),VC13(340,6));
r13 = abs(z13);theta13 = atan2(imag(z13),real(z13));

z14=complex(VC14(340,5),VC14(340,6));
r14 = abs(z14);theta14 = atan2(imag(z14),real(z14));

z15=complex(VC15(340,5),VC15(340,6));
r15 = abs(z15);theta15 = atan2(imag(z15),real(z15));

z16=complex(VC16(340,5),VC16(340,6));
r16 = abs(z16);theta16 = atan2(imag(z16),real(z16));

z17=complex(VC17(340,5),VC17(340,6));
r17 = abs(z17);theta17 = atan2(imag(z17),real(z17));

z18=complex(VC18(340,5),VC18(340,6));
r18 = abs(z18);theta18 = atan2(imag(z18),real(z18));

z19=complex(VC19(340,5),VC19(340,6));
r19 = abs(z19);theta19 = atan2(imag(z19),real(z19));

z20=complex(VC20(340,5),VC20(340,6));
r20 = abs(z20);theta20 = atan2(imag(z20),real(z20));

z21=complex(VC21(340,5),VC21(340,6));
r21 = abs(z21);theta21 = atan2(imag(z21),real(z21));

z22=complex(VC22(340,5),VC22(340,6));
r22 = abs(z22);theta22 = atan2(imag(z22),real(z22));

z23=complex(VC23(340,5),VC23(340,6));
r23 = abs(z23);theta23 = atan2(imag(z23),real(z23));

z24=complex(VC24(340,5),VC24(340,6));
r24 = abs(z24);theta24 = atan2(imag(z24),real(z24));

z25=complex(VC25(340,5),VC25(340,6));
r25 = abs(z25);theta25 = atan2(imag(z25),real(z25));

z26=complex(VC26(340,5),VC26(340,6));
r26 = abs(z26);theta26 = atan2(imag(z26),real(z26));

z27=complex(VC27(340,5),VC27(340,6));
```

```
r27 = abs(z27);theta27 = atan2(imag(z27),real(z27));

z28=complex(VC28(340,5),VC28(340,6));
r28 = abs(z28);theta28 = atan2(imag(z28),real(z28));

z29=complex(VC29(340,5),VC29(340,6));
r29 = abs(z29);theta29 = atan2(imag(z29),real(z29));

z30=complex(VC30(340,5),VC30(340,6));
r30 = abs(z30);theta30 = atan2(imag(z30),real(z30));

z31=complex(VC31(340,5),VC31(340,6));
r31 = abs(z31);theta31 = atan2(imag(z31),real(z31));

z32=complex(VC32(340,5),VC32(340,6));
r32 = abs(z32);theta32 = atan2(imag(z32),real(z32));

rz=[r0,r1,r2,r3,r4,r5,r6,r7,r8,r9,r10,...
    r11,r12,r13,r14,r15,r16,r17,r18,r19,r20,r21,r22,r23,r24,r25,r26,...
    r27,r28,r29,r30,r31,r32];
%rz=interp(rz,100);

tetaz=[theta0,theta1,theta2,theta3,...
    theta4,theta5,theta6,theta7,theta8,theta9,...
    theta10,theta11,theta12,theta13,theta14,theta15,theta16,theta17,...
    theta18,theta19,theta20,theta21,theta22,theta23,theta24,theta25,...
    theta26,theta27,theta28,theta29,theta30,theta31,theta32];
%tetaz=interp(tetaz,100);
z_experimental = rz.*exp(i.*tetaz);%experimental data

G1=z_experimental*exp(i*0.2*pi);
G2=z_experimental*exp(i*1.118*pi);
%G2=-G1;
z1=(1+G1)./(1-G1);
z2=(1+G2)./(1-G2);
ztot=z1+z2;
G=(ztot-2.2)./(ztot+2.2);
mag=interp(abs(G),100);
pha=interp(unwrap(angle(G)),100);
G3=mag.*exp(i*pha);
figure(10)
polar(angle(G3),abs(G3));
figure(3)
polar(angle(G1),abs(G1));
figure(4)
polar(angle(G2),abs(G2));
save('work1');
```

Radiation Pattern,

```
clear;
clc;
load work1.mat
z_2patch= G3;%2patch data

f=10e9;
c0=3e8;
lambda=c0/f;
s=lambda/6;%lenght of sample
beta=2*pi/lambda;
R=50*lambda;
F=100*lambda;
N=(R/s)+1;%number of SAMPLE

%Rayon central:
fi0=0;
x0=R/2;
teta0=asin(x0/F);
alpha=teta0/2;
lp0=abs(F-x0*tan(alpha));
l0=sqrt(x0^2+(x0*tan(alpha)-F).^2);
deltafi0=-beta*(l0+lp0)+fi0;
gama=ones(1,N);%ideal reflection

% array initialization
xx=linspace(0,R,N);%lenght of sample
NN=linspace(0,N,N);%Sample number

% calculating length of travelling wave versus number of samples
  for n = 1:N,
     % calculating length of travelling wave versus number of samples
       l(n)=sqrt(xx(n)^2+(xx(n)*tan(alpha)-F).^2);
       lp(n)=abs(F-xx(n).*tan(alpha));
       fi(n)=deltafi0+beta.*(l(n)+lp(n));
         % calculating cosine(sai) versus number of samples
     cos_sai(n)=(x0.*xx(n)+(x0*tan(alpha)-F)*(xx(n)*tan(alpha)-F))./...
            (l0.*l(n));
        % calculating change of magnitud in perfect reflectarray antenna
        %versus number of samples
        v(n)=(cos_sai(n).^12)./(l(n)+lp(n));% feed pattern and
spreading loss
  end;

z_d = abs(gama).*exp(i.*(fi));%reflection in the desirable reflectarray
z_p = z_d.*abs(v).*exp(i.*(-beta*(l+lp)));%perfect reflectarray,
aperture field
```

```matlab
    for n=1:N,
        for n_achiv=1:3300
      %  Z_t(n_achiv)=(z_d(n)-z_2patch(n_achiv));
          Z_t(n_achiv)=(angle(z_d(n))-angle(z_2patch(n_achiv)));
        end
    [Z_t_min,Index_min]=min(abs(Z_t),[],2);% achievable reflectarray
    r_t(n) = abs(z_2patch(Index_min));
    teta_t(n) = angle(z_2patch(Index_min));
    end

    for n=1:N,
        v_real_phase(n)=-beta.*(l(n)+lp(n))+teta_t(n);
        v_real_abs(n)=abs((v(n)).*r_t(n));
    end

% %----plot ------------------------------------
set(0,'defaultaxesfontsize',25);
clf
figure(1);
polar(fi,gama,'rs')%sample
hold on;
polar(angle(G3),abs(G3))%2patchdata
hold on;
polar(teta_t,r_t,'gp')% achievable reflectarray
hold on;
polar(angle(z_p),abs(z_p),'m<')%perfect
hold on;
polar((v_real_phase),v_real_abs,'-k')%real

legend('\Gamma(sample)','\Gamma(2patch)',...
    '\Gamma(achievable)','\Gamma(perfect)','\Gamma(real)',1);



% Radiation pattern
Ntheta=1800;
 %theta=linspace(-pi/4,pi/4,Ntheta);
theta=linspace(pi/4,3*pi/4,Ntheta);
v_achieved=v.*r_t.*exp(j*teta_t).*exp(i.*(-beta*(l+lp)));%unit pattern
%e_ff_achi=zeros(1,Ntheta)
for m = 1:Ntheta
    e_ff_achi(m)=v_achieved*exp(j*beta*xx*cos(theta(m))).';%achiv
    e_ff_ideal(m)=z_p*exp(j*beta*xx*cos(theta(m))).';%ideal
end
norm_ach=max(max(abs(e_ff_achi)));
norm_ide=max(max(abs(e_ff_ideal)));
figure(2)
theta=theta*180/pi-90;
plot(theta,20*log10(abs(e_ff_achi/norm_ach)),...
    theta,20*log10(abs(e_ff_ideal/norm_ide)))
```

```
xlabel('\theta(degrees)','FontSize',25);   ylabel('E-
plane(dB)','FontSize',25);
legend('achieved reflectarray','Perfect reflectarray',0);


figure(10)
polar(angle(e_ff_ideal),abs(e_ff_ideal))
hold on;
polar(angle(e_ff_achi),abs(e_ff_achi),'r-')

index=[1:1:301]
figure(3)
plot(index,angle(v_achieved),index,angle(z_p));
xlabel('Number of samples','FontSize',25);
   ylabel('angle(rad)','FontSize',25);
legend('achieved reflectarray','Perfect reflectarray',0);
figure(4)
plot(index,abs(v_achieved),index,abs(z_p)*0.11);
xlabel('Number of samples','FontSize',25);
   ylabel('Absolute magnitude ','FontSize',25);
legend('achieved reflectarray','Perfect reflectarray',0);
```